DEVELOPMENT OF NEAR INFRARED SPECTROSCOPY METHODOLOGIES TO PROVIDE PHYSICAL INFORMATION FOR PHARMACEUTICAL PROCESSES

by

Jorge Mario Ropero Vega
A dissertation submitted in partial fulfillment of the requirements for the degree of

DOCTOR OF PHILOSOPHY
in
Applied Chemistry

UNIVERSITY OF PUERTO RICO
MAYAGÜEZ CAMPUS
2013

Approved by:

_____   _____
Rodolfo J. Romañach, Ph.D.   Date
President, Graduate Committee

_____   _____
Nairmen Mina, Ph.D.   Date
Member, Graduate Committee

_____   _____
Félix Román, Ph.D.   Date
Member, Graduate Committee

_____   _____
Oscar Perales, Ph.D.   Date
Member, Graduate Committee

_____   _____
Dorothy Bollman, Ph.D.   Date
Representative, Graduate Studies

_____   _____
René S. Vieta, PhD   Date
Chairperson, Chemistry Department

ABSTRACT

This research focused on increasing the number of applications and establishing methods to monitor physical properties from pharmaceutical materials using Near Infrared Spectroscopy (NIRS). NIRS in combination with chemometric data analysis was used increasing the number of applications and understanding the physical information of pharmaceutical materials, this work opens interesting perspectives for pharmaceutical analyses in solid form without sample preparation. The development of new NIR analytical methods contributes to the process analytical technology (PAT) initiative and pharmaceutical manufacturing.

NIR spectroscopy was used to create a new method for in-line characterization of powder flow behavior. The spectra of flowing powders were used to measure the flow, continuity, and interruption of powder flow and evaluate the chemical heterogeneity of pharmaceutical powders. The main purpose of this work was used in-line NIRS to detect the flow uniformity, which in general depends on the flowability of the powder and their blends. The new NIRS method was used for the evaluation of active pharmaceutical ingredients (APIs) that have surface modified to improve their extremely poor flow properties. Near-infrared (NIR) spectroscopy was utilized as a novel approach to characterize the improved flow behavior of APIs and their blends. This NIRS application also involves a second study evaluating the performance of excipients and cohesive powders in a K-tron twin-screw gravimetric feeder. The evaluation used NIR spectroscopy and multivariate data analysis as an effective alternative for the real-time measure of flow behavior.

The second objective of this study was the real-time determination of tablet compaction pressure in pharmaceutical tablets. This study determined the concentration and compaction pressure in moving tablets with NIR spectra.

The third section of this dissertation describes the use of Near-infrared chemical imaging (NIR-CI) to study pharmaceutical tablets that decrease in compaction of particles (tablet relaxation). NIR-CI spectra of lactose monohydrate tablets were acquired and the spectral slope from each pixel and the data hypercube was used to assess tablet compaction and relaxation over the time.

Resumen

Este trabajo fue enfocado en aumentar el número de aplicaciones y métodos establecidos para monitorear propiedades físicas de materiales farmacéuticos usando espectroscopia de infrarrojo cercano (NIRS). NIRS en combinación con quimiometría fueron empleados en incrementar el número de aplicaciones y el grado de comprensión de la información física originada en materiales farmacéuticos, este trabajo abre perspectivas interesantes para el análisis farmacéutico de muestras solidas sin preparación de muestras. El desarrollo de nuevos métodos analíticos de NIR contribuye al mejoramiento de los métodos de manufactura farmacéutica y la iniciativa de tecnología de procesos analíticos (PAT).

La espectroscopia NIR fue usada para crear un nuevo método de caracterización en línea para el comportamiento del flujo de material particulado. Espectros de flujo de partículas fueron usados para medir el flujo, la continuidad, la interrupción del flujo al tiempo que evaluaron la heterogeneidad química del flujo de partículas. El propósito central de este trabajo fue emplear la espectroscopia NIR en línea para detectar la uniformidad del flujo, la cual en general depende de la fluidez del tipo de partículas estudiadas y de sus mezclas. El nuevo método NIR fue empleado en la evaluación de ingredientes activos farmacéuticos (APIs) que fueron modificados en la superficie para mejorar sus pobres propiedades de flujo. La espectroscopia de NIR fue empleada como una nueva aproximación para caracterizar el mejoramiento de las propiedades de flujo de APIs y sus mezclas. Esta aplicación NIRS también envuelve un segundo estudio evaluando el desempeño de excipientes y partículas cohesivas en un alimentador gravimétrico K-tron de tornillos gemelos. La espectroscopia NIR y análisis multivariado de datos es una alternativa efectiva de análisis para mediciones del comportamiento de flujo en tiempo real.

El segundo objetivo de este estudio fue la determinación en tiempo real de la presión de compactación de tabletas farmacéuticas. En esta parte del trabajo fue determinada la presión de compactación y la cantidad de ingrediente activo para tabletas en movimiento usando espectroscopia NIR.

La tercera sección de esta tesis describe el uso de imágenes químicas en infrarrojo Cercano (NIR-CI) para estudiar tabletas farmacéuticas con decrecimiento en la compactación de partículas (relajación de tabletas). Espectros NIR-CI de tabletas de lactosa monohidratada fueron adquiridos y la pendiente del espectro en cada pixel fue usada como indicador de la relajación de tabletas atreves del tiempo.

ACKNOWLEDGEMENTS

During the development of my doctoral studies at the University of Puerto Rico at Mayagüez campus, several persons and institutions collaborated directly and indirectly with my research. I want to express a sincere acknowledgement to my advisor, Professor Rodolfo J. Romañach Ph. D. for his invaluable scientific support, guidance and friendship.

I would also like to thank to Professor Nairmen Mina Ph. D., Carlos Velázquez Ph. D., Félix Román, Ph. D. and Professor Oscar Perales-Perez Ph. D. for their time and availability to help me during the progress of this research. I would like to thank the Engineering Research Center for Structure Organic Particulate System (C-SOPS) for the financial support.

Table of Contents

List of original publications

This thesis is based on the following original papers.

I.   Ropero, J.; Beach, L.; Alcalà, M.; Rentas, R.; Dave, R.; Romanach, R. Near-infrared spectroscopy for the in-line characterization of powder voiding part I: development of the methodology. *Journal of Pharmaceutical Innovation*.**2009**, 4, 187–197.

II.   Alcalà, M.; Ropero, J.; Vázquez, R.; Romañach, J. Deconvolution of Chemical and Physical Information from Intact Tablets NIR Spectra: Two- and Three-Way Multivariate Calibration Strategies for Drug Quantitation. *Journal of Pharmaceutical Sciences.***2009**, 98 (8), 2747-2758.

III.   Beach, L.; Ropero, J.; Mujumdar, A.; Alcalà, M.; Romanach, R.; Dave, R. Near-Infrared Spectroscopy for the In-Line Characterization of Powder Voiding Part II: Quantification of Enhanced Flow Properties of Surface Modified Active Pharmaceutical Ingredients. *Journal of Pharmaceutical Innovation*.**2010**, 5, 1–13.

IV.   Ropero, J.; Colón,Y.; Johnson-Restrepo, B.; Romañach, R.Near infrared chemical imaging slope as new method to study tablet compaction and tablet relaxation. *Applied Spectroscopy*. **2011**, 65 (4), 459-465.

In addition, I contributed to the following publications, which were very important in my overall training and development:

V.   Barajas, M.; Rodriguez, A.; Vargas, W.; Conde, C.; Ropero, J.; Figueroa, J.; Romañach R.Near-Infrared Spectroscopic Method for Real-Time Monitoringof Pharmaceutical Powders During Voiding.*Applied Spectroscopy*. **2007,** 65, 490-496.

VI.   Alcalà, M.; León, J.; Ropero, J.; Blanco, M.; Romañach, J. Analysis of low content drug tablets by transmission near infrared spectroscopy: Selection of calibration ranges according to multivariate detection and quantitation limits of PLS models. *Journal of Pharmaceutical Sciences*. **2008**, 97(12), 5318-5327.

List ofFigures

List of Tables

List of Abbreviations and symbols

AoR	Angle of repose
APIs	Active pharmaceutical ingredients
CDI	Control Development Inc.
FDA	Food and Drug Agency
InGaAs	Indium gallium arsenide
KT20	K-tron twin-screw gravimetric feeder
MCC	Microcrystalline cellulose
MLR	Multi-linear regression
NIR	Near-infrared
NIR-CI	Near-infrared chemical imaging
NIRS	Near-infrared spectroscopy
NJIT	New Jersey Institute of Technology
PARAFAC	Parallel Factor analysis
PAT	Process Analytical Technology
PbS	Lead sulfide
PC	Principal component
PCA	Principal component analysis
PCR	Principal component regression
PLS	Partial least squared
QC	Quality control
RMSE	Root Mean Square Error
RSD	Relative standard deviation
RSEP	Relative standard errors of prediction
SMCC	Silicified microcrystalline cellulose
SNV	Standard Normal Variation

Some basic notations that will be used throughout this work are resumed as follow:

n, i, j, k, x	Italics lowercase represent scalars
$E, K, X, Y,$	Italics uppercase represent vectors and functions
$\boldsymbol{X, Y, B, E, e, V}$	Bold italics Uppercase and lowercase represent vectors and Matrices
$\boldsymbol{I}$	Means the identity matrix.
$\boldsymbol{M+N}$	Mean sum of matrices
$\boldsymbol{MN}$ and $\boldsymbol{M^{.}N}$	Means multiplication of matrices
$\boldsymbol{M'}$	Means transpose of matrix $\boldsymbol{M}$

1. Introduction

1.1 Motivation

The physical properties of powders are very important to the pharmaceutical industry. For example, the flow properties of powders are of critical significance in operations such as blending, tablet compression, capsule filling, transportation, and in scale-up operations.[1] Pharmaceutical powders are described as heterogeneous systems with different physical and/or chemical compositions with a range of particle sizes that vary from a few micrometers to about a millimeter. Solid oral dosage forms constitute more than 80% of pharmaceutical production, with formulation which are powder mixtures.[2, 3, 4, 5]

Near-infrared spectroscopy (NIRS) is a fast and nondestructive technique that provides both chemical and physical information of pharmaceutical powders.[2] The use of NIRS to determine physical parameters is still under exploration.[1] For those reasons, it is necessary to develop near infrared spectroscopy to provide physical information for pharmaceutical processes; increasing the number of applications and understanding of the physical information in NIR spectra from pharmaceutical materials. The knowledge and subsequent control of the powders physical behavior is crucial in the development and processing of solid dosage forms.[1]

Regulatory requirements for pharmaceutical manufacturing consist of identification of the incoming raw materials, quality testing of in-process materials,[4] and the final analysis of physical, chemical and microbiological product properties due to quality control. The Food and Drug Agency (FDA) understands that the quality of the currently manufactured products is good, but obtained with a high cost and inefficient process.[4] In the eyes of the FDA changes are

necessary in the analysis of pharmaceutical processes, quality assurance, and manufacturing in general.

FDA has outlined a number of reasons for the needed transformation in pharmaceutical manufacturing. However, there are three reasons that should be highlighted. The first reason is "significant opportunities exist for improving pharmaceutical development, manufacturing, and quality assurance through innovation in product and process development, process analysis, and process control".[6] The second factor that FDA has emphasized is: "Efficient pharmaceutical manufacturing is a critical part of an effective U.S. health care system. The health of our citizens (and animals in their care) depends on the availability of safe, effective, and affordable medicines". Finally, the third reason is "respond to the challenges of new discoveries (e.g., novel drugs and nanotechnology) and ways of doing business (e.g., individualized therapy, genetically tailored treatment)".[6]

Many authors have discussed the two first *Process Analytical Technology* (PAT) motivations, and emphasized modernization of the current pharmaceutical industry, improving its quality and efficiency through the implementation of PAT.[2, 4, 7, 8] Few papers discuss that PAT is also the preparation for large changes in pharmaceutical manufacturing due to new scientific discoveries, and new necessities of the health care system.[7] For example, the successful application of nanotechnology opens new opportunities for drug discovery and construction of materials with new composition. The changing nature of technologies and methods used for chemical analysis is directly relevant to the pharmaceutical industry today. Some pharmaceutical applications of nanotechnology and advances in genomics, genetic testing and drug discovery; development of analytical biochips; molecular diagnostics; system to detect protein–protein

interactions,[9] will require changes in industrial pharmaceutical process and technology. It is necessary to increase the actual pharmaceutical process knowledge to adapt or create these future industrial processes. FDA encourages development and implementation of pharmaceutical manufacturing based on process knowledge. The Agency recommends real-time measurements of chemical, physical, mathematical and microbiological properties relevant to pharmaceutical manufactory processes. Novel analytical approaches are necessary to understand and measure the phenomena that take place during pharmaceutical manufacturing.

Near-infrared (NIR) spectroscopy is a fast and non-destructive method that has demonstrated its suitability for industrial and field deployment. Spectral absorptions in NIR are the result of overtone or combination bands in the region from 12800 to 4000 cm^{-1}. The overtones of fundamental stretching vibrations of C-H, O-H, and N-H bonds occur in the NIR spectral region.[10] The superposition of many different overtones and combination bands in the NIR region causes wide overlapping bands. In spite of the overlapping bands, NIR spectroscopy may be used to identify raw materials, perform in-line blend homogeneity, drug content in tablets, and quantitative analysis using on line tablet concentration,[11] and chemical concentration of pharmaceutical powder in flow process.[12] Because NIR spectroscopy does not require sample preparation, spectra are obtained in the solid or native state of the material. The spectra obtained include chemical information as evidenced by the absorption bands and features related to the scattering of the radiation that vary according to the physical properties of the material. Most of the NIR industrial applications use the chemical information in NIR spectra, and reduce the physical information of the samples; this reduction of physical information facilitates the observation of chemical variation. Other applications have involved the development of methods

for obtaining the physical information from NIR spectra for example: tablet compaction pressure, particle size and polymorphism determinations.[13] This study was dedicated to increasing the number of application and understanding of the physical information in NIR spectra from pharmaceutical materials, although some work in chemical applications was performed. This thesis describes the development of new NIR analytical methods that contribute to the PAT initiative and pharmaceutical manufacturing.

1.2 Research Objectives

1.2.1General Objectives

The research was aimed at understanding the physical information in NIR spectra of pharmaceutical materials, and establishing methods to monitor physical properties with in-line NIR methods.

1.2.2 Specific Objectives

One specific objective was developing a NIR method for in-line determination of powder flow properties. In this application NIR spectroscopy was used to measure and characterize the powder flow properties of powders voiding through a funnel. The physical information was employed to understand powder flow properties and control the voiding process of pharmaceutical materials.

NIR spectra provide chemical information by measuring changes in concentration during powder voiding. NIR spectroscopy also provides physical information by monitoring flow interruptions in powder flow process during powder voiding, providing the flow rate for pharmaceutical powder materials, and comparison of flow properties of different materials. For example, Davé and co-workers developed a nanoparticle dry coating particle to modify the flow of materials.[14] The powder flow properties of dry coated particles were measured using the NIR method, and compared to the non-coated material.

The second objective of this study was the real-time determination of tablet compaction pressure in pharmaceutical tablets. This study determined the compaction pressure in moving tablets with NIR spectra. In this study a multivariate model was developed to predict the

compaction pressure of tables. The study also includes methods to obtain the NIR information of moving pharmaceutical tablets, and deconvolute the obtained chemical and physical information. This information could be used to control an industrial tablet compaction machine. At the same time both physical and chemical information could be used to control the pharmaceutical process.

The study of tablet relaxation of pharmaceutical materials is the third objective in this study. After compaction process the pharmaceutical tablets may suffer relaxation, this process can affect dissolution characteristic or the coating process and affect product release. In order to achieve these goals this research included efforts to:

a.Determine changes in NIR spectra of tablets over the time

b.Provide a new application of NIR-CI to obtain an image of spectral slope that facilitates the study of tablet relaxation

The first approximation to follow tablet relaxation used linear least squares regression based on the measured applied compaction force of six lactose tablets and their average NIR-CI slope, determined as a mean value of all pixels on the top and bottom surfaces of those tablets.

The second method evaluated tablet relaxation from each pixel in a (NIR-CI) data hypercube and provided an image of the spectral slope which was used to follow spatial tablet relaxation.

1.3 Background (Literature Review)

Applications of NIR spectroscopy to pharmaceutical analysis (summary of chemical applications)

1.3.1 Powder characterization and analysis

Knowledge about flow properties of powders is very important when developing powder processes and handling procedures. Thalberg has emphasized that without knowledge of flow performance a number of problems can occur during a mixing, tableting, or capsulation.[15] In industrial processes the flow properties of powders can create production stoppages or poor quality product.[16] Benedetti developed an in process analytical technology (PAT) method based on near-infrared spectroscopy (NIR) for the in-line powder flow characterization of pharmaceutical formulations. Benedetti characterized the homogeneity of flowing powder mixtures during emptying of the hopper prior to the tableting or encapsulation steps. All NIR information was interpreted using chemometric algorithms. The results show that collection of real-time information of flowing cohesive powder mixtures is possible, and also the development of a PLS predictive model for quantification.[12]

Powder flow properties could change during processing and formulation work and affect pharmaceutical production. It is necessary to know the changes in flow properties during pharmaceutical production as materials are modified. Mehrotra described how the different shear rating and concentration of lubricants affects the blend properties: particle size and shape, bulk density, flow properties, and level of cohesion and tablet properties hardness, dissolution, friability, and weight variability, these variations are typical in pharmaceutical production.[17]

Various types of test devices have been developed for the characterization of the flow behavior of powders. For example, the direct Jenike shear cell, evaluates the angle of internal friction of highly consolidated granular materials. Essentially, Jenike shear cell measurements consist of compacting a powder sample with a known external load into a cylindrical cell composed of two metal rings one upon the other, then measure, the minimum steady state shear stress necessary to displace the upper ring horizontally with respect to the lower ring.[18] A second measure to characterize flow behavior is the flowability test. The flowability test is defined as the diameter of the smaller orifice through which a powder can flow. The test for flowability determines the ability of powders to flow under defined conditions, using funnels with different orifice diameters and angles.[18]

Another commonly used flow indicator is the time it takes for a powder to flow out of a funnel through a well defined orifice.[19] In addition, the commercially available AeroFlow (Automated Powder Flowability Analyzer -3250 Aero-Flow [TM]) equipment, characterizes the avalanching behavior of a powder rotated in a drum. A recent comprehensive review by Schwedes is focused on the shear tests but also mentions alternative ways to assess powder flow properties. All these techniques are off line, and need to take place in a laboratory.[20] The NIR applications to be studied in this project are ready for in-line process measurements in a non-destructive manner at the same moment when the industrial processes take place.

The NIR spectra of powder mixtures contain physical information. Barajas showed that NIR can detect differences in particle size of pharmaceutical powder in a voiding process. Barajas compared in-line NIR spectra with off line spectra and the results showed similar physical information. This study showed that the determination of particle size differences during voiding

was possible and the study found particle size segregation due to the air resistance to the movement of the pharmaceutical particles.[21]

In addition, NIR methods have been developed for real-time quantitative chemical determinations. A method for quantitative in-situ measurements of the chemical content of powder mixtures is presented by Berntsson et al. used NIR spectroscopy with a fiber-optic diffuse reflection probe inserted into the powder in the blender, and determined the powder mixture content during processing. In this work quantitative analytical information was obtained, the concentration of the drug in the powder mixture for each acquired NIR spectrum by means of a multivariate calibration model.[22]

1.3.1.2 Real time determination of tablet compaction pressure in moving tablets

Tablet hardness is an important quality control (QC) parameter that is usually measured during bulk tablet manufacturing. The role of hardness in disintegration and dissolution is well documented.[23] The current practice for its determination includes contact testing, either manual or automated. The major implications of the current method of hardness testing are delayed batch-release and labor-intensiveness, which may add expenditures to the manufacturing process.[24]

Kirsch, and Drennen evaluated tablet hardness in a non-destructive analysis using NIR spectroscopy. The variation on NIR spectra was only based on physical differences, and it is measured as a change in the slope of the spectrum. The slope approach offers advantages because the calculation of a spectral slope was out the influence of individual spectral absorbance.[25]

Blanco and Alcala showed the effect of physical parameters on NIR-PLS models when the physical differences between calibration samples and production samples are not taken into account. Calibration models were constructed from the spectra for laboratory samples at 300 Mega Pascal (MPa) of tablet compact pressure, close to production compact pressure but not the same. In a principal component analysis (PCA) to determine the production compaction pressure, the physical properties had a marked influence on the spectrum for a tablet, and constituted to the primary source of variability among samples. For a 3 factor partial least squared (PLS) model, with a calibration set that only contained laboratory samples of production, the relative standard errors of prediction (RSEP) over 10% was obtained. The PLS model that contained laboratory samples and production samples gave a production RSEP of 2.8%.[11]

Peinado et al used a Parallel Factor (PARAFAC) model to separate and model the sources of information, where the NIR spectra were obtained at different temperatures. The variation of temperature originates changes in the vibration modes of the molecules and affected the NIR spectra directly. The strategy of this method was the combination of chemical variation and physical variation in parallel form to obtain a more robust model.[26]

Skibsted et al explained why real time release of products is a paradigm shift for the pharmaceutical industry, and suggested the NIR as a useful tool to maintain the pharmaceutical production inside their limit of variation.[27] This variation can be tablet compact pressure, temperature, particle size, drying temperature, and others. Every change in physical properties affects NIR spectra, and contains information of pharmaceutical particles and the process; this advantage can be used to maintain pharmaceutical production in control.[27] Even though near infrared (NIR) spectra provides both physical and chemical information, most research efforts

have been directed to chemical applications where drug or moisture concentrations are determined.[13] Very few research efforts have been directed to obtaining physical information from NIR spectra.[28]

1.3.1.3 Tablet relaxation

Tablet relaxation is normally considered as a fine balance between stored elastic energy as driving force for expansion and particle bonding as counteracting force.[29] Zuurman et al measured tablet dimensions and pore proportions at least 16 h after compaction with an electronic micrometer. Zuurman showed that for microcrystalline cellulose porosity under pressure was equal for unlubricated tablets and for tablets containing 0.5% magnesium stearate. However, the lubricated tablets show a much larger relaxation in the time, than the tablets without magnesium stearate. The author suggests that the difference can be ascribed to the reduction of interparticle bonding by the lubricant, because a strong interparticle bonding counteracts tablet relaxation. The measurement of this relaxation was made using mercury intrusion porosimetry.[30]

B. van Veen et al analyzed the effect of coprocessing colloidal silicon dioxide with microcrystalline cellulose (MCC) on different compaction parameters in tablet relaxation of MCC, silicified microcrystalline cellulose (SMCC) and tablet strength. Alterations in tablet strength of MCC and SMCC by addition of magnesium stearate are compared with those of physical mixtures containing colloidal silicon dioxide and MCC. The results show small negative effect of colloidal silicon dioxide on the interparticle bonding strength of unlubricated MCC. However, for lubricated MCC a larger increase in tablet relaxation at a high compression speed was found than for lubricated SMCC tablets.[31]

1.3.2 NIR Spectroscopy

NIR spectroscopy is a fast and non-destructive analytical method that provides physicochemical information of virtually any organic matrix.[2] NIR spectroscopy covers the wavelength range from 780 to 2500 nm, or 12800 to 4000 cm^{-1} to the mid infrared and extends up to the red in visible region. Historically, the discovery of the NIR region in 1800 is ascribed to Herschel, in his "Experiments on the Refrangibility of the Invisible Rays of the Sun," presented to the Royal Society in 1800,[32] Hershel separated the electromagnetic spectrum with a prism and observed that the temperature increased markedly towards and beyond the red, in the region that is now called the near-infrared.[33] Two years later in 1882 Abney and Festing using pictures of the NIR absorption spectra showing correlations between absorption bands and the presence of some functional groups.[34] The first modern NIR investigations were done by Coblentz in 1905, Coblentz recorded the spectra of 19 compounds between 800 and 2800 nm using a spectrometer equipped with a quartz prism and a radiometer, the motion of the radiometer was used to measure the intensity of NIR bands.[34]

NIR spectroscopy was ignored as an analytical technique for nearly 150 years following it discovery until 1962, when Hart, Norris and Golumbic used NIR spectroscopy for the quantitative determination of seed moisture using methanol extraction. This work was followed by transmission measurements of moisture in intact seeds with carbon tetrachloride.[35]

Karl Norris from the U.S. Department of Agriculture who recognized the potential of NIR method applied to food industry.[2] Over the past 20 years, the development of NIR analytical methods has been strong; NIR applications have increased together with computer and chemometric progress. Chemical industries have also applied NIR methods as an industrial

quality- and process-control tool, coinciding with the introduction of efficient chemometrics data processing techniques.[2] Petrochemical, pulp and paper, and pharmaceutical industry have taken advantage of the characteristics of NIR spectroscopy.[28]

1.3.2.1 Basic principles Origin and characteristics of NIR absorption bands

Infrared (IR) Spectroscopy is based on the interaction between electromagnetic radiation and electromagnetic field in the molecules. The IR region is divided as near-infrared from 0.7-2.5 μm (12800-4000 cm^{-1}), mid infrared from 2.5-50μm (4000-200 cm^{-1}) and far infrared from 50-1000μm (200-10 cm^{-1}). The far infrared (FIR) is due to molecular rotations, while the mid-infrared (MIR) comes from the fundamental molecular vibrations. The near infrared (NIR) region is the result of overtones and combination bands. The molecule, absorbing infrared radiation, changes in its dipole moment and its state vibrational or rotational energy. Vibrational energy refers to the oscillations of atoms through their bonds in a molecule; much like two balls could oscillate if they were connected by a spring.[35]

The length of the vibration movement of atoms in molecules is on the order of 10^{-9}–10^{-10} cm. The movement of the atoms in a molecule is confined by a potential energy well, formed between the binding potential of the bonding electrons, and the repulsive force between the atomic cores.[36] A particle undergoes harmonic motion if it experiences a restoring force proportional to its displacement;[37] the potential energy of the bond defined by a simple harmonic oscillator is given by the expression:

$$E = \frac{1}{2}kX^2 \qquad\qquad (1.1)$$

Where k is the bond force constant and X the distance between atoms. The equations of classical mechanics do not completely describe the vibrational behavior of molecules. The mechanical models do not reflect the dual nature of molecular bonds, and the quantized molecular vibrational energy.

To describe the properties of molecular bond systems according to quantum mechanics the appropriate Schrödinger equation must be solved. For two atoms m_1 and m_2, confined within a simple harmonic potential well the Schrödinger equation is (1.2).

$$-\left(\frac{\hbar^2}{2\mu}\right)\frac{d^2\psi}{dX^2} + \frac{1}{2}KX^2\psi(X) = E\psi(X) \qquad (1.2)$$

Where $\hbar = \frac{h}{2\pi}$, μ is the reduced mass, $\mu = \frac{m_1 m_2}{m_1 + m_2}$, X is the displacement respect the minimum of the curve. The potential energy $\frac{1}{2}KX^2$, rises to infinite values at sufficiently large displacement. Solving the quantum mechanical wave function for a simple harmonic oscillator, the discrete amount of energies for vibration can be calculated by equation (1.3)

$$E_n = \left(n + \frac{1}{2}\right)\hbar\omega, \omega = \left(\frac{K}{\mu}\right)^{\frac{1}{2}} \qquad (1.3)$$

Where $n = 0, 1, 2, 3, ...$the first important observation from this solution is that the gap between adjacent energy levels is the same $\Delta E = E_{n+1} - E_n = \hbar\omega.$ The interaction between the electromagnetic radiation and the chemical bond is quantized. Only a set of discrete energy levels is allowed, with equal intervals of energy between the energy levels as shown in Figure1.1.[36]
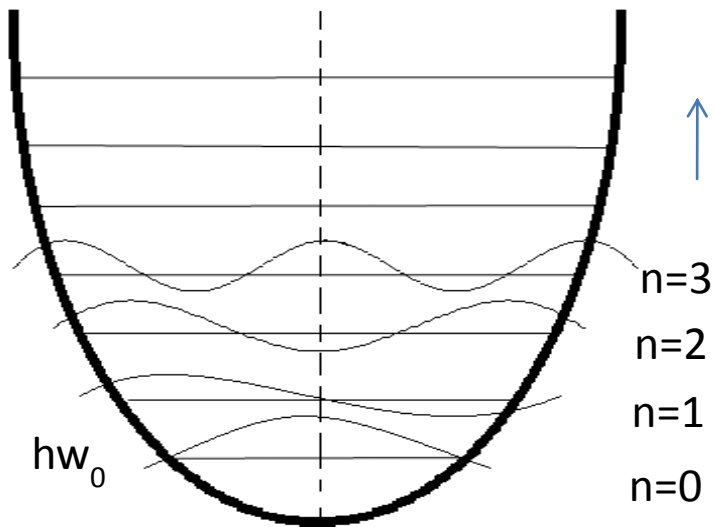
Figure 1.1 Potential energy in the harmonic oscillator model.[(adapted from ref. 36)]

The simple harmonic oscillators explain quite well the mid-IR absorption bands due to the fundamental modes of molecular vibration$\Delta n = \pm 1$. Thus in the case of the simple harmonic model described above, NIR spectroscopy would not exist.

1.3.2.2 Anharmonicity of the potential well

Real molecules are not perfect harmonic oscillators as evidenced by near infrared spectra. In the cases of harmonic oscillator, the potential energy rises equally with displacement in both positive and negative directions from the equilibrium position. This is only an approximation because the forces responsible for the potential energy are different in the two directions.[36] When two atoms come near, coulombic repulsion increases between the core and against the motion, which implies a rapid increase in its potential energy well. On the other direction when two

atoms are moving away, the interatomic distance is close to breaking the bond distance, with a decrease in potential energy.

The molecular vibration then becomes anharmonic, because the restoring force is no longer proportional to the displacement.[37] The Morse potential energy is a very realistic approximation to the potential energy well in real molecular bonds (1.4). Real molecules are closer to anharmonic behavior. Both the harmonic and anharmonic models are similar at low energy levels. One approach to the calculation of the energy levels in the presence of anharmonicity is to use a function that resembles the true potential energy more closely.

The expression for potential energy within the well becomes:

$$V(r) = hcD_e\left[1 - e^{-a(r-r_e)}\right]^2 \qquad (1.4)$$

Where D_e is the depth of the potential minimum, and $a = \left(\frac{\mu\omega^2}{2hcD_e}\right)^{1/2}$. When the function $V(r)$ is used in the vibrational Hamiltonian of the simple harmonic, the quantized vibrational energy levels are:

$$E_n = \left(n + \frac{1}{2}\right)\hbar\omega - \left(n + \frac{1}{2}\right)^2 X_e \hbar\omega \qquad (1.5)$$

The new parameter X_e is called the anharmonicity constant $X_e = \frac{a^2\hbar}{2\mu\omega}$. There are two effects of the anharmonicity of the quantized energy levels described above, which have significance for NIR spectroscopy. The first effect is observed in the difference between adjacent energy levels which are no longer constant. The energy levels become closer as n increases. Secondly, the

rigorous selection rule that $\Delta n = 1$ is relaxed, so that weak absorptions can occur with $\Delta n = 2$ (first overtone band), or $\Delta n = 3$ (second overtone band).[36]

In addition to the overtones, the NIR region also includes other absorption bands, called combination bands, due to the interaction between different vibration fundamental frequency polyatomic molecules. Combination bands appearing between 1900 nm and 2500 nm are the result of vibrational interactions, i.e. their frequencies are the sums of multiples of each interacting frequency.[2]

$$v_{comb} = b_1 v_1 + b_2 v_2 + b_3 v_3 \qquad (1.6)$$

Where b_i are integers and v_i, the frequencies of transitions that contribute to the combination bands. The most frequent combination bands are those in which $b_1 = b_2 = b_3 = 1$.

1.3.2.3 Instrumentation and sample presentation

The fundamental design of a NIR spectrophotometer consists of: emission source (lamp), a mechanism for wavelength selection, sample compartment allowing for transmittance or reflectance measurements and detector system.[2] Figure1.2 shows the scheme of basic NIR spectrometer.

The light source is typically a tungsten lamp, since it is small and rugged.[38] The source of radiation is capable of providing a continuous spectrum the region of 320-2500 nm. Tungsten halogen lamps require selection system for wavelengths.[36] The detectors commonly used in NIR spectroscopy are constructed semiconductors such as indium gallium arsenide (InGaAs), lead sulfide (PbS) and Silicon detectors.[2] Silicon detectors are fast, low noise, small and highly sensitive from the visible region to 1100 nm.[2] The most expensive InGaAs detector combines the

speed and size characteristics of the silicon detector with the wavelength range of the PbS detector. Measurements in solids using InGaAs detectors, operating from 850 to 1750 nm and extended-InGaAs operate from 1100-2200nm.[38]

Diffuse Reflectance
Detector

Light
Source

Monochromator

Sample

Transmittance
Detector
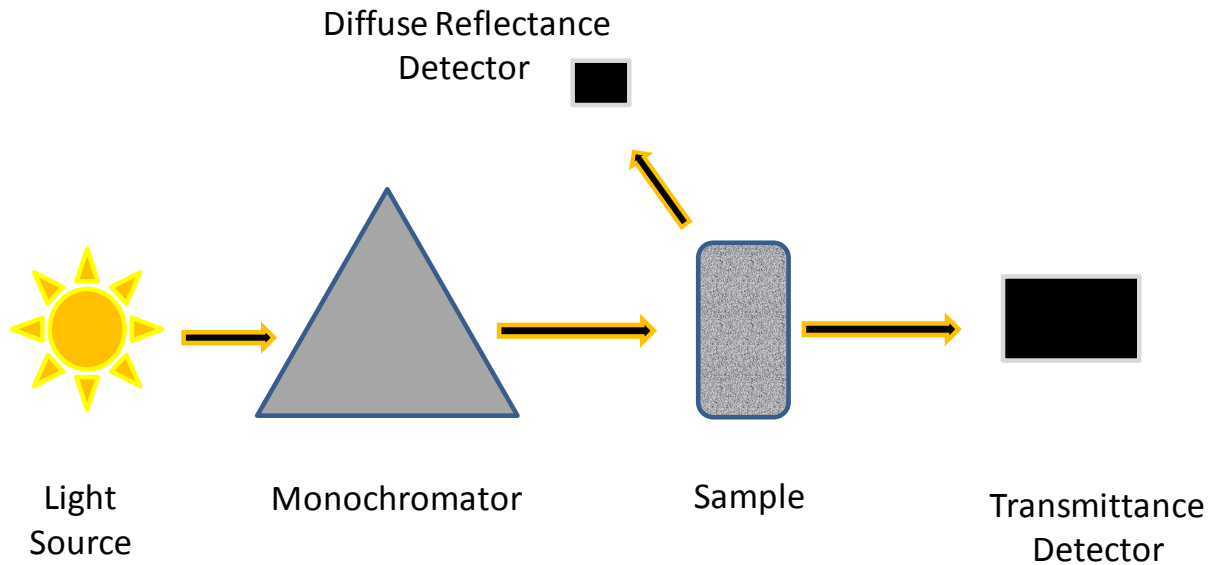
Figure 1.2 Configuration of a basic NIR spectrometer.[adapted from ref. 2]

1.3.2.4 Sample presentation

The appropriate NIR measuring mode depends on the optical properties of the samples (Figure 1.3) Transparent materials are typically measured in transmittance (Figure1.3 a). Turbid liquids or semi-solids and solids samples could be measured in diffuse transmittance (Figure 1.3 b), and diffuse reflectance (Figure1.3 c).[2]
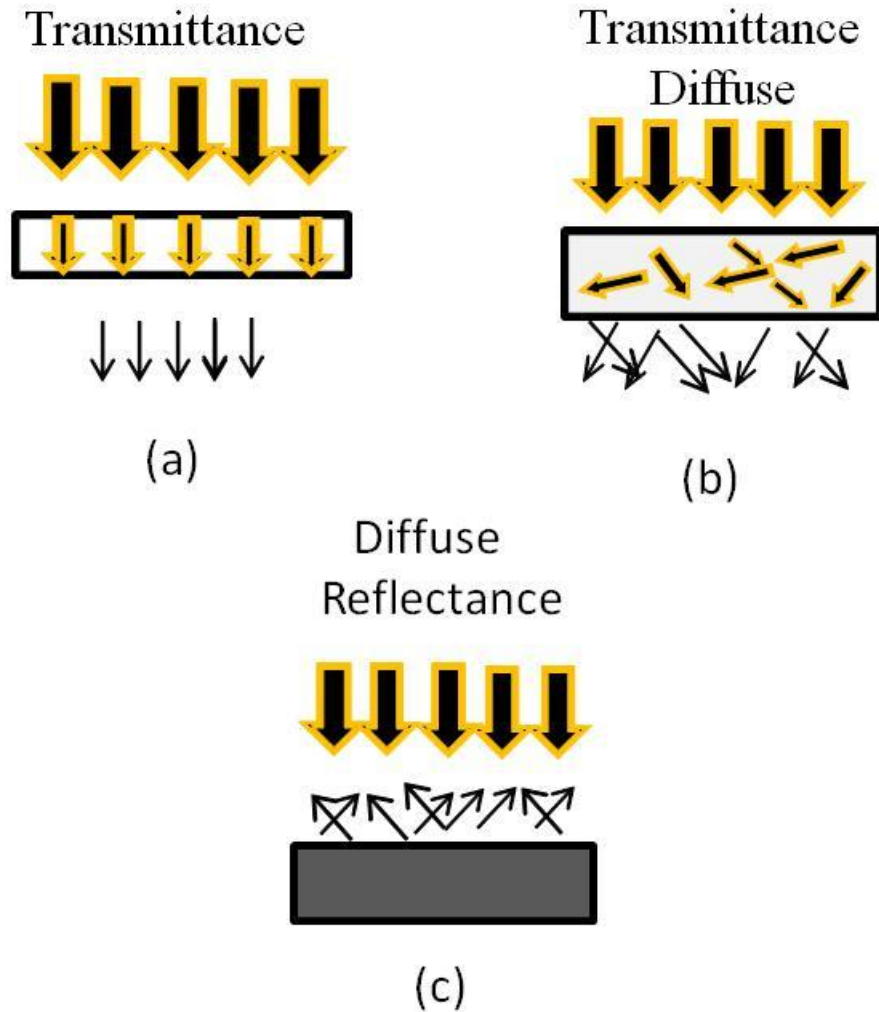
Figure 1.3 NIR measuring modes (a, b) transmittance, (c) diffuse reflectance.[(adapted from ref. 2)]

1.3.2.5 Transmission measurements

The absorption of radiation follows the law of Lambert-Beer in a non-scattering medium. The transmittance solution is the fraction of incident radiation transmitted by the solution.[36] The transmittance and absorbance measurements are related to the following expression:

$$A = log\frac{1}{T} = Log\frac{P_0}{P} = abc \qquad\qquad (1.7)$$

Where A is the absorbance of the sample, transmittance T, P_0 intensity incident radiation, P the intensity of radiation transmitted, a the molar absorptivity, b the optical path and c the concentration.[36] Divergences from this law can be to the result of reflection and/or scattering of radiation, very high concentrations, chemical interactions of the sample, etc.

1.3.2.6 Reflectance measurements

The reflection of radiation can be specular or diffuse. Specular reflectance described by Fresnel's law does not provide information on the composition of sample.[35] Diffuse reflectance occurs in all directions as a result of absorption and scattering processes. Diffuse reflectance dominates when the material is weakly absorbing at the incident wavelength and when the penetration of radiation is large relative to the length of wave. The frequently used expression is an empirical application of the relationship between concentration and reflectance relative similar to the Beer- Lambert law (although this law only applies to non-scattering samples):

$$A = -logR = log\frac{1}{R} = Log\frac{R_{Reference}}{R_{Sample}} \qquad\qquad (1.8)$$

where A is the apparent absorbance, and R the reflectance, $R = \frac{R_{Sample}}{R_{Reference}}$.

Figure 1.4 representing the apparent absorbance (A) in function of the sample reflectance R_{Sample} according to the equation (1.8), assuming $R_{Reference} = 1$. The combination of light scattering and absorbance of radiation determines the amount of radiation that returns to the NIR detector (R_{Sample}). The relationship between absorption and particle size can be described by the difference in absorption of copper sulfate pentahydrate at various particle size ranges (Figure

1.5). Particle size determines the effective pathlength, As the particle size increased the absorption due to the copper sulfate pentahydrate increased and increased the intensity of blue. The crystals appeared dark as a result of the relatively large interaction between the copper sulfate pentahydrate and the radiation. For smaller particles (<75um), the absorbance of the material is less and the material shows less color because the scattering of radiation. The scattering of radiation is inversely proportional to the mean pathlength and is the result of the reflection and the refraction of radiation.[25, 35]

A reduction of particle size increases the amount of radiation that returns to the detector. In the same way the decrease in pressure of tablets compaction increases porosity of the material and increases the amount of radiation which returns to the detector.[35] These reflectance characteristics of NIR spectroscopy allows to monitor the particle size and the compaction pressure of pharmaceutical particles.[35]
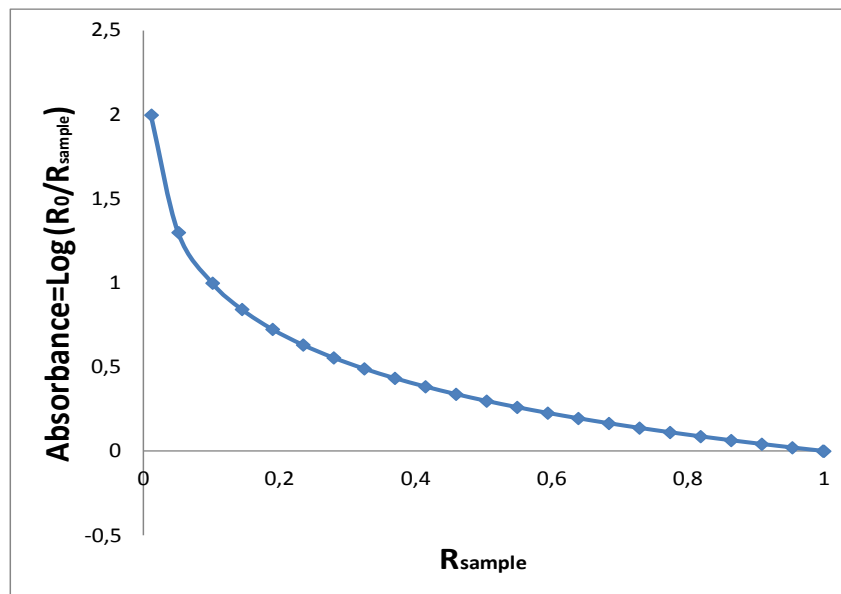
Figure 1.4 Apparent absorbance (A) in function of the sample reflectance (R_{sample}) assuming R_0=1.
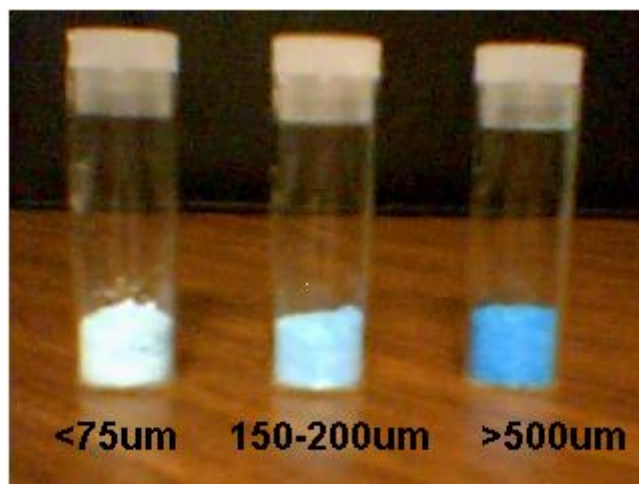
Figure 1.5 Absorption of copper sulfate pentahydrate at various particle size ranges

1.3.2.7 Light interaction with solid particles

The reflection and scattering properties of a particle are dependent on the relation between the wavelength of the radiation and the dimensions and orientation of the particle.[39] Assuming that all particles are large compared with the wavelength of incident radiation; the reflection from a surface may be calculated by the application of geometrical optics.[40] Two important factors in these phenomena are the refractive index and the absorption coefficient of the material that compose the particle. The refractive index, n, is given as the ratio of the velocity of light in a vacuum, c, to that in the sample, n, so $n = \frac{c}{v}$. An optical interface is the boundary between two media having different indices of refraction.[41] When a radiant beam finds an interface, the beam is divided into two parts, the transmitted ray, T, and the reflected ray, R. as shown in figure 1.6. The direction of the transmitted ray is defined by Snell's Law as:

$$(\sin \theta_i)n_i = (\sin \theta_r)n_r \qquad (1.9)$$

In the interaction of solid particles with a beam of visible or NIR radiation, the beam is divided in different interactions. Some rays experiment specular reflectance, diffuse reflectance, diffuse transmittance, and absorbance, transmittance or transflectance Figure 1.6. Specular reflectance and transflectance takes place at particle interfaces and depend of physical properties of surface. The diffuse reflectance, diffused transmittance, absorbance, transmittance and transflectance are functions of shapes, thickness, and its refractive index relative to its surroundings.[37] NIR diffuse reflectance is an interface phenomenon, which contains chemical and physical information of particles.

NIR absorption bands are broad, overlapping and 10–100 times weaker than their corresponding fundamental mid-infrared absorption bands. This aspect is actually an analytical advantage, since it allows direct analysis of strongly absorbing and even highly scattering samples, such as turbid liquids or solids in either transmittance or reflectance mode without sample pretreatments. In the other hand due to the broad and overlapping of NIR signals, mathematical and statistical tools (chemometrics) are needed to process recorded NIR spectra. Chemometrics is the tool to extract the relevant information for qualitative or quantitative analysis using NIR spetroscopy.[2]
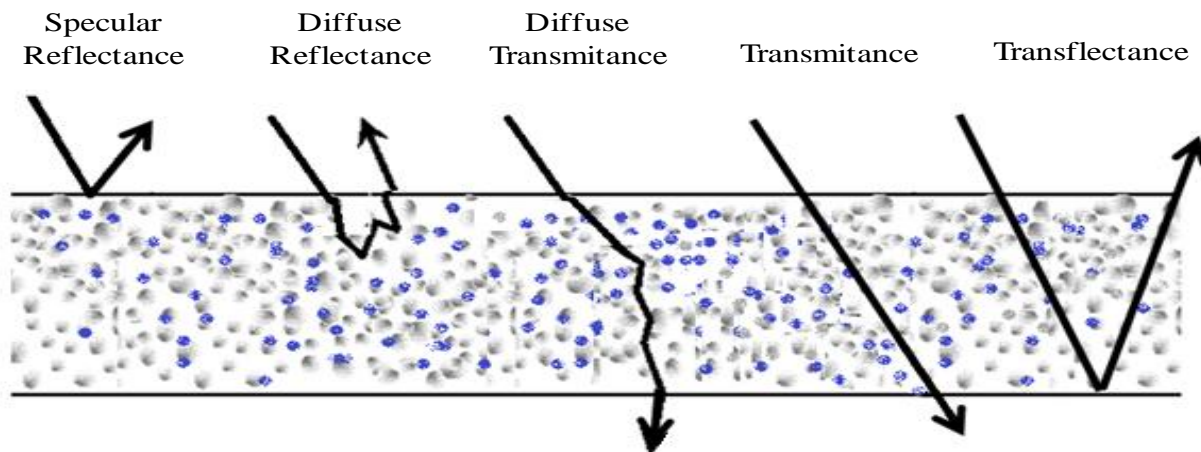
Figure 1.6 Reflection, transmission, transmittance and diffuse reflectance for a ray of optical radiation incident on a plane interface.

1.3.3 Chemometrics

NIR spectroscopy has also some drawbacks, such as the complexity of the spectra due to their overtones and combination bands of NIR spectra. At the same time it is difficult to obtain relevant chemical or physical information using univariate measurements.[13] The bands observed at the NIR region are overtone and combination bands, and the selectivity of NIR is relatively poor in comparison with, e.g., mid-IR region.[41] The spectra at the NIR region contain chemical and physical information of the sample, at the same time are broad and overlapping. Therefore, the spectral analysis requires application of chemometrics tools, which involve experienced analyst and specific sofware.[41]

The continuous advance in the analytic instrumentation has allowed obtaining larger volumes of data from every sample group. Chemical measurements are essentially multivariate data. The conversion of multivariate data into useful information requires the use of mathematical, statistical tools and formal logic tools that have grouped in the discipline

denominated Chemometrics.[42] This means that more than one measurement can be made on a sample at the same time. An example of this is NIR spectroscopy where, one spectrum contains hundreds of wavelengths on a single sample. Chemometrics represent the NIR spectra as a matrix of data, where the 'X' matrix represents NIR spectral intensities at different wavelengths (Figure 1.7).

The three main chemometric techniques are grouped on: data pretreatment (Mathematical pretreatments), Classification methods, and regression methods.[42] Data pretreatment is a tool that decreases spectral variation, such as light scattering, path length variations and random noise, resulting from variable physical sample properties or instrumental effects.[2] Classification methods are tools that group samples together according to their spectra and samples properties. Regression methods relate spectra to quantifiable properties of the samples.[42]

1.3.3.1 Data pretreatment applied to NIR spectra

The NIR spectral data can be mathematically transformed to highlight the differences and similarities between spectra. Pretreatment could improve the robustness of a multivariate model.[2] The most commonly used methods are briefly discussed with respect to the effect they are able to correct. Some pretreatments used in this work were mean centering, normalization, baseline correction, Standard Normal Variation (SNV) and derivatives.

$$j \text{ Wavelength (nm)}$$

$$X_{ij} = \quad i \text{ Samples}$$

$$
\begin{array}{cccccccc}
x_{11} & x_{12} & x_{13} & x_{14} & \cdots & x_{1j} & \cdots & x_{1m} \\
x_{21} & x_{22} & x_{23} & x_{24} & \cdots & x_{2j} & \cdots & x_{2m} \\
x_{31} & x_{32} & x_{33} & x_{34} & \cdots & x_{2j} & \cdots & x_{3m} \\
 & & \cdot & & \cdot & & \cdot & \\
 & & \cdot & & \cdot & & \cdot & \\
 & & \cdot & & \cdot & & \cdot & \\
x_{k1} & x_{k2} & x_{k3} & x_{k4} & \cdots & x_{kj} & \cdots & x_{km}
\end{array}
$$
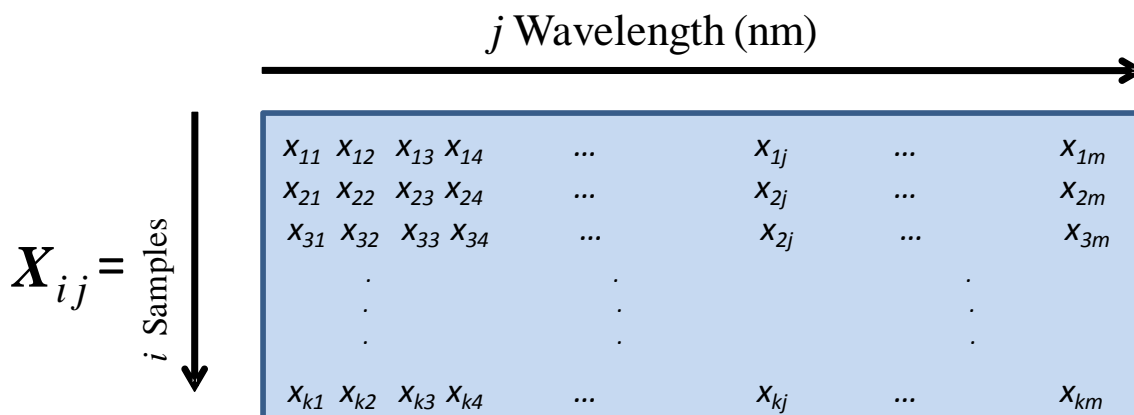
Figure 1.7 Graphical representation of a matrix X with spectral data. Where i and j are the number of rows and columns respectively.

1.3.3.2 Mean centering

Mean centering consists of subtracting the mean of each column, equation (1.10). Where x_{ij} is the original data, $mc\ x_{ij}$ is the mean-centered data, and $\bar{x}_j$ is a vector that contains the mean response values for every of the j-variables.[43]

$$mcx_{ij} = x_{ij} - \bar{x}_j \tag{1.10}$$

1.3.3.3 Baseline correction

Baseline pretreatment is used to correct the baselines of the samples as shown in equation (1.11), where x is a variable and X denotes all selected variables for this sample. For each sample, the value of the lowest point in the spectrum is subtracted from all the variables. The result of that the minimum value is set as 0 and the rest are positive values.[23]

$$f(x) = x - \min(X) \tag{1.11}$$

26

Polynomials grade 1, 2 or superiors can be used, to adapt the correction to the characteristics of the variation of the line it bases. When polynomials of grade 1 or 2 are used, this correction is called detrending.[44] Figure 1.8 shows the base line correction using polynomial function.
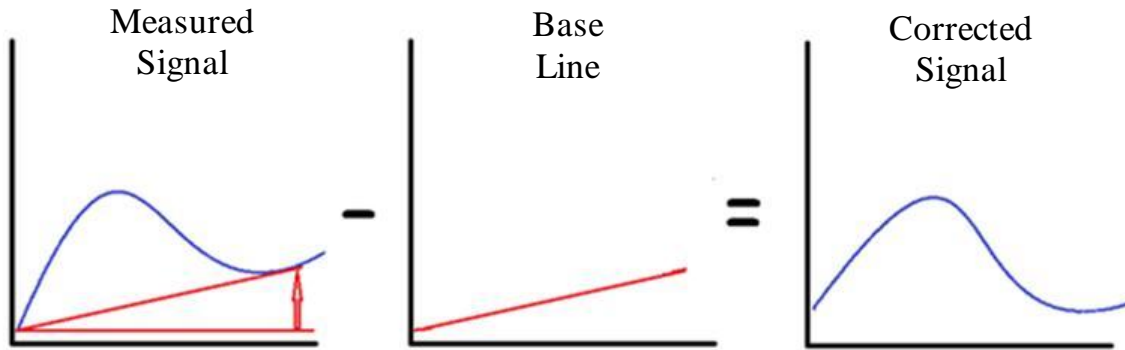
Figure 1.8 Base line correction using a linear explicit model.

1.3.3.4 Standard Normal Variation (SNV)

This pretreatment is a row-oriented transformation which centers and scales the acquired spectra. Each value in a row of data is transformed according to the equation (1.12)

$$\text{SNV}x_{ij} = \frac{(x_{ij}-\bar{x}_j)}{\sqrt{\sum_{i=1}^{I}\frac{\left(x_{ij}-\bar{x}_j\right)^2}{I}}} \tag{1.12}$$

1.3.3.5 Derivatives

Derivative pretreatment removes the signal which is the same between the two variables and leaves only the part of the signal which is different. Derivative pretreatment resolve overlapped picks and it eliminates linear and quadratic displacements of the line it bases.[45] The first

27

derivative is obtained as the difference between two absorbance values at two consecutive wavelengths or wavenumbers, equation (1.13).

$$dx = \frac{x_{j+1} - x_j}{\lambda_{j+1} - \lambda_j}$$ (1.13)

The simplest form of a derivative is a point-difference first derivative, in which each variable in a sample is subtracted from its immediate neighboring variable.[44] A second derivative would be calculated by repeating the process. In this study derivatives were calculated using the Savitzky-Golay algorithm. The derivative algorithm essentially fits individual polynomials to windows around each point in the spectrum. The algorithm requires selection of size of the window and order of the polynomial.

1.3.3.6 Classification methods

1.3.3.7 Principal component analysis (PCA)

PCA is a technique of variable reduction that facilitates visualization of the similarities or differences between a group of samples in a space of multiple dimensions.[2] PCA is a data compression method that reduces a set of data collected on j-variables over i samples to a simpler representation that uses a much lower number of compressed variables, called principal components (**PCs**). The number of **PCs** is much less than the initials variables j. PCA method is described in equation (1.14).

$$X = TP' + E$$ (1.14)

Where **T** is a i-by-c matrix containing the scores of the c **PCs**, and **P** is a j-by-c matrix that contains the loadings of the **PCs**. **E** is the i-by-j matrix that contains the variation not encompassed by the PCA model. The scores are the intensities of each of the new 'compressed'

variables for all of the i samples (Figure 1.9 a). The loadings are the 'definitions' of the c new variables in terms of the j-original variables.[36] The new PCs variables correspond to the largest eigenvalues of the covariance matrix calculated for X. The first PC is a vector that represents maximum variance amongst all linear combinations and each successive variable accounts for as much of the remaining variability as possible.[44] The loadings of PCA correspond to the eigenvectors of the covariance matrix and the PCs scores correspond at the multiplication of PC loadings by the mean centered X variables.

The steps to develop a principal component analysis consist of the following list:

- Create an X data matrix, apply mean center to the data (X_{mc})

- Calculate the covariance of X_{mc} data

- Calculate the eigenvalues and eigenvectors of the covariance matrix. Eigenvectors correspond to the PCs loadings in the principal component analysis.

- Calculate principal component scores (T), using the equation $T=X_{mc*}P'$.

1.3.3.8 Outliers

An "outlier" is the term given to an observation that does not fit a pattern.[36] In an analytical problem in process analytical chemistry, several different types of outliers can be encountered. X samples that have an extreme spectral profile. Samples that have an extreme Y value of the property of interest are outliers. Different outlier types are predictor variables that behave quite differently than the rest of the predictor variables. Outlier does not imply that a measurement or calculation is incorrect. An outlier could be caused by an error or an incorrect analytical action, but it could be caused by a real phenomenon relevant to the problem.

a)

m wavelengths

P_a loading

X $=$ T P'

n objects

T_a scores

$$X = T \cdot P'$$

b)

MLR $\rightarrow$ PCR

Independent *variable*

scores

Coefficients (Solution)

Residuals (noise)

Y $=$ T_a B $+$ E
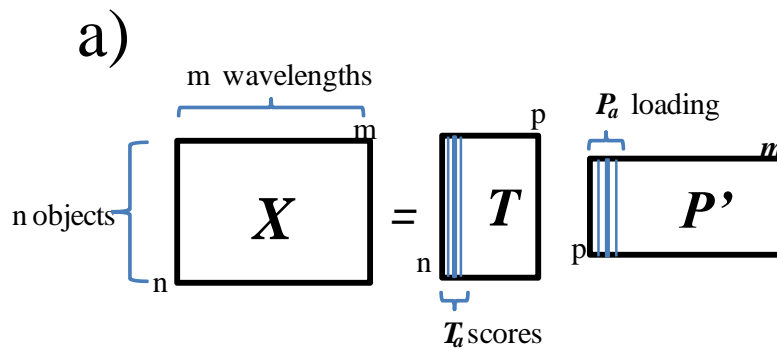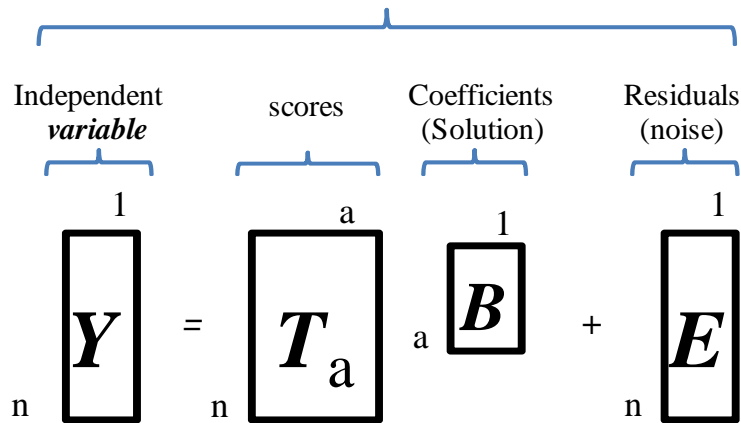
Figure 1.9 a) Graphical representation of matrices involved in principal component decomposition PCA b) Graphical representation of matrices related with principal component regression

Outliers demand attention in chemometrics for several different reasons. In calibration data, they will add error to the calibration model. Even if they represent informative data, it might be determined that this specific information does not need to be included in the model. PCA representation of samples and spectral data is a good opportunity to find outliers in the data.

1.3.3.9 Parallel Factor Analysis (PARAFAC)

PARAFAC is a decomposition method that can be considered as a generalization of the bilinear Principal Component Analysis (PCA) for two and higher multi-way arrays.[46] The principle behind the PARAFAC decomposition is to minimize the sum of squares of the residuals e_{ijk} as indicated in equation (1.15), where x_{ijk} is a data matrix for i samples, with variables j and k. The rank of the PARAFAC model is given by the number of factor or components, F, needed to describe the variation in the data array X_{ijk}. Each component, F, consists of one score or loading vector in the first mode, a_{if}, and two loading vectors, b_{jk}, and c_{kf}, for, respectively, loading vectors in the second and third mode.[46]

$$X_{ijk} = \sum_{f=1}^{F} a_{if} b_{if} c_{if} + e_{ijk} \qquad (1.15)$$

1.3.3.10 Regression methods

1.3.3.11 Multi-linear regression (MLR)

MLR allows to modeling the relationship between a group of X_j spectral data and an Y_j response by fitting a linear equation. The prediction Y_j property can be described with the equation (1.16)

$$Y_j = b_0 + \sum_{k=1}^{i} b_k X_k + e_{k\,l} \qquad (1.16)$$

1.3.3.12 Principal component regression (PCR)

Principal component regression is an extension of the PCA analysis. The principal component regression (PCR) is divided into two steps. First the spectral data are treated with a PCA. Then a multi-linear regression (MLR) is performed on the scores as predictive variables.[42]

MLR allows establishing a link between a reduced number of scores $\boldsymbol{T}$ and $\boldsymbol{Y}$ property of the samples (i.e. concentration). The prediction $\boldsymbol{Y}_j$ property can be described with the equation (1.17)

$$\boldsymbol{Y}_l = b_0 + \sum_{k=1}^{i} b_k \boldsymbol{T}_k + \boldsymbol{e}_{k\,l} \qquad (1.17)$$

Where $\boldsymbol{b}_k$ is the computed coefficient, $\boldsymbol{T}_k$ the $\boldsymbol{PCs}$ scored at each selected $\boldsymbol{PC}$ component and $\boldsymbol{e}_{k\,l}$ is the error. Each score is studied one after the other and correlated with the $\boldsymbol{Y}_l$ studied property. The selection is based on the predictive ability of the score. The prediction equation is written $\boldsymbol{Y}_{samples} = \boldsymbol{T}_{samples}*\boldsymbol{b}$ with $\boldsymbol{T}_{samples}$ are the scored of samples, $\boldsymbol{Y}_{samples}$ the reference values and b is the coefficient vector. The calculation of $\boldsymbol{T}_{samples}$ used the relation (1.18)

$$\boldsymbol{T}_{samples} = \boldsymbol{X}_{Samples}\boldsymbol{P}' \qquad (1.18)$$

Where $\boldsymbol{X}_{samples}$ are the spectra of the samples, and $\boldsymbol{P}'$ the loadings of the PCA analysis (Figure 1.9 b).[42]

1.3.3.13 Partial least squares regression (PLS)

PLS is a multivariate regression method that computed with least squares algorithms to establish a linear link between two matrices $\boldsymbol{X}$ and $\boldsymbol{Y}$. The PLS method involves modeling of the spectral data $\boldsymbol{X}$ and the reference values $\boldsymbol{Y}$ to find out the variables in $\boldsymbol{X}$ matrix that will best describe the $\boldsymbol{Y}$ matrix. PLS method is described in equations (1.19), (1.20) and (1.21)

$$\boldsymbol{X} = \boldsymbol{T}_{PLS}\boldsymbol{P}'_{PLS} + \boldsymbol{E} \qquad (1.19)$$

$$\boldsymbol{Y} = \boldsymbol{T}_{PLS}\boldsymbol{C} + \boldsymbol{F} \qquad (1.20)$$

$$\boldsymbol{Y} = \boldsymbol{T}_{PLS}\boldsymbol{U} + \boldsymbol{G} \qquad (1.21)$$

Where T_{PLS} are the scores predictors of Y and also model X, P are the loading that explain the variation of X matrix, and C the loading of Y. E and F represent the residuals in the X and Y modeling respectively. The PLS-regression used the coefficients matrix B to predict Y variables in function of new X spectral data.

$$Y_{pred} = X_{spectra} * B \qquad (1.22)$$

$$B = W * C \qquad (1.23)$$

$$T = X * W \qquad (1.24)$$

Where B is the regression coefficient, for prediction of Y from X. W are coefficients or weights to the scores calculation. The NIPALS is the most common PLS algorithm used for calculation, for a detailed calculation see their calculation.[47] The difference between PLS and PCR is the manner in which the T scores are calculated. T scores in PCR method, are estimated exclusively on the basis of explained variance in X followed by subsequent regression (a simple 'two-step' process), on PLS data compression is done such that the most variance in both X and Y is explained.

1.3.3.14 Evaluation of prediction models

During the development of calibration models, the number of factors that the model requires must be determined. With a greater number of factors, the percentage of information included in the model is larger and errors decrease calibration, however the model complexity increases.[11] The model should be the simplest model with better predictive ability.[35] One of the criteria set for the factor selection is the choice of the number of factors provided the lowest

prediction error. The Root Mean Square Error (*RMSE*) was used to evaluate the calibration errors

and prediction models, the equation (1.25) indicate their calculation.

$$RMSE = \sqrt{\left(\frac{\sum_{i=1}^{n}(Y^{Predicted} - Y^{acepted})^2}{n}\right)}$$ (1.25)

Where n are the number of samples, $Y^{predicted}$ and $Y^{accepted}$ are the value of Y properties predicted

and accepted respectively.[1]

1.4 Main achievements

Main achievements of this research (and related publications) are summarized as follows:

1.4.1 Chapter 2 - Near-infrared Spectroscopy for the In-line Characterization of Powder Voiding: Development of the Methodology and Quantification of Enhanced Flow Properties of Surface Modified Active Pharmaceutical Ingredients

This study reports a novel use of NIR spectroscopy, as an in-line characterization method of

powder flow behavior. The spectra of flowing powders were used to measure the flow,

continuity, and interruption of powder flow and evaluate the chemical homogeneity of

pharmaceutical powders. The main purpose of this work is to demonstrate that NIR may be used

in-line to detect the flow uniformity, which in general depends on the flowability of the powder.

Two similar dynamic indices of powder flow were developed using the noise or the change

in baseline of NIR spectra. The method is based on the observation of large changes in baseline

and increases in noise for powders that flow poorly. The method described may be used to understand the flow behavior of powders but may also be used with already implemented NIR applications such as blend uniformity. The same NIR spectra that provide blend uniformity information may also be used to understand the flow behavior of powders. Thus, NIR spectra from a blend uniformity application or any application involving flowing powders will yield information on the flow properties of the powders.

1.4.2 Chapter 3 - In-Line Quantification of Enhanced Flow Properties of Surface Modified Active Pharmaceutical Ingredients Using NIR Spectroscopy, Powder Flow in Free Fall and Gravimetric Feeders Process

This chapter describes methods to improve the flow properties of pharmaceutical materials and the use of near-infrared spectroscopy for in-line evaluation improvements. Consequently, the main purpose of this work is to demonstrate that NIR may be used in-line to detect the flow uniformity, which in general depends on the flowability of the powder. In order to corroborate the observations from the in-line NIR signals of the powder sample being discharged, a simple independent method to characterize the powder flowability based on the angle of repose was employed. Results of the angle of repose, which is not an in-line method, are expected to provide a supporting evidence of the powder behavior based on the extent of surface modification. Overall, the purpose of the study was to investigate: (a) whether NIR may be used via the inverse of the noise signal to obtain the flow intensity as well as the indication of flow uniformity through the relative standard deviation (RSD) of flow intensity; (b) if the dry coating improves the flow and flow uniformity of otherwise cohesive pharmaceutical powders and NIR provides the rank order of flow improvement; (c) whether the flow improvement measured during voiding

via in-line NIR spectroscopy generally corresponds with the flowability improvement as measured via off-line means such as the angle of repose.

1.4.3 Chapter 4 -Deconvolution of Chemical and Physical Information from Intact Tablets

This chapter presents a three-way method for developing an NIR spectroscopic determination of drug content in tablets that present a wide variation in tablet compaction pressure. Since NIR methods contain both chemical and physical information, the use of two way models may require the development of several calibration models as the tablet compaction pressure is changed. The study also describes a number of calibration models developed with two-way PLS calibration, and discusses the effect of pressure changes on these models. The novel method utilizes a multivariate calibration strategy based on three-way methods (PARAFAC and MLR tensor based models), to provide a single calibration model to quantify the drug concentration on tablets that present a huge variation in compaction pressure.

In addition a new method for analysis of the Near-infrared chemical imaging (NIR-CI) data is described, calculating the slopes between two wavelengths in each pixel from a NIR-CI. The NIR slope in each pixel describes tablet compaction along the surface of the tablet, in a form that is not affected by differences in tablet height or positioning, and therefore is independent of base line variation. The slope of NIR-CI spectra measures differences in compaction throughout the tablet surface and also provides information on tablet relaxation as shown in this study.

Chapter 2. Near-infrared Spectroscopy for the In-line Characterization of Powder Voiding: Development of the Methodology and Quantification of Enhanced Flow Properties of Surface Modified Active Pharmaceutical Ingredients

2.1 Summary

This chapter describes the uses of in-line near-infrared spectroscopy (NIR) spectra acquired and analyzed to assess the relationship between physical and chemical properties of voiding powders and their spectral changes. NIR spectra were obtained for powders voiding from a conical glass funnel while the powder flow was recorded with a digital camera. Two different approaches using in-line NIR spectra were developed to measure the flow interruptions in the powder voiding process. The first approach uses the noise in the spectra and the second is based on the baseline changes. The new method was also used to evaluate the effects of humidity on the flow of microcrystalline cellulose samples and to evaluate the effect of mixing method on the flow properties of the blends obtained. The method described may be applied to other applications that involve powder flow, and the same spectra may be used to determine drug concentration.

2.2 Materials and Methods

2.2.1 Materials

The materials chosen for this study were Lactose fast flo (Pharmatose DCL-11, DMW International, Veghel, The Netherlands), ibuprofen (70 grade USP/BP/EP, Albemarle, Baton Rouge, LA, USA), colloidal silicon dioxide Mutchler INC, magnesium stearate (Mallinckrodt),

and several commercial microcrystalline cellulose (MCC): VIVAPUR 101, EMCOMCEL 50 and 90, and PROSOLV SMCC 50 and 90 (JRS Pharma).

Table 2.1 Composition of powder mixtures and the flow rates when emptied from funnel

Lactose (%)	Ibuprofen (%)	Average Flow Rate (g/s) (n = 3)	Flow Interruption (#)	Standard Deviation (n =3)
84.3	0	29.5		0.5
79.3	5	20.0		0.4
74.3	10	13.5		0.6
69.3	15	9.5		0.9
59.3	25	1.1	1	0.8
54.3	30	0.5	2	-
34.3	50	0	Did not flow	-
9.3	75	0	Did not flow	-

2.2.2 Instrumentation

A CDI (Control Development Inc, South Bend, IN, USA) Blend Uniformity Analyzer NIR spectrometer was used to acquire the spectra of the voiding powders. This instrument includes a 5.4 W dual tungsten halogen light source and an indium gallium arsenide (InGaAs) diode array that is thermoelectrically cooled and has 256 elements to cover the 908 to 1,687-nm spectral area. Reference spectra were obtained with an AutoCal feature that includes an internal Hg/Ar lamp used for wavelength calibration. NIR diffuse reflectance measurements were obtained from samples in movement during powder voiding and collected with an integration time of 50 ms. A chronometer was used to measure 120 s, and during this time, the spectrometer collected about 650 spectra. This experiment was repeated three times; the calculated average time for each spectrum was 180 ms, with a standard deviation of 11 ms.

2.2.3 Experimental Setup for voiding powders

Previous efforts have shown that NIR spectroscopy may be used to obtain physical information from flowing blends.[21] Barajas showed that NIR can detect differences in particle size of pharmaceutical powders during voiding and observed particle size segregation as a result of air resistance to the movement of the pharmaceutical particles. Barajas employed an experimental setup that includes a stainless steel pipe with a height of 6.3 feet, an inner diameter of 0.9 inches, and an outer diameter of 1 inch.

The objectives of this study were to measure the flow, continuity, and interruption of powder flow and evaluate the chemical homogeneity of pharmaceutical powders. To complete these objectives it was necessary to eliminate the stainless steel pipe in the previous setup,[21] minimizing the air resistance to the movement of the pharmaceutical particles.

The setup used in this study include, a conical glass funnel made of KIMAX borosilicate glass with a stem length of 35 mm, a wall inclination of 63°, a top diameter of 150 mm, and an orifice with an inner diameter of 15 mm (Fisher Scientific Catalog Number 29020 150). The 150 g of mixtures were split into two aliquots of 75 g, for the voiding experiments. The funnel was carefully clamped to ensure minimal lateral motion when a stainless sheet in the bottom of the funnel was removed. The powder mass was measured before and after the voiding process. The powder samples were discharged from the glass funnel as shown in Figure 2.1, and all spectra described in this study were obtained for powders voided from this funnel. Each powder sample was voided three times, and spectra were obtained for each voiding experiment. Diffuse reflectance NIR spectra were collected with the spectrometer positioned at 10 mm from the powder flow. The spectrometer was placed without any physical barrier or separation from the

voiding powder flow. Thus, the diffuse reflectance spectrometer is able to obtain spectra just outside of the funnel, about 0.5 cm below the end of the funnel. The powder voiding process was recorded with a Logitech camera 2 megapixel, and the time record option was used. The recording of all the experiments with the camera was useful in reviewing the flow interruptions that occurred in a number of experiments.

Figure 2.1 Photograph of set up used for voiding experiments showing the near-infrared spectroscopy probe and flowing powder

2.2.4 Software and NIR data processing

Spectra were collected with the Spec 32 (version 1.6.0.6) software provided by Control Development (South Bend, IN). The Pirouette 4.0 software developed by Infometrix (Bothell, WA) was used to evaluate and extract information from the spectra obtained. All spectra were mean centered before principal component analysis (PCA). PCA is a common method used in

multivariate analysis where data is transformed into orthogonal components (uncorrelated to each other) which are linear combinations of the original variables. The spectral data matrix (X) is decomposed in the combination of scores (T) and loadings (P) plus a residual matrix (E) (equation 1.14)

2.2.5 Determination of flow rate

Average flow rate during discharge from the funnel was estimated by measuring the time needed to empty the funnel used in this study.[12] This flow rate was calculated by measuring mass in grams and time was determined by counting the number of NIR spectra during powder flow and multiplying by 180ms (average time for collecting a spectrum). The flow rate is the ratio of the mass in grams between the duration of the emptying of particles. The flow rate units were expressed in grams per second (g/s).

2.2.6 NIR spectral noise

In this work spectral noise was estimated by measuring the standard deviation of raw spectra throughout the 1050 – 1070 nm regions, where the powders do not have absorbance bands. The noise obtained was expressed in absorbance units (AU). This noise was observed to be minimal for a continuous flow; increasing when the flow is interrupted and particles do not reflect the NIR radiation. The noise was found to be inversely proportional to powder flow, thus the inverse of noise can be considered a measure of flow intensity.

2.2.7 Flow continuity

The inverse of the noise was useful to deduce the beginning, the continuity and the end of the powder flow. The inverse of the noise was represented as a function of time, and the graphic

obtained related the flow process and the variation in powder flow rate. If powder flow takes place, it is possible to use the standard deviation of the inverse of the noise to measure the variation in the flow rate. This variation indicates whether the flow is continuous or interrupted, and the variation in the inverse of the noise can be considered as an index for flow uniformity. The noise index is the inverse of the noise and is expressed in 1/AU.

2.3 Results and Discussion

2.3.1 NIR spectra of powder flow

NIR spectra with large baseline and noise differences were obtained in real time during the voiding of a 5% w/w ibuprofen powder mixture powder as shown in Figure 2.2 a) The 5% w/w powder mixture is considered to have good consistent powder flow, without significant interruptions in the powder flow. When a large number of particles from the powder interact with the NIR beam the resulting spectra have a low baseline and minimum noise in the NIR spectra. The change in baseline is clearly explained by the following equations:

$$I_{det} = 1/c \ \ x \ I_{refl} \tag{2.1}$$

$$A_{det\,ected} = -\log(R_{det\,ected}) = -\log\left(\frac{I_{det}}{I_0}\right) = -\log\left(\frac{1}{c}\right)\left(\frac{I_{refl}}{I_0}\right) = \log c + A \tag{2.2}$$

Where I_0 is the total intensity of the radiation focused on the flowing powder, and 1/c is the fraction of the reflected radiation (I_{refl}) that reaches the detector.[48] The base line depends on 1/c, the fraction of the reflected radiation that reaches the detector. This fraction is sample dependent and varies as the flow rate changes and the number of particles that interact with the radiation changes. When a high flow is observed diffuse reflectance is strong, and the spectra will

resemble spectra of a static powder sample. However, if the powder flow decreases fewer particles are in contact with the beam, the diffuse reflectance decreases, while the baseline and noise of the NIR spectra increases yielding the spectra with medium baseline observed in Figure 2.2 a) The low baseline and medium baseline spectra show the absorbance bands of the voided material, providing chemical information. The high baseline spectra are obtained when powder particles do not interact with the NIR radiation. These high baseline spectra do not have absorbance bands; appearing as a line and noise related to the lack of radiation returning to the detector. Thus, the baseline is a function of the flow making it possible to use the NIR spectra to study powder flow.

Figure 2.2 a) shows NIR spectra obtained for a powder voiding process where the flow was continuous without interruption. The NIR spectra obtained for this powder voiding process included a larger number of low baseline spectra and some medium baseline spectra. The larger number of low baseline spectra with minimum noise indicate a continuous flow of powder during the voiding process. Figure 2.2 a) shows very few medium baseline spectra. In Figure 2.2 a) the high base line spectra indicate the beginning and end of powder flow.

Figure 2.2 b) were obtained for a powder voiding process of a 25% w/w ibuprofen blend with intermittent poor powder flow, where the powder did not flow continuously. The NIR spectra obtained for this intermittent powder flow process shows a greater number of high baseline noise NIR spectra than low baseline spectra, as a consequence of several interruptions in the powder flow during the voiding process.
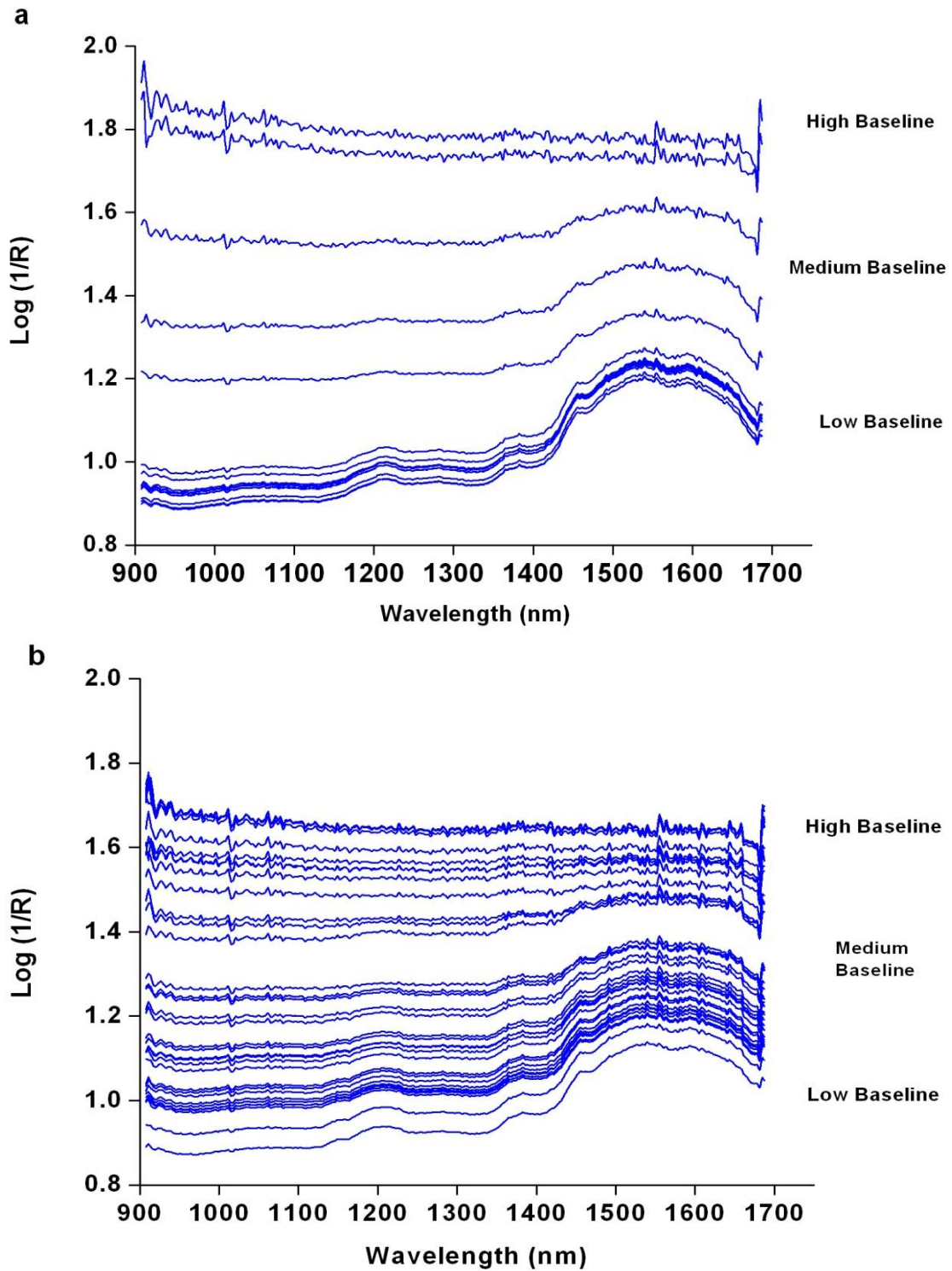
Figure 2.2 a) NIR spectra of 5% w/w ibuprofen mixture in free fall. b) NIR spectra 25% w/w ibuprofen mixture in free fall

2.3.1.2 Optimal distance between powder flow and NIR spectrometer

A number of experiments were performed to further evaluate the ability of the NIR spectrometer to monitor the powder flow. The first experiment consisted in evaluating the possible effect of probe distance to powder flow. The distance between the NIR probe and the sample could be a source of spectral noise, where if the probe is too far away, the fraction of the reflected radiation that reaches the detector is reduced. The optimal distance was evaluated for the powder voiding process of a 5% w/w ibuprofen blend with consistent powder flow with spectra acquired at several distances, as shown in Figure 2.3 a) The standard deviation in the region of 1050-1070 nm was used as an indicator of noise. The lowest distance used was 2 mm and the largest distance was 30 mm. However, at distances of 2 mm significant fouling of the NIR probe was observed and the short distance affected the powder flow. Figure 2.3 b), shows the average of standard deviation of the NIR spectra. The selected probe distance for all other experiments was 10 mm where a standard deviation of 0.00075 mm was measured. The magnitude of the spectral noise was considered to be similar at all the distances evaluate.

The noise and baseline changes are an essential component of this method. Thus, the spectral noise and its possible sources were studied to better understand the method. In this application the NIR spectral noise could be associated with the distance from the probe to the sample, stray light,[49] and sample absorbance. Five experiments were performed to evaluate the effect of different parameters on the noise in the region of 1050-1070 nm as shown in Figure 2.4. The noise was measured as 0.0056 in the absence of particles interacting with the NIR beam and with efforts to isolate the probe from possible sources of stray light. The standard deviation was very similar: 0.0080, in the absence of efforts to reduce the possible effects of stray light. The third case with continuous powder flow showed a standard deviation of 0.00075 in the region of

1050-1070 nm. The fourth test was with the NIR beam reflected from a reference ceramic disc where the standard deviation was about 0.00053 in the region of 1050-1070 nm. The test with the ceramic disk is important since it leads to a low baseline as a high portion of the radiation is returned back to the detector. The noise is lower with both the ceramic disc and the continuous powder flow, while it is higher when a limited amount of radiation is returned to the detector. Thus, the source of the increased noise observed when the powder stops flowing is the result of the low signal (few number of photons) received in the detector.

The approach described in this paper will work in situations where the number of photons reaching the detector is reduced due to lack of particle flow. The approach will not be suitable within a pipe or equipment where a shiny surface reflects the radiation back to the detector, therefore saturating the detector.
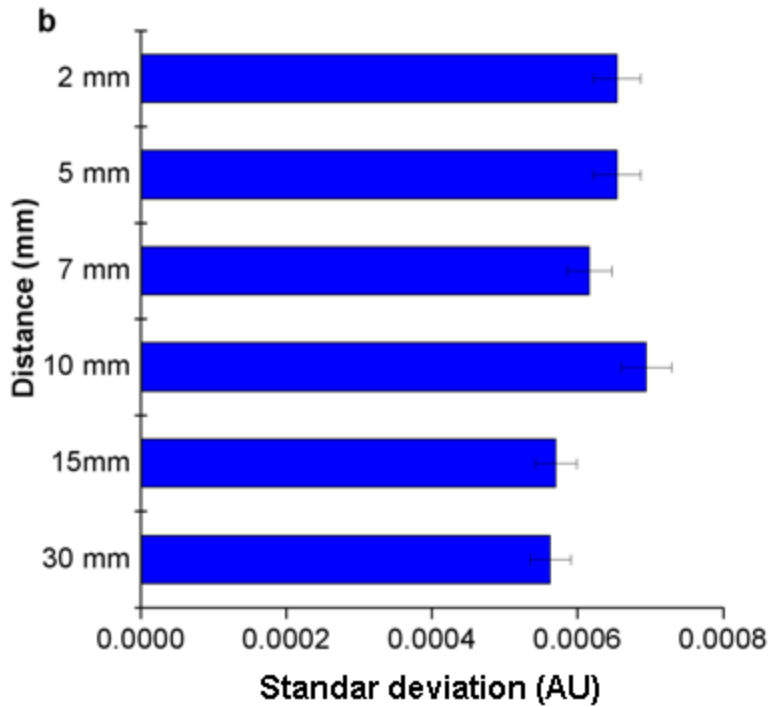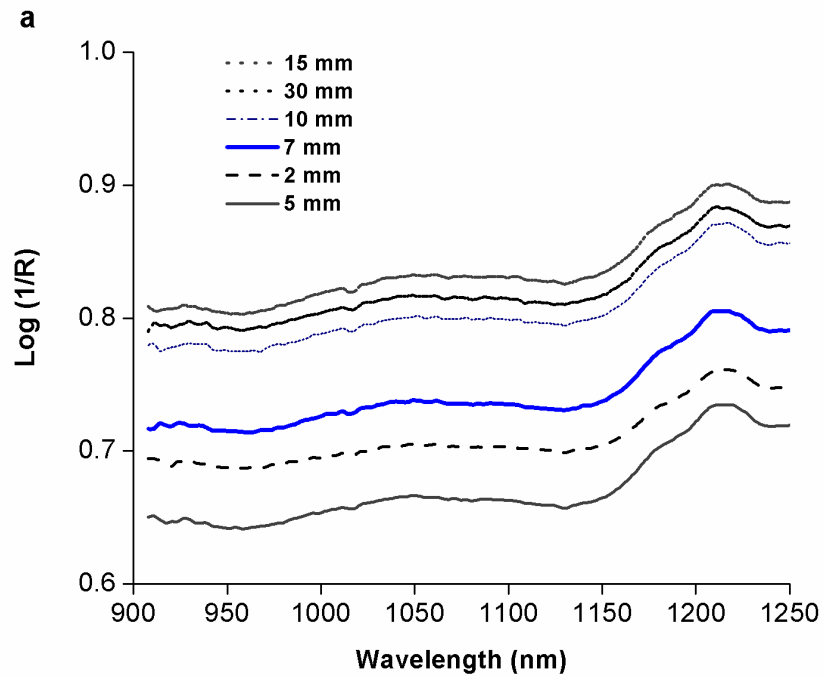
Figure 2.3 a) NIR spectra obtained at various probe distances to powder. b) Standard deviation (noise) as probe distance to powder was varied.
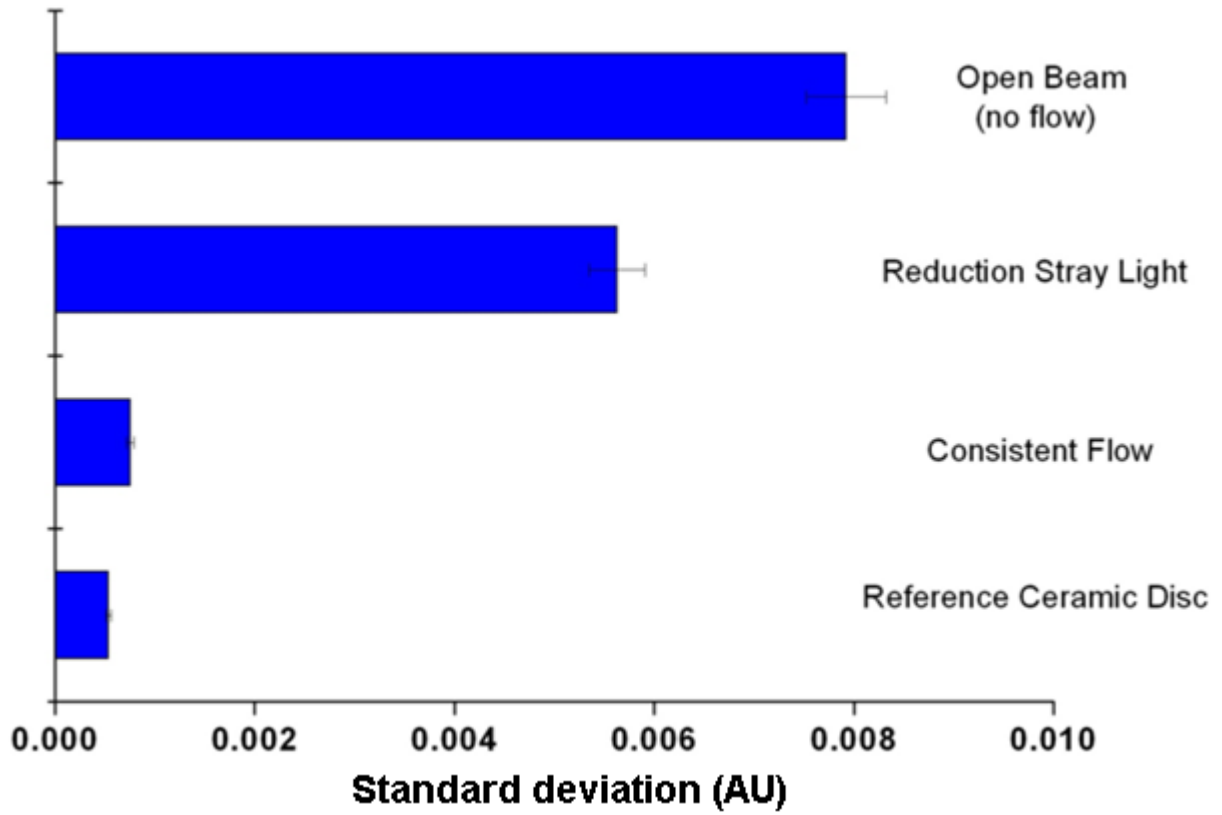
Figure 2.4 Determination of noise (standard deviation) under various conditions

2.3.2 Continuity of powder flow and data evaluation
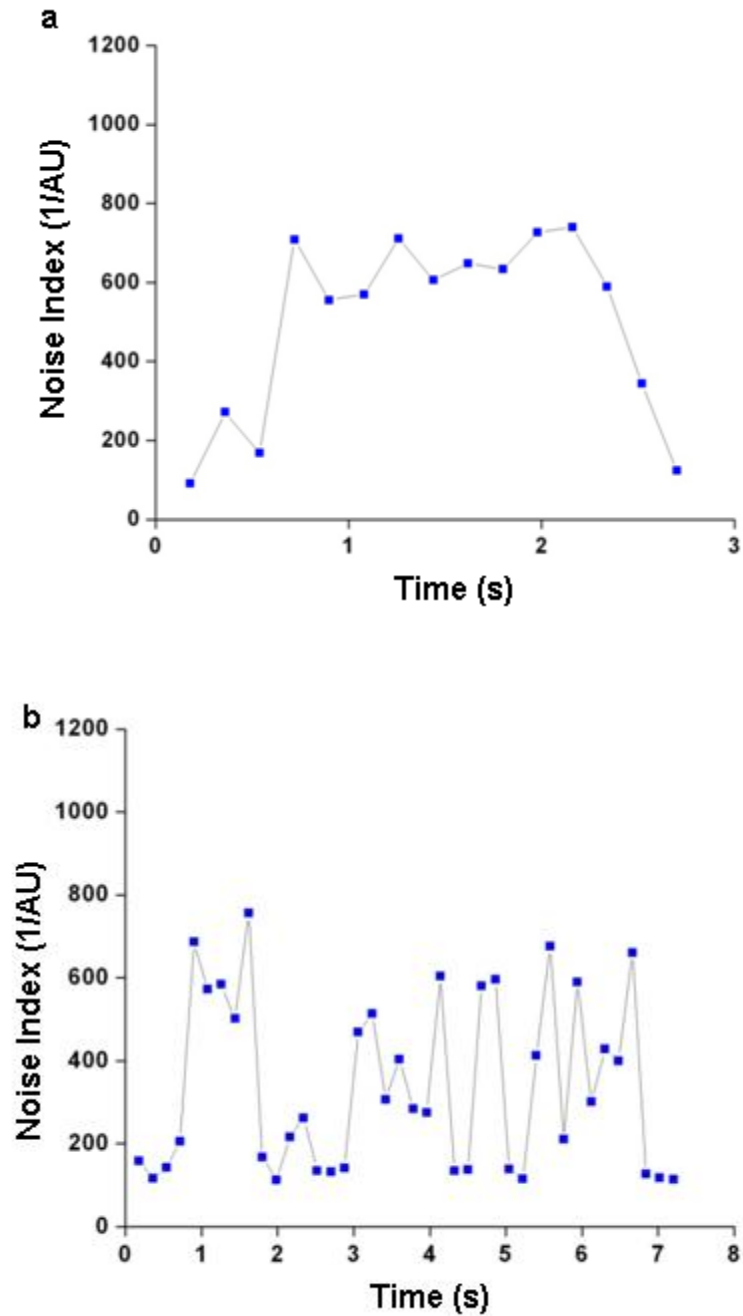
Figure 2.5 a) 1/Noise versus voiding time for a 5% w/w ibuprofen powder mixture with good (consistent) powder flow and b) 25% w/w ibuprofen mixture with interrupted powder flow.

Two blends with very different flow properties, the 5% w/w and 25% w/w ibuprofen powder mixtures, were used to evaluate the method's ability to monitor the continuity of powder flow. The 5% w/w ibuprofen mixture does not show visible powder flow interruptions as previously indicated, while 25% w/w ibuprofen exhibits multiple powder flow interruptions. The inverse of the noise (1/noise) versus time was used to evaluate the continuity of the flow, to describe the beginning, interruption and the end of voiding process as indicated in Figures 2.5 a) and 2.5 b). The noise was estimated using the standard deviation in the 1050-1070 nm regions, where the spectra do not show absorbance bands. The 1/noise value has been termed flow intensity and is shown in Figure 2.5 a) for the 5% w/w ibuprofen powder blend, where the highest values were obtained during, high level, continuous flow of the mixture, and the lowest values (maximum noise) obtained when the flow stopped. Figure 2.5 b) indicates a number of occasions where the flow was interrupted, providing lower flow intensity values. Figure 2.5 b) describes the flow process of the 25% w/w ibuprofen mixture, where the flow was not continuous and tapping of the funnel was required to force the flow to continue, with the corresponding interruptions of flow. Figures 2.5 a) and 2.5 b) also show that the voiding process took longer for the 25% w/w ibuprofen powder mixture. Figure 2.5 shows that the NIR method follows the voiding process, detects the beginning of flow process, indicates discontinuities in the flow and detects the end of the powder flow.

PCA was also used as a possible alternative to evaluate the continuity of powder flow in the voiding experiments. PCA was performed over the 936 – 1634 nm wavelength range for spectra obtained during the voiding experiments with the 5% w/w and 25% w/w ibuprofen powder mixtures.
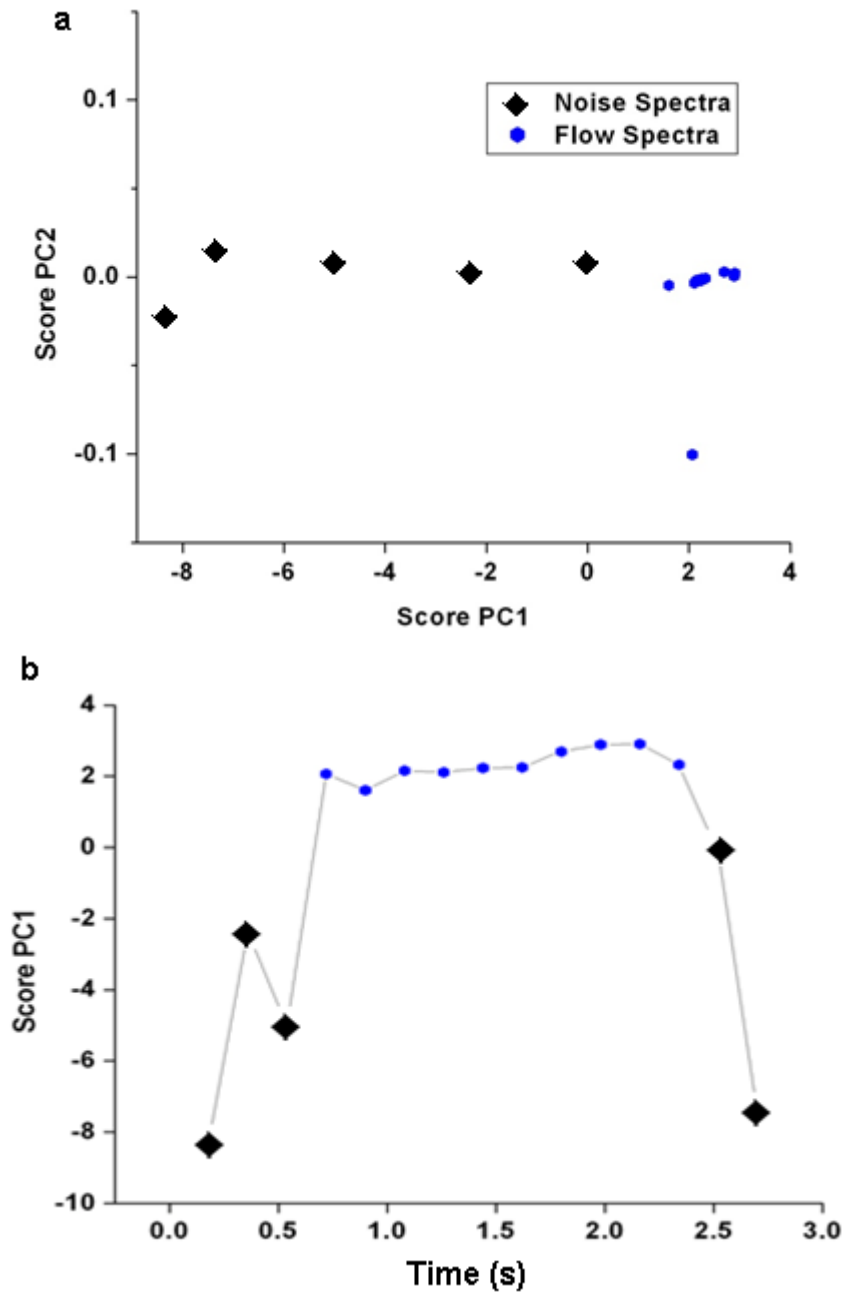
Figure 2.6 a) Principal Component Analysis for flow continuity of 5%w/w ibuprofen powder mixture. b) Score PC1 vs time.

Figure 2.6 a) shows the scores plot for the NIR spectra acquired during the powder flow process of the 5%w/w ibuprofen mixture. Figure 2.6 a) shows that spectra are characterized according to their baseline along *PC1*. The first loading (not shown) is a horizontal line, indicating that the baseline is the principal source of variation. Figure 2.6 b) shows that when *PC1* is plotted versus time a plot similar to that of the inverse of noise was obtained. Thus PCA is also an alternative to study the flow behavior of a voiding powder. The advantage of PCA is that it does not require the selection of a region without absorbance bands in the NIR spectra of the flowing powder.

2.3.3 NIR Cross-sensitivity

NIR infrared instruments are cross-sensitive,[48] where one sensor or instrument can be used to provide both chemical and physical information.[11] In this study in-line NIR spectra were obtained during voiding of six different powder blends with 1, 10, 15, 20, 25 and 30% w/w ibuprofen. The spectra obtained contain low, medium and high baseline NIR spectra for every concentration. To obtain chemical information, all spectra with high base line were removed from the spectral data set. The remaining spectra were analyzed by PCA to visualize the spectral variability due to chemical properties. Figure 2.7 shows the scores plot (*PC1* vs *PC2*) after applying Standard Normal Variate (SNV) pretreatment. The scores plot easily differentiates among the powder blends with different ibuprofen concentrations. *PC1* describes 66.4% of the spectral variation, and separates the spectra of the voiding samples according to the ibuprofen concentration. Thus, the same spectra used to study differences in concentration can also be used to study the flow behavior of the powder mixture.
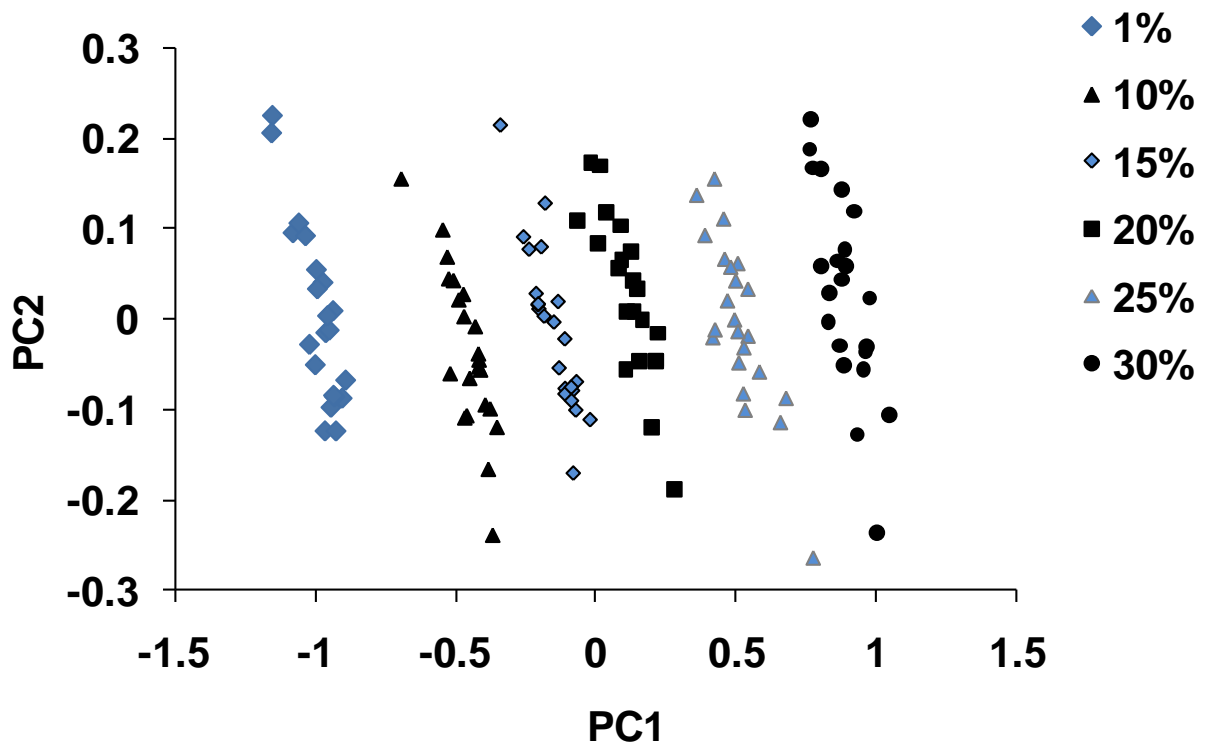
Figure 2.7 Principal component analysis of in-line NIR spectra of powder flow at different ibuprofen concentrations
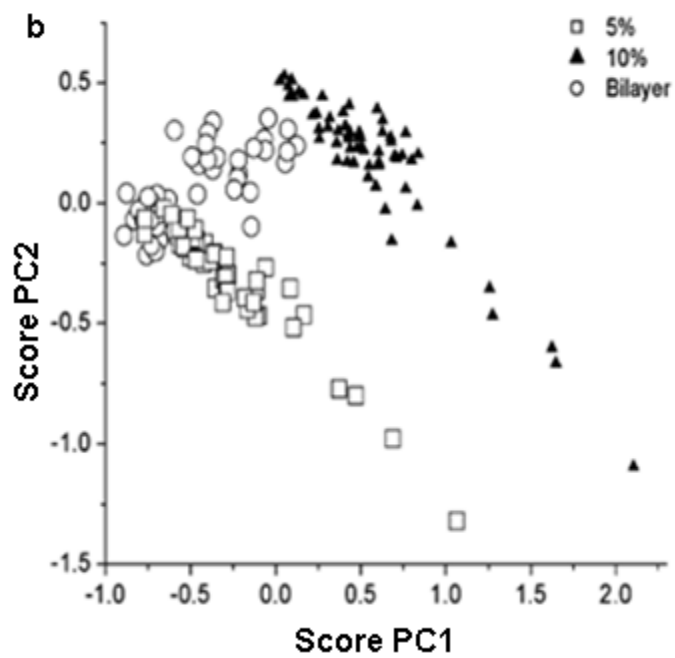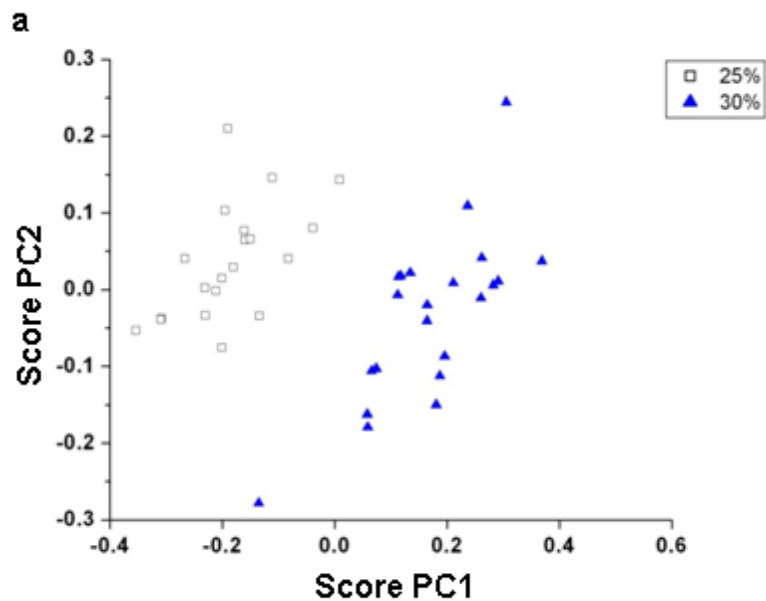
Figure 2.8 a) PCA scores plot for layers 25% w/w and 30% w/w ibuprofen powder mixtures. b) PCA scores plot of ibuprofen mixture of 5% w/w, 10% w/w and bilayer (5% w/w and 10% w/w)

The NIR system was also challenged to detect changes in the drug concentration of the blends during voiding. A previous study showed that NIR diffuse reflectance spectra responded to changes in powder composition after voiding of two different materials placed in layers in a funnel.[21] In this experiment, the funnel was charged with two layers of powder blends with different ibuprofen concentration. The first layer contained 75g of a mixture of 25% w/w ibuprofen, and the second layer of 75g was a mixture at 30% w/w ibuprofen. Furthermore, the flow of the 30% w/w blend is much more intermittent and it was necessary to tap the funnel to force its flow. Figure 2.8 a) shows the PCA scores plot for this experiment. The first 24 spectra (group A) obtained are observed on the left half of the scores plot. Group A spectra correspond to the 25% w/w blend, while the group B spectra in the right side correspond to the 30% w/w blend; these observations were confirmed by obtaining spectra of each individual blend in separate experiments. The two spectra not included in group A or B are likely intermediate spectra, resulting from mixing in the funnel or during flow. These experiments demonstrate that the method is able to provide both physical and chemical information. Figure 2.8 b) shows a similar experiment where the bottom layer was a 5% w/w blend, and the top layer was a10% w/w. The flow properties of the blends caused mixing of the two layers during voiding.

Table 2.1 shows the flow rate calculated for the different mixtures of ibuprofen and lactose. The fast flow lactose has a flow rate of 29.5 g/s, the ibuprofen has a flow rate of 0 g/s; thus the flow rate of the blends depends on the ibuprofen concentration. The 30% w/w of ibuprofen mixture was helped with tapping to complete the process. The 50%, 75% and 100% w/w of ibuprofen mixtures did not flow at all, even after repeatedly tapping the funnel.

2.3.4 Flow rate and consistency of powder flow in commercial microcrystalline cellulose samples

Table 2.2 Flow rate of microcrystalline cellulose using NIR spectral method.

Material	Flow rate (g/s) n =3	Flow Interruption	Standard Deviation n =3
EMCOCEL50	0	No Flow	0
EMCOCEL90	14.3	X	0.9
PROSOLV 50	10.5	X	0.6
PROSOLV 90	21.4		0.5

The NIR method can also be used to evaluate the differences in the flow properties of excipients, and the environmental effects such as exposure to humidity. The flow rates of several commercial MCC samples were measured using the new in-line NIR method and the experimental setup for voiding powders. The samples used were EMCOMCEL 50 and 90, PROSOLV SMCC 50 and 90. Table 2.2 shows the flow rate (g/s) measured using the NIR spectra. All measurements were made with 150 g of material and the samples were measured in triplicate. The EMCOMCEL 90 sample flow when the valve was opened, then the flow stopped, and then continued after the funnel was tapped. EMCOMCEL 50, did not flow even with tapping, the flow was interrupted forming a rat hole. PROSOLV 50, which is 98% w/w microcrystalline cellulose and 2% w/w colloidal silicon dioxide, flowed when the valve was opened but then the flow was interrupted, and tapping was necessary to continue the flow. PROSOLV 90 flowed continuously and with a flow rate 21.4 ± 0.5 g/s.

It is emphasized however, that the principal value of the method is not in evaluating the flow rate, but in evaluating the consistency of the powder flow. The effect of humidity on the

consistency of powder flow was evaluated. Samples of 150 g of PROSOLV 90 were exposed to a humid environment of 85% relative humidity for 1, 2, and 3 hours. Notable differences were observed in the consistency of powder flow when the PROSOLV 90 was exposed to high humidity. The consistency of powder flow was evaluated through the relative standard deviation of the flow intensity measurements, obtained as the powder flowed. Table 2.3 shows the results, with an increase in the variation of the flow intensity as function of the humidity exposure time. The exposed PROSOLV 90 shows higher flow intensity variation upon voiding from the funnel as shown in Figure 2.9. PROSOLV 90 voided immediately after opening the suppliers' package (0 hours of humidity) provided flow intensity greater than 1000 and an RSD of 13.5% while PROSOLV 90 exposed to 3 hours of humidity showed a flow intensity of 697 and RSD of 33.1% and three interruptions in powder flow. Thus, the variation in flow intensity may be used to assess flow uniformity and hence compare the flow properties of the material exposed to humidity.

Table 2.3 Noise index variation for different humidity exposure time of PROSOLV 90, measures using NIR spectra method

Humidity exposure time (h)	Interruptions	Noise Index (1/AU)
0	0	35±10
1	0	112±7
2	0	132±6
3	3	231±25
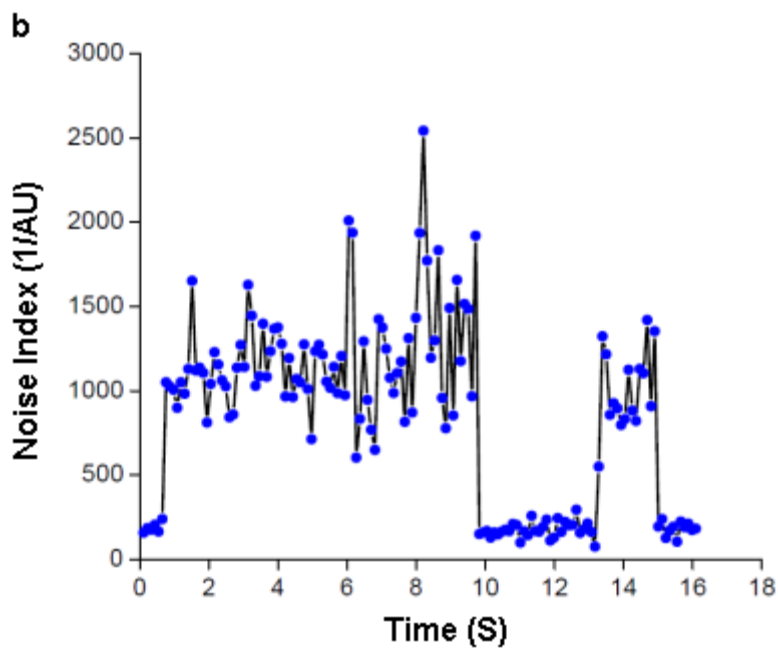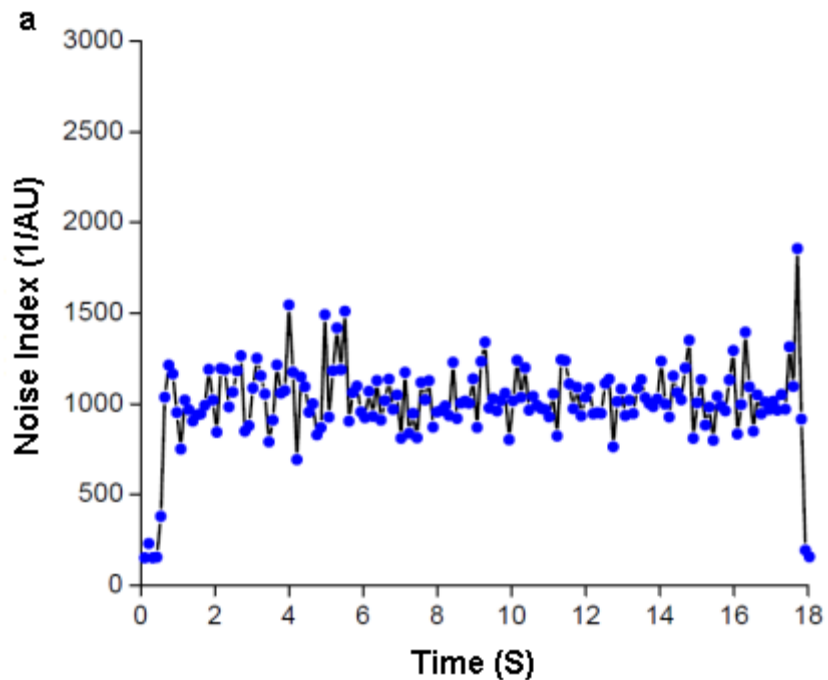
Figure 2.9 a) Noise index (1/AU) for Prosolv 90 as removed from sample container. b) Noise index (1/AU) for Prosolv 90 exposed to humidity for 3 days

2.3.5 Relationship between powder flow rate and mixing method

Blends were prepared to determine whether changes in the mixing method affect powder flow properties during voiding. The blends were prepared using ibuprofen 5% w/w, 15% w/w VIVAPUR 101, colloidal silicon dioxide 0.2% w/w, magnesium stearate 0.5% w/w and lactose as filler, but with two mixing methods. In the first mixing method the powders were first passed together through a sieve, as discussed in the Experimental section, and then placed in the V-blender. In the second mixing method the powders were placed directly in the V-Blender and then mixed. Each set of mixtures were prepared in duplicate and mixed at 14 rpm at different time sets. Table 2.4 compares the sieve and the V-blender method flow properties for the 5% w/w ibuprofen mixtures. The V-blender method provided blends where flow properties varied according to the mixing time used. The sample exposed to a blending time of 0 seconds at the V-blender showed a flow rate similar to the mixture of 0% w/w ibuprofen (Table 2.1) as a consequence of not mixing the components (the components were only passed together through the sieve). The average flow rate for a mixture of 5% w/w ibuprofen was very similar for the three blending times: 17.7 g/s after 60 seconds of blending, 19.0 g/s after 300 seconds, and 18.0 g/s after 600 seconds of blending.
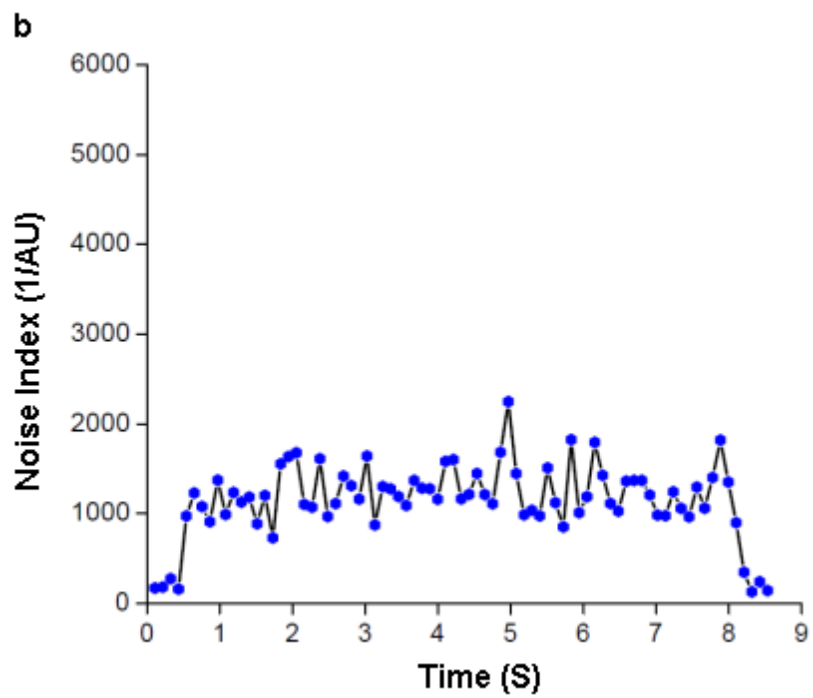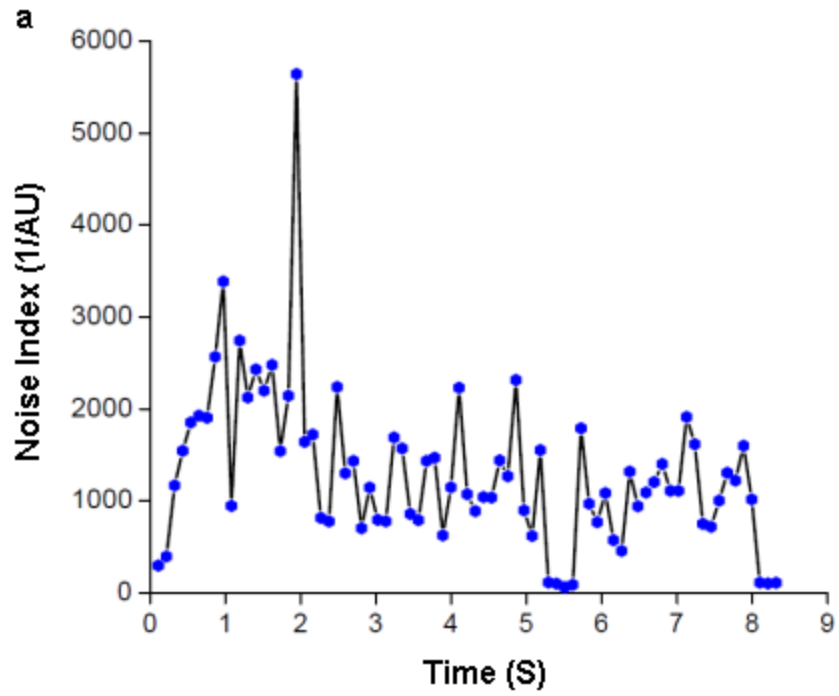
Figure 2.10 a) Noise index vs time for ibuprofen 5% w/w blend and b) 5% w/w sieved blend

When the powders were passed together through the sieve the average flow rate was almost constant as indicated in Table 2.4. Figure 2.10 shows flow intensity versus time plots for the two mixing methods. The 5% w/w sieving mixture does not show visible powder flow interruptions; and less variation is observed in the flow intensity than when the powders are blended directly. Thus, the variation (RSD) of the flow intensity could be used as a measure of the flow uniformity (consistency of powder flow). The flow uniformity was significantly better for the sieving method. Figure 2.10a) shows that for the 5% w/w blending mixture the first 3 seconds showed significant changes in powder flow rate, the flow rate changed less in the next 2 seconds, an a discontinuity in powder flow was observed between the 5 and 6 seconds. These results show that the NIR method provides the flow intensity and flow uniformity to compare blending methods.

Table 2.4 Flow properties of 5% w/w of ibuprofen mixture comparison V-blend method and sieve method.

Methods	Mixing Time (s)	Flow rate average (g/s) n = 3	Standard Deviation Noise Index	Noise Index
V-blend	0	29.85±0.60	1530	1562
	60	17.70±0.21	949	2090
	300	19.04±0.32	954	1898
	600	18.01±0.40	1066	1925
Sieve & V-blend	0	25.44±1.71	323	735
	60	20.41±0.61	223	668
	300	20.35±0.87	242	631
	600	20.35±0.91	223	638

2.4 Conclusion

The noise in the NIR spectra of flowing powders may be used to gain information on their flow properties. Flow interruptions will change the spectral baseline and increase noise. The consistency of powder flow may be evaluated through plots of 1/noise versus time as well as PCA score plots. The new method could be used to increase process understanding of the flow properties of excipients and API. The same spectra used to evaluate powder flow could also be used to evaluate drug concentration in the powder mixtures produced. The new method is not limited to the study of powder voiding and may be used in other applications that involve powder flow.

Chapter 3. In-Line Quantification of Enhanced Flow Properties of Surface Modified Active Pharmaceutical Ingredients Using NIR Spectroscopy, Powder Flow in Free Fall and Gravimetric Feeders Process

3.1 Summary

This chapter describes the application of the NIR method described in Chapter 2 to the evaluation of active pharmaceutical ingredients (APIs) that have been surface modified to improve their extremely poor flow properties. Near-infrared (NIR) spectroscopy was utilized as a novel approach to characterize the improved flow behavior of APIs and their blends. Acetaminophen and ibuprofen were coated with nano-sized silica at two different coating levels (0.5% and 1% w/w of the API). Surface modified (dry coated) APIs were then blended with excipients (spray dried lactose monohydrate) in a V-blender. As a baseline comparison to dry coating, the silica addition was also accomplished by two commonly used industry methods, i.e., passing a portion of API with silica through a sieve (sieve blending method) or blending a portion of API powder with silica in a V-blender (pre-blending method). Flow results showed that dry particle coated acetaminophen as well as ibuprofen blends performed significantly better than uncoated API blends at higher API concentrations. In addition, examination of the flow intensity from NIR spectra (inverse signal to noise ratio of spectra) and its standard deviation revealed that dry particle coated blends showed better uniformity of flow as compared to the other methods. Angle of repose measurements corroborated these results, showing that the majority of the blends prepared from coated APIs stayed in either passable or fair category.

This chapter also involves a second study evaluating the performance of excipients and cohesive powders in a K-tron twin-screw gravimetric feeder. The evaluation used NIR spectroscopy and multivariate data analysis as an effective alternative for the real-time measure of flow behavior. Microcrystalline cellulose was used as a representative excipient material since various grades are available with differences in particle size. The NIR system was used to evaluate the effect of feed rates, particle size, and feeder control settings on the continuity of powder flow. Additionally surface modified ibuprofen was evaluated to evaluate the effect of coating effect on powder feeding. This second study was performed at Pfizer Research labs in Groton, CT. and was important for the development of continuous mixing systems.[50]

3.2 Materials and Methods

3.2.1 Materials for powder flow in free fall

Highly cohesive and poorly flowable APIs such as acetaminophen (micronized grade with primary mean size ~20μm, supplied by Mallinckrodt, Inc., Hazelwood, MO, USA) and ibuprofen (70 grade USP/BP/EP, mean size ~70μm, supplied by Albemarle, Baton Rouge, LA, USA) were used for the characterization of the enhanced flowability after surface modification by utilizing an in-line measurement technique (NIR spectroscopy). Hydrophobic fumed silica (R972 grade supplied by Evonik Degussa, particle size 16 nm) was used for the surface modification of these APIs carried out by the various routes such as the dry coating, sieve mixing, and preblending method discussed below in details ("Operational Procedures for the Preparation of API Blends" section). R972 is hydrophobic due to the surface treatment by dimethyldichlorosilane, as per the information supplied by Degussa. All particle sizes reported are from the manufacturer. Powder

blends for the characterization of flow properties were prepared with the excipient; spray dried lactose monohydrate (Pharmatose DCL-11, DMW International, Veghel, The Netherlands) at the Analytical & Pharmaceutical labs at UPR-Mayagüez.

3.2.2 Materials for gravimetric feeder study

Dry coated ibuprofen, V-blender ibuprofen and microcrystalline cellulose were used as representative materials since its various grades differ in terms of particle size, density, and flow properties. The material was used in evaluating the flow performance in a K-tron twin-screw gravimetric feeder.

Table 3.1 describes the microcrystalline cellulose used in this study. The material properties listed are per certificate of analysis from the supplier. All materials were supplied by Pfizer Research labs.

Table 3.1 Physical properties of microcrystalline cellulose supplied for gravimetric feeder study.

Comercial Name	Nominal Particle size (µm)	Particle size d50 (µm)	Moisture, %	Bulk Density, g/cc
PH101	50	60.4	3.0 - 5.0	0.26 - 0.31
PH102	100	89.7	3.0 - 5.0	0.28 - 0.33
PH105	20	21.1	3.0 - 5.0	0.20 - 0.30
PH112	100	90.1	0.5 - 1.5	0.28 - 0.34
PH302	100	90.0	3.0 - 5.0	0.35 - 0.46

3.2.3 Instrumentation and setup

3.2.3.1 Instrumentation and setup for powder flow in free fall

For powder voiding experiments, a CDI (Control Development, Inc., South Bend, IN, USA) NIR spectrometer was used to obtain the spectra of the voiding powders from the funnel. The CDI NIR spectrometer includes a 5.4 W dual tungsten halogen light source and an indium gallium arsenide (InGaAs) diode array that is thermoelectrically cooled and has 256 elements to cover the 908 to 1,687-nm spectral area. NIR diffuse reflectance measurements were obtained from samples in movement during powder voiding and collected with an integration time of 200 ms.

The setup includes a conical glass funnel made of KIMAX borosilicate glass with a stem length of 35 mm, a wall inclination of 63°, a top diameter of 150 mm, and an orifice with an inner diameter of 15 mm (Fisher Scientific Catalog Number 29020 150). Aliquots of 75 g of material were used for the voiding experiments. The funnel was carefully clamped to ensure minimal lateral motion when a stainless sheet in the bottom of the funnel was removed. Powder samples were discharged from the glass funnel, and diffuse reflectance NIR spectra were collected with the spectrometer positioned at 10 mm from the powder flow. The spectrometer was placed without any physical barrier or separation from the voiding powder flow (Figure 3.1a).

In the powder flow in free fall process, the flow rate was calculated by the ratio of the mass in grams between the duration of the emptying of particles. The flow rate units were expressed in grams per second (g/s).

3.2.3.2 Instrumentation and setup for gravimetric feeder

The second part of the experimentation includes studying the powder flow from a K-tron twin-screw gravimetric feeder (KT20), with interchangeable feeding tools mounted on a weighing bridge. The feeder included a weight loss control unit with an internal balance. Each second the KT20 feeder calculates the flow rate using the ratio between the mass change and time change. In the control software of KT20 the flow rate units were expressed in grams per minute (g/min).

The powder from the feeder was emptied into a stainless steel funnel as shown in Figure 3.1b). A second NIR spectrometer was used to study the gravimetric feeder process. The NIR spectrometer used was from CDI (Control Development Inc, South Bend, IN), equipped with a thermoelectrically cooled InGaAs diode array detector of 256 elements that provides a spectral range from 1097 to 2200nm. Diffuse reflectance spectra were obtained with a miniature probe consisting of a dual tungsten halogen light source, equipped with gold diffuse reflectors positioned at a 45 degree angle from the fiber optic probe and fixed at a distance of 11 mm over each tablet. The inner diameter of the fiber optic is 400 microns and its length is three meters. NIR diffuse reflectance measurements were obtained from samples in movement during powder feeding and collected with an integration time of 200 ms.

The probe from the NIR spectrometer was placed at the bottom funnel as shown in Figure 3.1 b). A second external balance was used to continuously weigh the material received from the feeder, and then monitoring the rate at which the system loses weight. The second scale was used as a backup in case of differences between measurements made by NIR and the primary balance. Both balances measured the applied load, using a variable magnetic field, an electrified wire and

the change in the electric signal frequency (10-15 KHz measurement range) caused by changes in weight. The balance used in the setup, required about 1 second to provide a result. The gravimetric feeder setup was used to evaluate the effect of feed rates, particle size, and control settings on the continuity of powder flow.

A total of three feed rates were evaluated and these were summarized as A= 10 g/min = 0.17 g/s, B= 30 g/min = 0.5 g/s, and C was 50 g/min = 0.83 g/s. At the same time the gravimetric feeder control system incorporates Screw Speed Modulation, when the flow rate appears out of limits, the system recovers the gravimetric flow rate using invariable acceleration (non optimal settings) or variable acceleration (optimal settings). The control settings were classified in two levels of variation, optimal control has values of 1 and non-optimal control has value of 0. The effect of control settings (optimal and non optimal) was evaluated over the RSD of the powder feeding process. Each experiment was performed for 5 minutes and in every experiment NIR spectra were acquired during the entire process and the weight was recorded using the two balances.
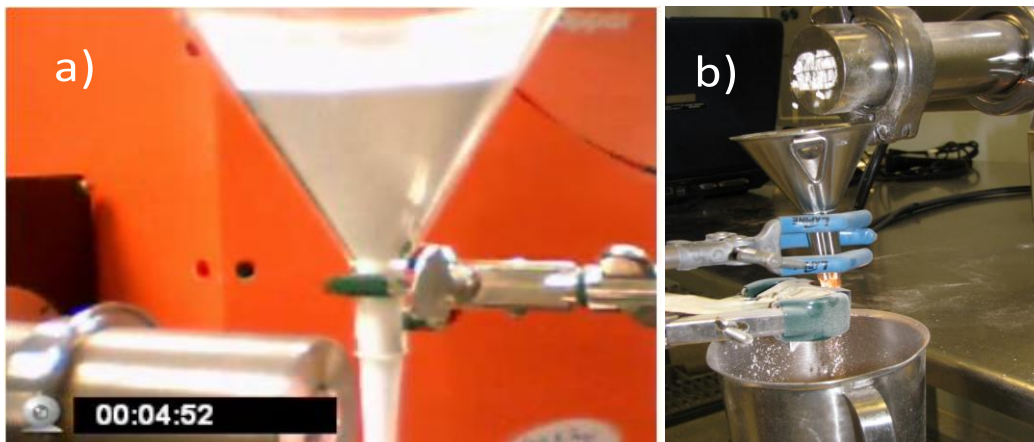
Figure 3.1 a) Photograph of set up used for voiding experiments showing the near-infrared spectroscopy probe and flowing powder b) Photograph of set up used for voiding

experiments showing K-tron twin-screw gravimetric feeder stainless steel funnel and the NIR probe.

3.2.4 Methods for surface modification

Surface modification of APIs by coating with silica was carried out in dry-coating equipment. The dry coating devices commonly employed by the Davé group for the coating of smaller size particles (guest) onto the surface of relatively larger size particles (host) are based on the principle of application of high impact and shear forces.[51, 52, 53, 54] In addition to the dry coating devices, V-blender (Patterson-Kelley, BlendMaster, East Stroudsburg, PA, USA), the most commonly employed blending device in the pharmaceutical industries, was used for preparing the blends of nano-size silica-coated APIs and the excipients.

3.2.5 Hybridizer method

The Davé lab also employed the Hybridizer from Nara Machinery, Tokyo, Japan, which consists of a high-speed rotor with six blades, a stator, and a powder recirculation circuit.[55] The powder (host and guest particles) placed in the processing part of the vessel is subjected to high impaction and dispersion due to the high rotating speed of the rotor. The particles undergo many collisions, and this allows for break-up of fine agglomerates and powder coating due to the embedding or smearing of the guest particles onto the surface of the host particles.[53, 54, 55]

3.2.6 Dry coating method

Acetaminophen and ibuprofen were coated with 0.5% and 1.0% w/w hydrophobic fumed silica, respectively, in the dry coating device. The operating conditions were described in Near-Infrared Spectroscopy for the In-Line Characterization of Powder Voiding Part II: Quantification of Enhanced Flow Properties of Surface Modified Active Pharmaceutical Ingredients.

3.2.7 Sieve mixing method

In this method, the API was placed on a US standard wire mesh test sieve (25, 750 μm mesh size). Hydrophobic fumed silica (0.5% and 1.0% w/w of API) was placed on the top of API. The remaining 90% w/w of the API was placed on top of the silica layer, and the powders were sieve mixed into a collection container. The sieve mixed material was then combined with the excipient and blended in a V-blender for 4 min at 15 rpm.

3.2.8 Characterization techniques

The objective of this study was to utilize the novel method based on the use of NIR spectroscopy, described in detail in Chapter 2, for the purpose of quantitatively understanding the effect of dry-particle coating on the flow properties of APIs. The powder samples were discharged from the glass funnel or gravimetric feeder system, and diffuse reflectance NIR spectra were collected with the spectrometer positioned at 10 mm from the powder flow. The spectrometer was placed without any physical barrier or separation from the voiding powder flow. In this work, spectral noise was estimated by measuring the standard deviation throughout the 1050–1070 nm regions to lactose mixtures, and 1100-1200 nm for microcrystalline cellulose, acetaminophen and ibuprofen, where NIR spectra of the powders do not have absorbance bands. This noise was observed to be minimal for a continuous flow, increasing when the flow is interrupted, and particles do not reflect the NIR radiation. The noise was found to be inversely proportional to powder flow, thus the inverse of noise can be considered a measure of flow intensity. The variation in the flow intensity indicates whether the flow is continuous or interrupted, and hence the standard deviation in the inverse of the noise can be considered as an index for flow uniformity.

3.2.9 Angle of repose measurements

Angle of repose (AoR) measurements was performed by the Davé lab at New Jersey Institute of Technology (NJIT) as described in the published article (Near-Infrared Spectroscopy for the In-Line Characterization of Powder Voiding Part II). To measure the AoR, the powder is placed in the powder holder in the device. The equipment is then set to run for 180 s and a suitable vibration rate depending on the powder is chosen. At the end of the run, the measuring pin is aligned parallel to the slanting surface of the powder and the resulting angle obtained is recorded. The results obtained from this established methods were compared to the obtained results with NIR spectroscopy.

3.3 Results and Discussion

3.3.1 Powder flow in free fall process

The variation in the baseline was studied by estimating the spectral noise throughout the 1050 – 1070 nm spectral area for lactose mixtures, Figure 3.2. The standard deviation of the baseline was measured for each sample and a graph of sample (or time) vs. inverse of noise described the continuity of the powder flow.

The most important feature of NIR spectroscopy for flow monitoring is its use for real time evaluation of powder flow. As discussed in Chapter 2, the inverse of noise signal provides information regarding the strength of the flow, which is termed flow intensity. In addition, the standard deviation of the continuously acquired data on flow intensity also gives an indication of the flow uniformity. The average flow rate may be computed during the voiding experiment since the spectra give a clear indication of the beginning and end of the voiding process, which could be automated in the future using software. The average flow rate can also be easily

determined with a stop watch, but in this case, the NIR signals provide additional information, including chemical and physical properties, such as the average flow rate. The flow characteristics of dry-coated API blends were compared with the uncoated API blends, where the NIR signals provide average flow rate estimates. The flow of ibuprofen and acetaminophen blends was evaluated. The main feature of the NIR inverse noise signal methodology was used to examine the flow intensity and flow uniformity of the API blends. This was done for the case when the flow aid such as nano silica is blended using the industry standard methods that were described in "Sieve Mixing Method" and "Preblend (V-Blender) Method" sections as well as dry coating.
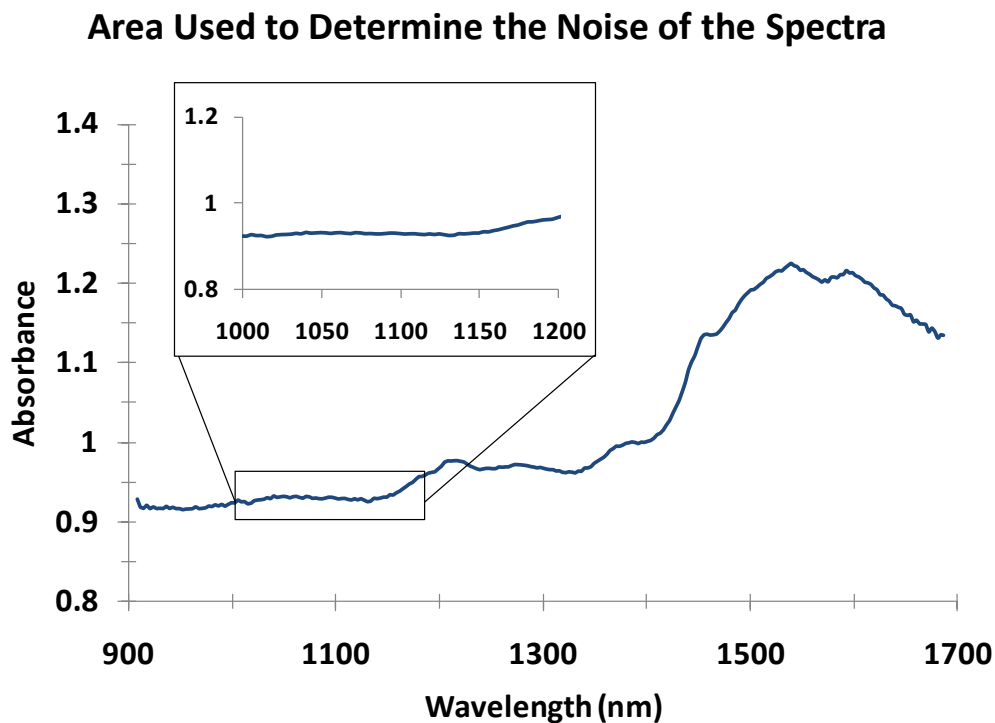
Figure 3.2 NIR spectra region used to estimate noise by measuring the standard deviation throughout the 1050–1070 nm regions (lactose mixtures cases).

3.3.2 Flow characteristics of uncoated and dry-coated ibuprofen blends

NIR spectroscopy was used to evaluate the flow of dry-coated acetaminophen and ibuprofen for the basic understanding of flow. The flow rate was based on the mass of powder voided and the time of voiding computed from the intensity of the inverse of the noise spectra (also called the flow intensity) of the NIR signals. In each case, a minimum of three replicates were done. Table 3.2 and Figure 3.3 illustrate the averaged flow rates of ibuprofen blends (Table 3.2 also lists the standard deviation of the flow rate) for either no coating (listed as 0% w/w) or two different levels of silica coatings (0.5% and 1% w/w). The blends were prepared in the V-blender by mixing lactose with previously dry-coated ibuprofen in 5%, 25%, 50%, 75%, and 100% w/w proportions. The general trend of better (or higher) flow rate was observed for 1% w/w nano-coated blend of ibuprofen as compared to 0.5% w/w coated blend for all the different compositions of blends. For the blends prepared from uncoated ibuprofen, an uninterrupted flow was observed for the 5% w/w of ibuprofen concentration only. However, flow with increasing level of interruptions was observed for the blend with uncoated ibuprofen concentration of 25%, 50%, and 75% w/w, while there was little or no flow for pure ibuprofen (i.e., 100% w/w).

Significantly improved flow rates were observed for the coated ibuprofen blends for the similar blend compositions. The flow rate was found to increase for higher proportions of coated ibuprofen blends up to 75% w/w, the opposite trend as compared to uncoated ibuprofen blends. The ibuprofen-coated (100%) sample resulted in lesser flow rates compared to the other compositions with 5%, 25%, 50%, and 75% w/w ibuprofen concentrations for the same coating levels of silica. The standard deviation in the flow rates was found to be low for the lesser concentrations of uncoated as well as coated ibuprofen in the blends and increased gradually as

the concentration of ibuprofen in the blends increased from 5% to 100% w/w. These results showed that dry-particle coating of ibuprofen improved flow for the pure API as well as its blends. The most improved flow rates were observed for the blends with higher loading of 75% ibuprofen concentration in the blend of (1% silica coated) ibuprofen. For 5% w/w API blends, uncoated ibuprofen blend had a better flow rate than the dry coated ones. This may be attributed to the fact that there was appreciable size reduction for the coated ibuprofen due to the dry coating process and the reduced size leads to higher cohesion of the blend despite having surface modification. The reduction size effect was observed by NJIT collaborator Lauren Beach using SEM Images of the Hydrophobic Silica-coated and Uncoated APIs.

Table 3.2 Flow rate results for uncoated and dry coated ibuprofen, blended with lactose at various concentrations.

Ibuprofen Concentration	Nano Coated Level (% w/w)	Flow (g/s)	Standard Deviation	Flow Interruption
5%	0	27.3	0.5	
	0.5	20.25	0.1	
	1	22.5	0.2	
25%	0	13.8	0.9	Yes
	0.5	18.6	0.3	
	1	22.95	0.3	
50%	0	0	N.A	Yes
	0.5	22.65	0.8	
	1	24.15	0.9	
75%	0	0	N.A	Yes
	0.5	20.85	2.1	
	1	31.5	1.6	
100%	0	0	N.A	No Flow
	0.5	13.95	2.6	
	1	20.25	0.9	

The results show that with a significant concentration of well-flowing excipient in the blend, there is no need to employ dry-coating. Nevertheless, the results shown in Figure 3.3 and Table

3.2 clearly indicate that dry coating is necessary when the API amount in the blend is 25% w/w or higher. As evidenced in the study even 100% API blends flow well due to the surface modification via dry coating.
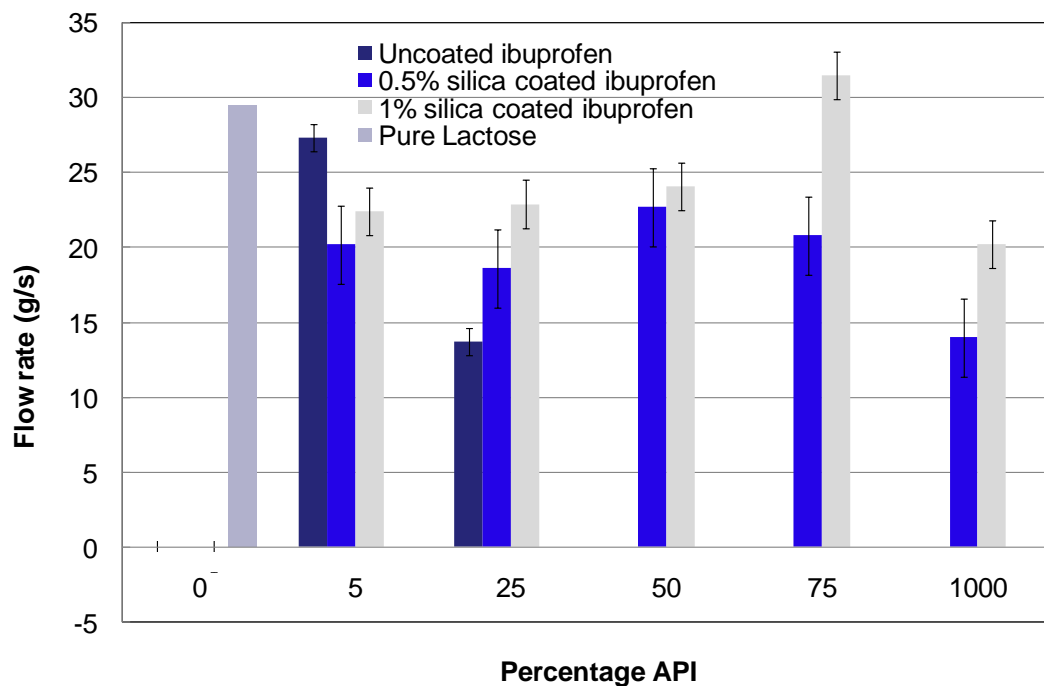
Figure 3.3 The average flow rates of uncoated ibuprofen blends with blends of two different levels of dry-coated silica; note 0% w/w API blend is composed of spray dried lactose monohydrate only. Also note that no flow was observed for uncoated blend beyond 25% w/w API.

3.3.3 Flow characteristics of uncoated and dry-coated acetaminophen blends

Acetaminophen flow rates were also characterized using the NIR method. The acetaminophen used in the study was very cohesive with electrostatic charges making it extremely difficult to handle during the processing by the NJIT collaborators in various devices for coating and in blending with excipients. Acetaminophen was dry coated with 0.5% and 1.0% w/w silica and further blended with lactose in a V-blender before voiding and evaluation by the

NIR method. The results of experiments, where a total of 75 g powder was voided, are presented in Tables 3.3 and 3.4, respectively, and Figure. 3.3 and 3.4.

In Tables 3.3 and 3.4, n represents the number of spectra recorded during the time taken by the powder sample to fully discharge from the funnel as indicated in the time column. The uncoated acetaminophen blends did not flow; not even at the lowest concentration of 5% w/w. The numerical results for the flow rates are only shown for the dry-coated API blends in Figure 3.4 and Tables 3.3 and 3.4.
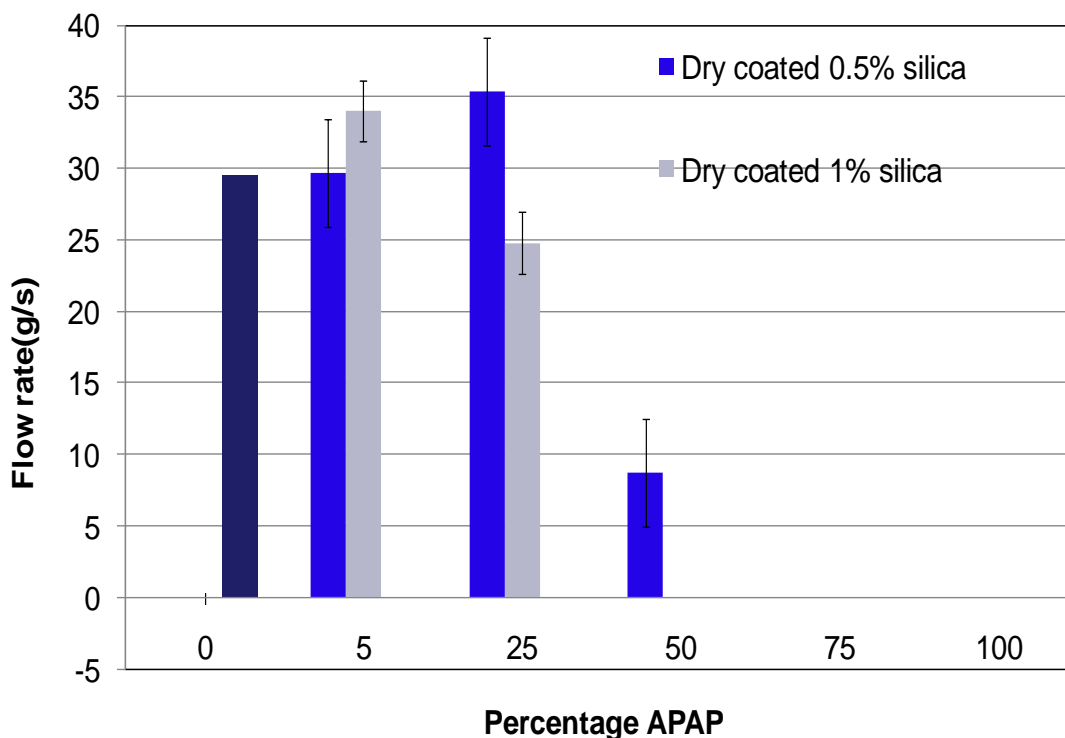
Figure 3.4 Average flow rates of uncoated acetaminophen (APAP) blends with blends of two different levels of drycoated silica; note 0% w/w API blend is composed of spray dried lactose monohydrate only. No flow was observed for any of the uncoated blends. Also no flow was observed for 75% and 100% blends of API having dry-coated silica.

Two different samples from the same batch (A and B) were used for the reproducibility of the characterization tests. The same powder sample from each blend was tested twice (results are

shown as A1 and A2 as well as B1 and B2 in Tables 3.3 and 3.4) for the repeatability of the tests. When the acetaminophen concentration in the blend was increased up to 25% w/w, the time taken by the blend to void completely also increased along with a corresponding decrease in the flow rate. In contrast to ibuprofen, acetaminophen blends were more poorly flowing, and at 50% w/w and higher API contents, flow interruptions occurred and the funnel required tapping to promote the flow and complete the voiding. This behavior was expected because of the much finer size of the APAP as well as its apparent high cohesion in comparison to ibuprofen. The number of taps can facilitate the flow as indicated by the fewer number of recorded spectra (9 as opposed to 50, 84, and 49) for the same sample, when no tapping was performed even though interruptions were observed in the flow. For 75% and 100% w/w of acetaminophen in the blend, no flow through the funnel was observed. For the blends prepared from 1% w/w silica-coated acetaminophen, good flow was observed until 25% w/w of acetaminophen concentration in the blend as opposed to the 50% concentration of acetaminophen in the 0.5% w/w silica-coated case (Table 3.3). The blends with more than 25% w/w acetaminophen concentration did not flow. In addition, the number of taps required to ensure the smooth flow were also more for 1% w/w coated blends as compared to the 0.5% w/w silica-coated blends of acetaminophen. The flow rate values calculated when tapping was required are only for the illustrative purpose and do not represent the continuous flow rates. Tables 3.3, 3.4 and Figures 3.3, 3.4, show that the dry-coated APIs blended with excipients performed significantly better than the blends prepared from uncoated APIs. Since acetaminophen is more cohesive and much finer than ibuprofen, the flow properties of its blends were poorer. The results indicate that the dry coating of the API is a viable and promising alternative for the higher drug loading scenarios of poorly flowing APIs.

Table 3.3 Flow rate results for 0.5% w/w silica dry-coated acetaminophen, blended with lactose at various concentrations.

APAP (%)	Run	Mass(g)	n	n (Average)	Time (s)	Flow rate (g/s)	Interruptions	Funnel Tapped
5%	A1	75	9	14	2.52	29.76		
	A2	75	15					
	B1	75	16					
	B2	75	16					
25%	A1	75	10	12	2.12	35.46	Yes	
	A2	75	10					
	B1	75	12					
	B2	75	15					
50%	A1	75	9	48	8.58	8.74	Yes	Once
	A2	75	50				Yes	
	B1	75	84				Yes	
	B2	75	49				Yes	
75%, 100%	A1	75	0	0	0.00	0.00	No Flow	
	A2	75	0				No Flow	
	B1	75	0				No Flow	
	B2	75	0				No Flow	

Table 3.4 Flow rate results for 1.0% w/w silica dry-coated acetaminophen, blended with lactose at various concentrations.

APAP (%)	Run	Mass (g)	n	n (Average)	Time (s)	Flow rate (g/s)	Interruptions	Funnel Tapped
5	A1	75	10	12	2.21	34.01		
	A2	75	10					
	B1	75	11					
	B2	75	18					
25	A1	75	17	17	3.02	24.88		
	A2	75	20					
	B1	75	15				Yes	Yes
	B2	75	15				Yes	Yes
50 75 100	A1	75	0	0	0.00	0.00	No flow	
	A2	75	0				No flow	
	B1	75	0				No flow	
	B2	75	0				No flow	

3.3.4 Flow uniformity results for blends of dry-coated APIS versus blended APIS from noise inverse signals

Flow aids such as nano silica are commonly used in pharmaceutical manufacturing to improve flow of API powders. The flow improvement was evaluated when the flow aid was added/blended as per the procedures described earlier ("Sieve Mixing Method" and "Preblend (V-Blender) Method" sections). In general, the flow observed from these two methods was poorer as compared to the dry-coated blends.

The time to void, and hence the average flow rate alone did not adequately characterize the flow. Many discharge experiments had interruptions, unevenness of the flow, or no flow without the gentle tapping of the funnel. The visual observation of the blends indicated better smoothness of flow for the dry-coated samples, and a number of experiments were filmed and included in the publication (Near-Infrared Spectroscopy for the In-Line Characterization of Powder Voiding Part II). For the purpose of quantification, information from NIR measurements was extracted by computing the inverse of the noise as described in Chapter 2. This measurement has been called the flow intensity index, with the higher values obtained for continuous flow and the lower values observed when the flow was less. The results for uncoated, sieve blended, pre-blended, and dry-coated flow of ibuprofen 50% w/w blends are illustrated in Figure 3.5 a), b), c), and d), respectively. As shown in Table 3.2, uncoated ibuprofen (50% w/w concentration) blend did not flow, which is clear from the very low value of the inverse noise signal. Figure 3.5 shows that the flow intensity was highest for the dry-coated blends, followed by the pre-blended, and then sieve-blended. In addition to computing the flow intensity, the NIR signals are used to

understand flow uniformity because higher fluctuations for flow intensity (evaluated via taking a RSD) indicate higher fluctuations in the flow of the powder.

The RSD of flow intensity can be used to quantify and assess the consistency in the powder flow, and it may be then called the flow uniformity index. Therefore, in addition to the flow intensity plots during the voiding experiment, their average value as well as RSD were computed and illustrated in Figure 3.6 for ibuprofen blends. Figure 3.6 clearly shows that the flow performance of dry-coated blends is the best, since the average flow intensity is highest while the RSD, i.e., the flow uniformity index, is the lowest, indicating the flow smoothness. The average flow intensity values obtained from the sieve mixed and pre-blended methods are significantly lower than the dry-coated blends and thus indicate poor flow compared with the dry-coated case. Moreover, the dry-coated blends have the lowest RSD of the three cases and the most uniform flow.

The flow intensity and the flow uniformity are also computed for the 5% and 25% w/w API concentration blends prepared for the coated samples of acetaminophen because the average flow rate for those concentrations was not better than the case of uncoated API blends. However, the results for the flow intensity and the flow uniformity index, shown in Figure 3.7, indicate equal (for 5% w/w) or better (for 25% w/w) flow properties for dry-coated blends as compared to their respective uncoated counterparts.
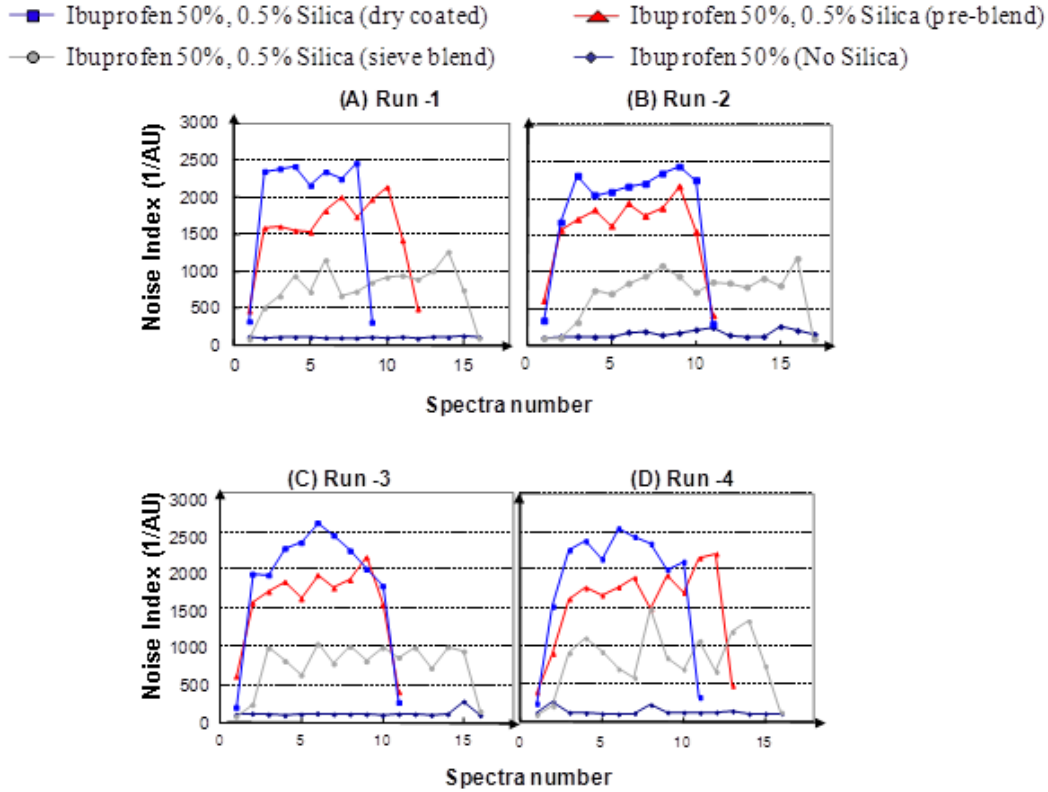
Figure 3.5 Signal to noise ratio for ibuprofen processed using various methods. Higher signal indicate higher flow intensity and lesser fluctuations indicate the flow smoothness.
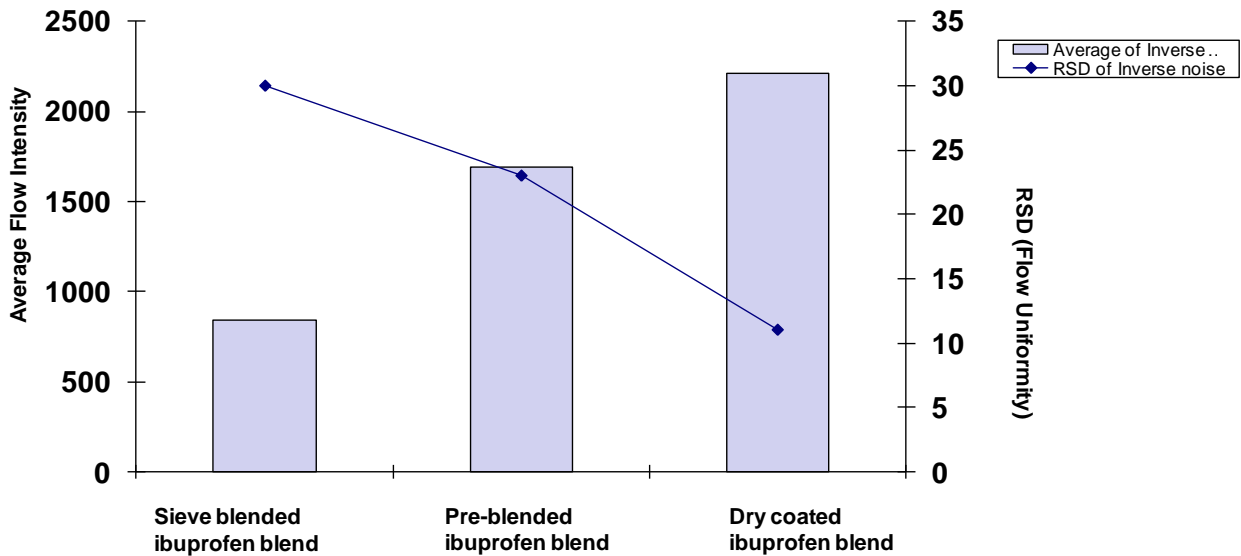
Figure 3.6 Average values and relative standard deviations for the flow intensity for 50% w/w ibuprofen with 0.5% w/w silica blends prepared using different methods. The RSD of the flow intensity represents the uniformity of the flow.
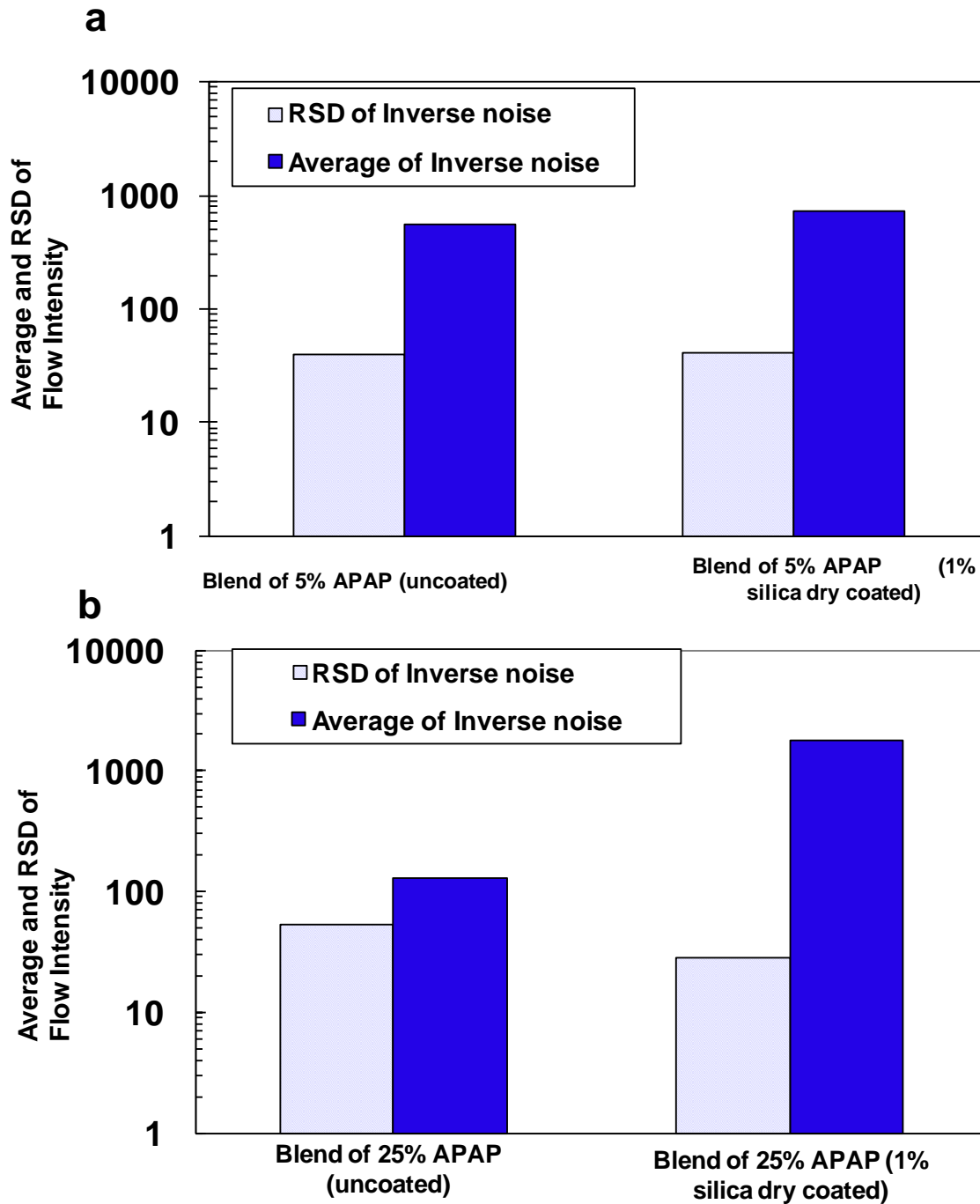
Figure 3.7 Log plot of average and relative standard deviation of flow intensity for acetaminophen blends prepared using a) 5% w/w and b) 25% w/w, uncoated and coated APIs, respectively. The RSD of the flow intensity represents the uniformity of the flow.

Although the average flow rate of 5% w/w uncoated acetaminophen blend was higher than the dry coated acetaminophen blend, the flow intensity as well as the flow uniformity for the 5% w/w uncoated and coated blends was similar despite the size reduction after dry coating. On the other hand, for 25% w/w blends, the flow intensity and the flow uniformity were enhanced for the dry-coated blends as showing the plot employing the log scale (Figure 3.7).

3.3.4.1 Surfaces distribution of flow aid particles

The   results for the flow intensity and the flow uniformity index, indicate better flow performance for dry-coated APIs particles as compared to uncoated, pre-blender and sieve-mixed API particles (figure 3.5). Yang et al. explained that for coating process using the same amount of silica (1%) as flow aid particles, the flow performance is a function of coating efficiency method.[54] Yang compared SEM images of coated cornstarch obtained from dry-coated, V-Blender and hand mixing methods. For dry-coated particles the SEM images show that the silica particles are dispersed evenly onto the cornstarch particles and there are no observed large silica agglomerates with surface coverage of 10.72%. The V-blender is also capable of coating fumed silica onto cornstarch, but the distribution of the fumed silica on the surface of cornstarch is not uniform. For V-blender coated particles Yang described agglomerates of fumed silica look like ''patches'' on the cornstarch surface and some small silica agglomerates, as well as uncoated cornstarch surfaces with surface coverage of 6.74%. Hand mixing method is only capable of coating part of cornstarch surface, and large individual agglomerates nano silica are observed on the coated particle with surface coverage of 1.72%.[54]

the SEM images of acetaminophen and ibuprofen dry-coated particles show that silica particles were discretely and uniformity coated (Near-Infrared Spectroscopy for the In-Line

Characterization of Powder Voiding Part II: Quantification of Enhanced Flow Properties of Surface Modified Active Pharmaceutical Ingredients). The ibuprofen and acetaminophen powders have poor flowability due to the cohesion force arising mainly from Van der Waals attraction. nano silica particles discretely coated onto the surface of cohesive to improve the flowability. However, nano silica particles have a tendency to form agglomerates. in the case of sieve mixed the results indicate that sieved process particles, breaking the agglomerates of ibuprofen and in the mixed achieve a better distribution of silica on the surface of ibuprofen. the pre-blender without sieve step, still contains agglomerates of ibuprofen and presents a poor distribution of silica on its surface. Thus, proper dispersion of the flow agent is a very important issue for obtaining discrete coating and flowability improvement.

3.3.5 Angle of repose of blends of coated APIs

In order to corroborate and compare the observations from the in-line NIR signals of the powder; the angle of repose of the blends of uncoated as well as dry-coated APIs was evaluated in a commercially available device, Hosokawa Micron Powder Tester by the NJIT collaborations to provide an independent flow property index to compare against NIR results. Results are shown in Figures 3.8 and 3.9 for acetaminophen and ibuprofen, respectively. In these figures, lower AoR values indicate better flow; each figure also shows the general flow categories as per the ASTM standard. The results with angle of repose are equivalent to those shown in Figure 3.3 obtained using in-line NIR signal of powder flow. Both APIs showed trends of improved flow similar to those observed via NIR approach; i.e., for the blends with lower API concentrations (5% and in some cases, 25%) uncoated blends are better, while for higher API concentrations,

dry-coated blends clearly outperform. The dry coating performed induced size reduction, which may be the cause of poorer performance of lower API concentration blends. In both the cases, the flowability of dry-coated samples was remarkably better than uncoated samples for the higher API concentrations, an important result that enables the use of high drug loaded blends which would not be otherwise possible.
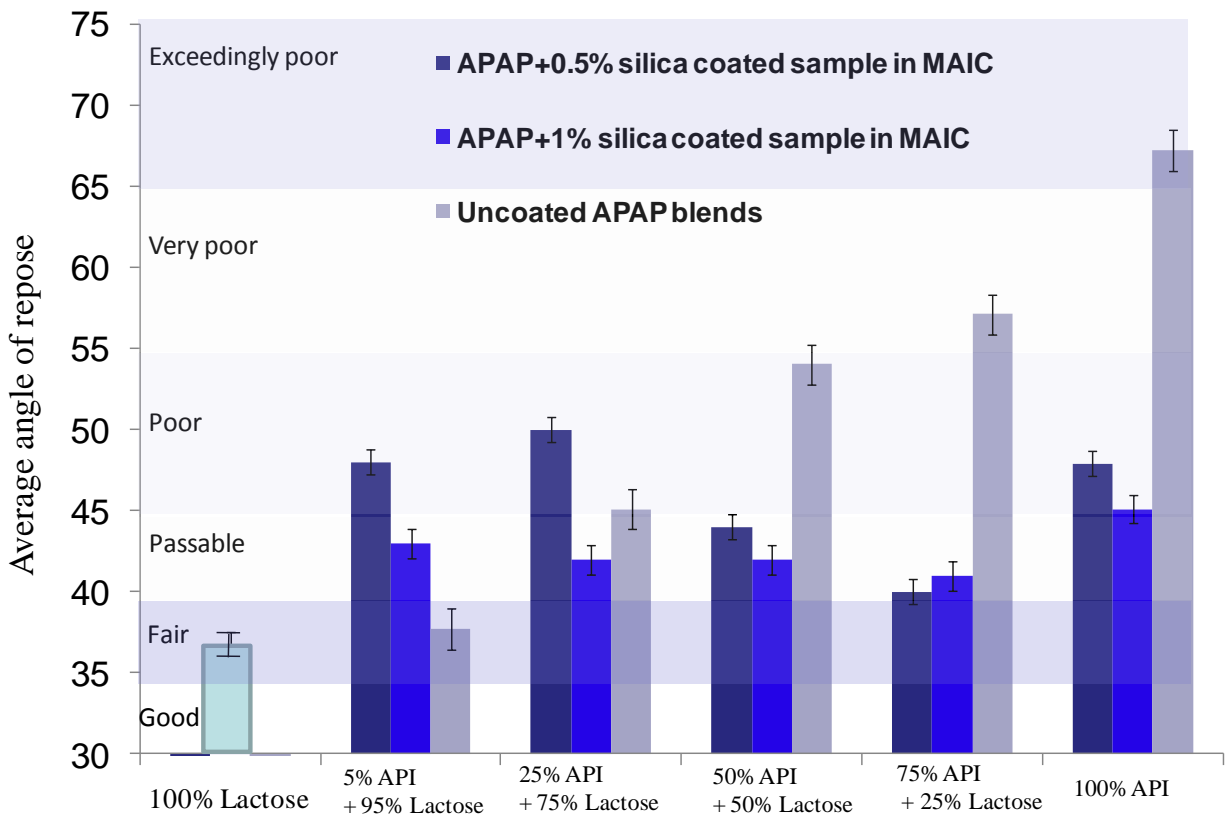
Figure 3.8 Averaged angle of repose of silica dry-coated acetaminophen blended with spray dried lactose monohydrate.
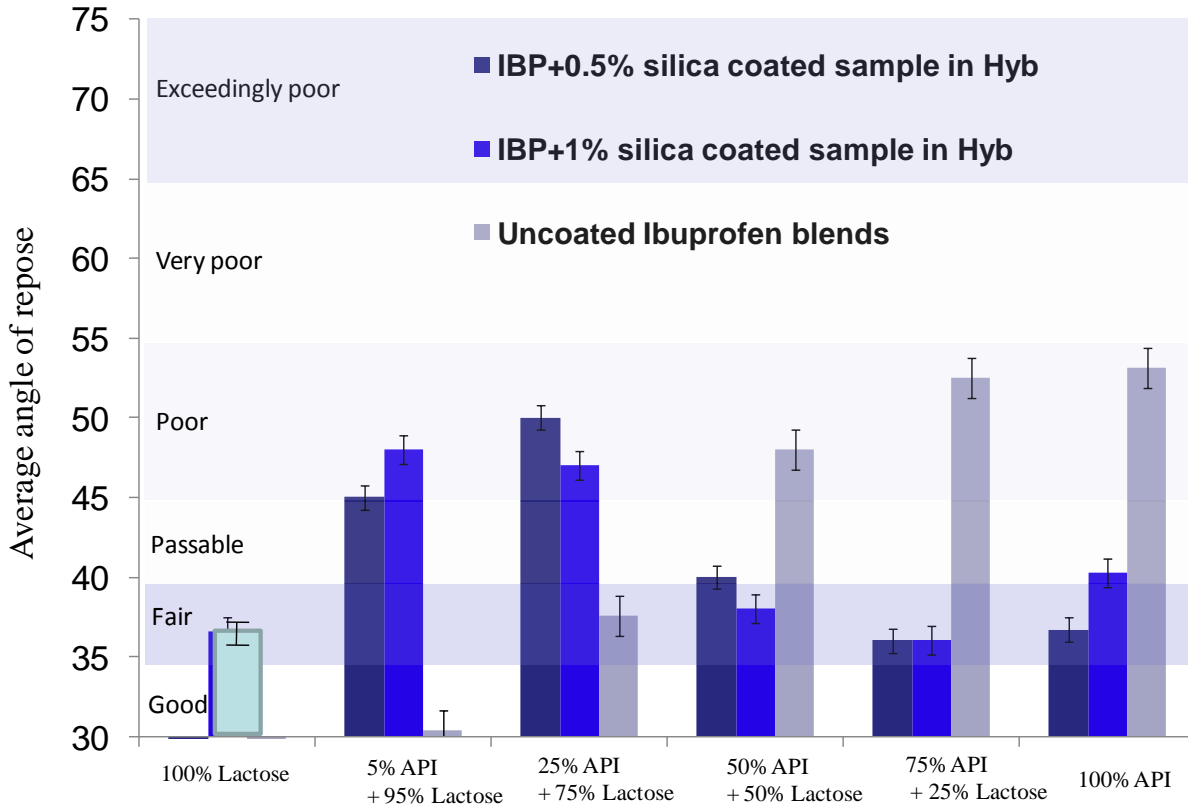
Figure 3.9 Averaged angle of repose of silica dry-coated ibuprofen blended with spray dried lactose monohydrate.

3.3.6 Gravimetric feeder study using real time NIR evaluation

NIR real time evaluation of flow continuity and in-line gravimetric measures were compared in the study of powder feeders. The obtained results show higher RSD for the 1/noise measures in contrast to lower RSD from in-line gravimetric measures of the same feeder operation. Figure 3.10 presents the in-line NIR and gravimetric measures from one selected feeder condition. Figure 3.10a) shows the in-line NIR and gravimetric data, using MCC PH302 (~100 μm particle size), at nominal flow rate of 10 g/min and Non-optimal settings in the KT20.

This experiment (Figure 3.10) shows differences and equivalences using the two methods to follow the feeding process. The first difference was the units, gravimetric measures appear in g/min and the spectroscopic measures have unit of 1/noise. The second observation between gravimetric and NIR method was difference in RSD. The different RSD of the same process is explained by the frequency of data acquisition. In-line Gravimetric measures acquire a measurement per second and the RSD obtained was 17.3%. In-line NIR spectroscopy acquire data every 200 ms and the RSD obtained was 29.1%. Thus, the larger acquisition time was equal to average sequential measures. The results of RSD for in-line gravimetric measure and in-line NIR spectroscopic flow measured were in agreement whit the reported by Li et al 2003, the standard deviation increase significantly when the sampling size decrease.[56]

Gravimetric flow rate and 1/noise average were compared to evaluate the response of NIR method when flow rate changes. Figure 3.11 shows 9 feeding processes at 3 levels of flow rate and 3 different MCC. The average flow rate and the average 1/Noise show a direct relation for the 3 different MCC. As explained in Chapter 2, the principal value of the NIR method is evaluating the consistency of the powder flow, but the observation using gravimetric flow rate can be matched with NIR spectroscopic method.
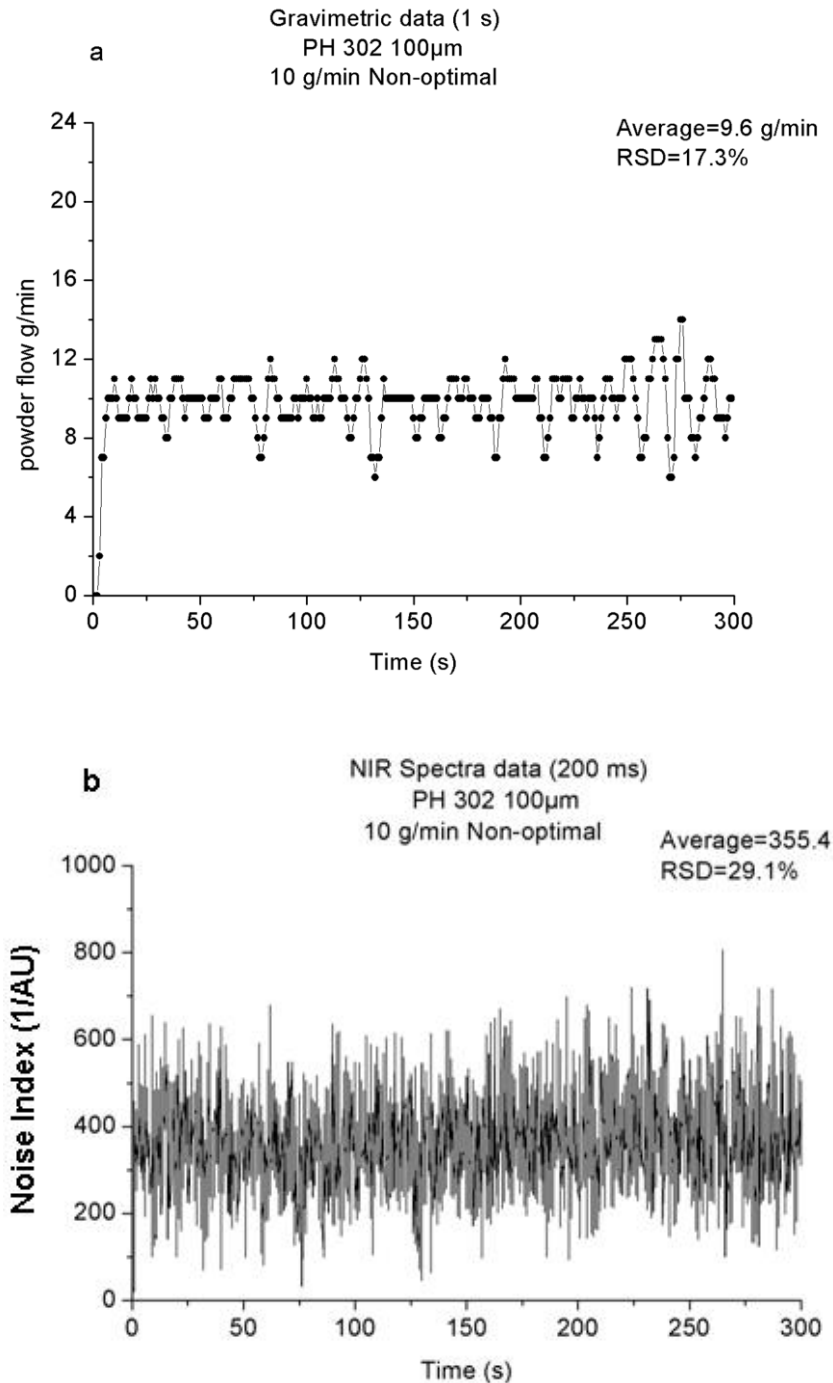
Figure 3.10 Gravimetric data of flow rate (g/min) continuity during a powder feeder of MCC PH302, obtained by KT20, acquisition time 1 second. b) 1/noise of NIR spectroscopic data from powder flow continuity, obtained during a powder feeder of MCC 302, operation, acquisition time 200 milliseconds.
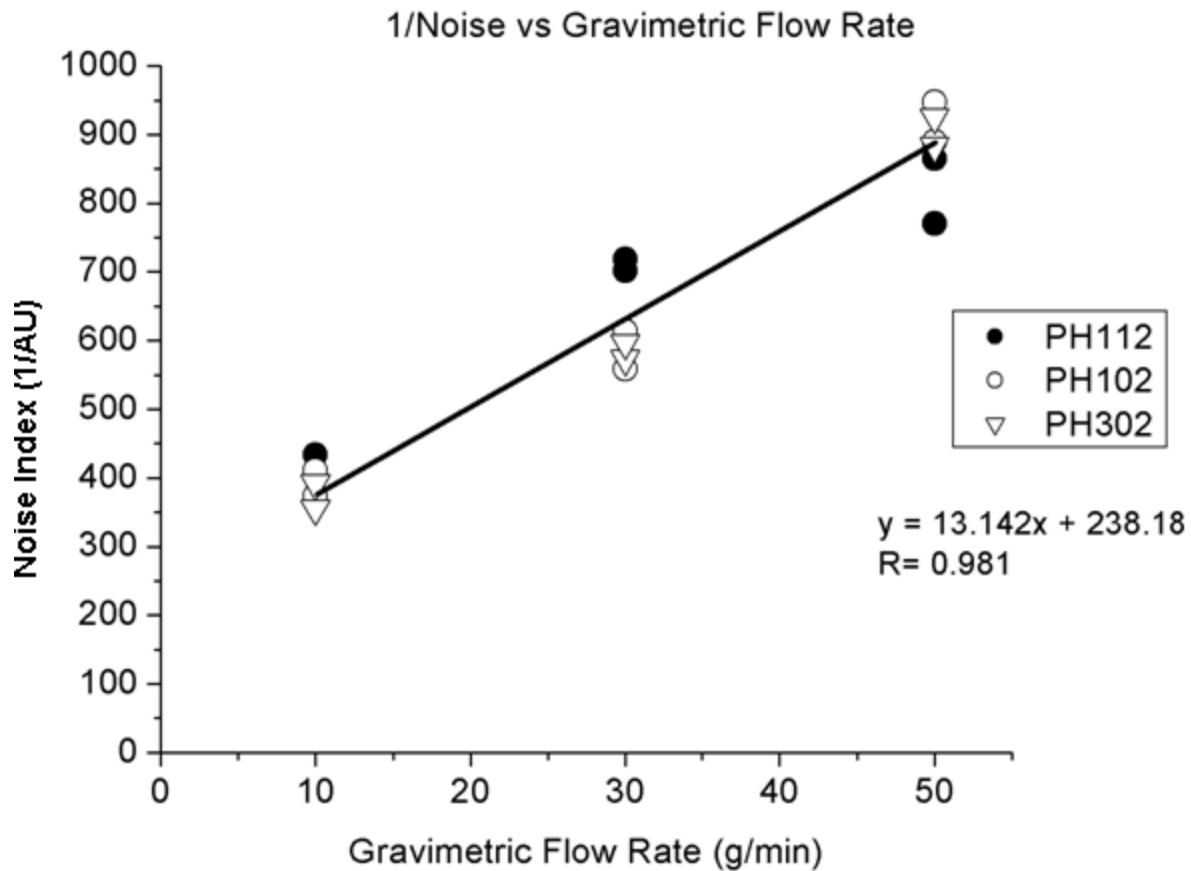
Figure 3.11 Gravimetric flow rate and 1/noise average for 3 different feeding processes at 3 levels of flow rate, every process performed for 5 minutes.

3.3.7 NIR flow continuity and flow rate

In general the RSD obtained from NIR real time sensor of flow continuity; show that the flow rate was inversely proportional to RSD. In the specific case of a particle size of 20μm and the same control settings the inverse relation was easy to follow (Table 3.5). The obtained relation between NIR RSD and flow rate was not easy to follow in the cases of 50 and 100 μm at the three flow rates. Table 3.5 shows the RSD results in function of flow rate, particle size and control settings.

3.3.8 Powder flow continuity and particle size effect

Particle size shows a decreasing relationship with the obtained RSD at constant levels of flow rate and control settings, as shown in Figure 3.12. The obtained results of RSD and particle size were summarized in the Table 3.5. The results showed that particle size and RSD relationship was intertwined with flow rate and control settings conditions.
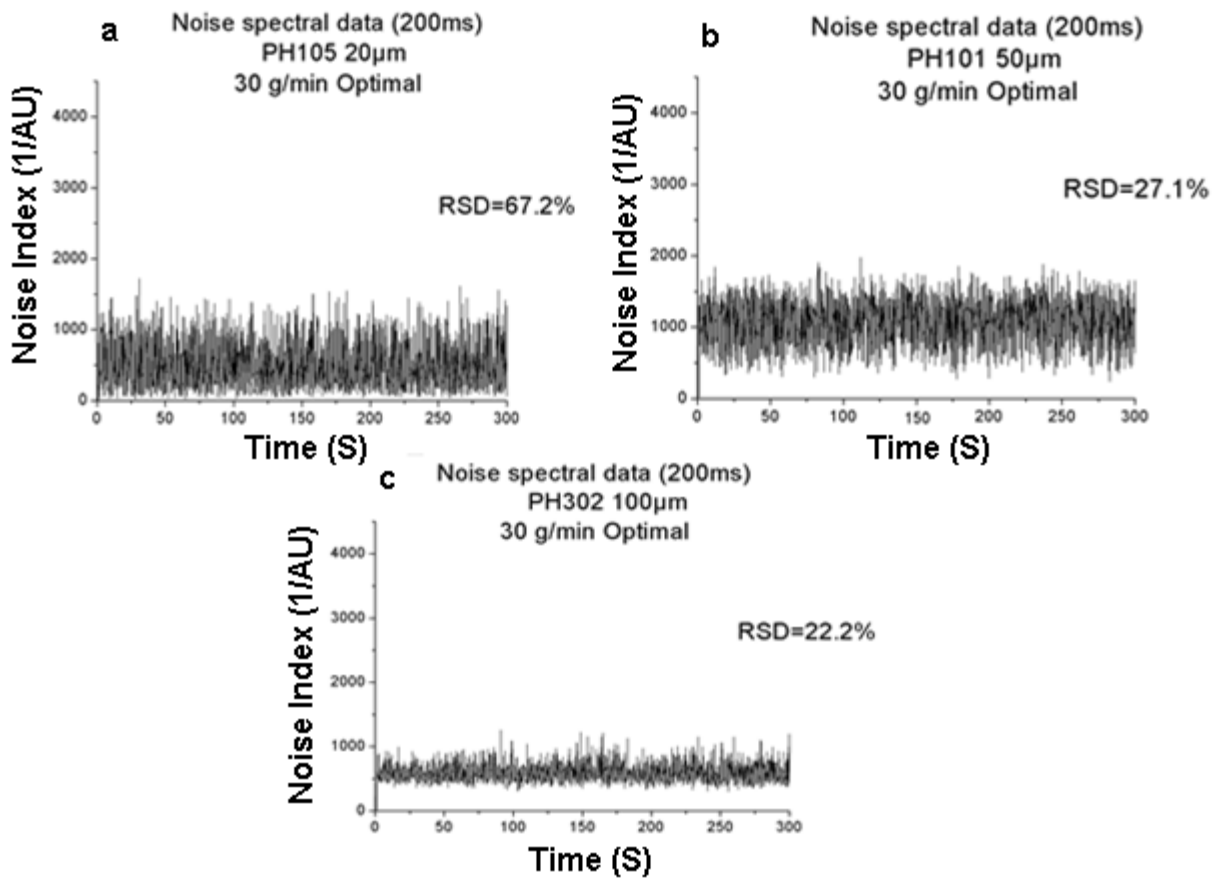
Figure3.12 1/Noise spectroscopic data from powder flow feeder operation at three different particle size levels a) 20 µm of average particle size b) 50 µm of average particle size c) 100 µm of average particle size.

3.3.9 Powder flow continuity and control settings

Control settings modulate the screw speed variation. Alterations in the speed set for the material flow, require adjustments in the screw speed. The adjustment screw speed is made by the process controller. The process controller makes adjusting speed using constant acceleration (non optimal settings) or Variable-acceleration (optimal settings).Constant acceleration of feeder screw was designed by non optimal settings and represented by 0 in control setting column Table 3.5. Optimal settings mean a variable acceleration of screw speed variation and were represented by 1 in control setting column (Table 3.5).

The effect of control settings (optimal and non optimal) was evaluated over the RSD of powder feeders process (Table 3.5). In general cases (particle size of 50 and 100 µm) the results shows higher RSD values using non optimal settings and lower values of RSD using optimal setting; but a clear tendency was not observed for 20 µm particle size. The relation between RSD, control setting and flow rate, show less influence of control settings that the influence of flow rate over the resulting RSD.

The interdependency of variables in the gravimetric feeder process required a method that allows visualize in multiple dimensions, how similar or different are the variables that control RSD in gravimetric feeder process. PCA was the selected method to visualize the relation of variables in a multiple space.

Table 3.5 RSD results of microcrystalline cellulose feeding at different particle size, flow rate and control settings condition.

	NIR RSD (%)	Particle size d50(μm)	Flow Rate (g/min)	Control Settings
PH101AN	56.8	50	10	0
PH101BN	29.7	50	30	0
PH101BO	27.1	50	30	1
PH101CN	29.2	50	50	0
PH101CO	25.5	50	50	1
PH102AN	25.2	100	10	0
PH102AO	20.5	100	10	1
PH102BN	25.2	100	30	0
PH102BO	19.4	100	30	1
PH102CN	27.3	100	50	0
PH102CO	24.6	100	50	1
PH105AN	91.2	20	10	0
PH105AO	107.2	20	10	1
PH105BN	68.2	20	30	0
PH105BO	64.3	20	30	1
PH105CN	46.9	20	50	0
PH105CO	49.0	20	50	1
PH112AO	20.1	100	10	1
PH112BN	24.9	100	30	0
PH112BO	20.5	100	30	1
PH112CN	39.7	100	50	0
PH112CO	26.4	100	50	1
PH302A N	29.7	100	10	0
PH302A O	27.5	100	10	1
PH302B N	25.1	100	30	0
PH302B O	22.2	100	30	1
PH302C N	29.3	100	50	0
PH302C O	26.6	100	50	1

3.3.10 Principal component analysis (PCA)

A principal component analysis of MCC gravimetric feeder observation (Table 3.5) was performed to understand the relationship between particle size, flow rate and control settings with NIR RSD. The first step in the principal component analysis consisted of applying autoscaling to the data. The autoscaling transforms the measures, dividing each value in the column (variable) by the standard deviation in the selected column; after transform the new standard deviation by variable was 1.

The results of PCA analysis appear summarized in Figure 3.13 a) and b), showing the variable distribution described by loadings plot, and the sample alignment described by scores plot. Loading 1 described 46% of the variation of the data, and revealed an inverse relationship between the RSD and the particle size (Figure 3.13). The PC loading 2 described 25% of the variation, showed an inverse relation between the RSD and control settings but presented a direct relation between flow rate and RSD. The PC loading 3 describes 24% of the variation of the data (not shown), and indicates the direct variation between control settings level and RSD. All the loadings results obtained on the PCA using the chemometric software PLS Toolbox v4.2 (Eigenvector Research) under Matlab (v 7.0, The Mathworks), appear listed in Table 3.6; all the scores of PCA appear listed in Table 3.7.

Table 3.6 PC loadings result of PCA analysis of gravimetric feeder process.

	Variation (%)	RSD	P size		C Settings
PC-1	46	-0.70263	0.66090	0.22516	0.13712
PC-2	25	0.035841	0.17723	-0.77620	0.60399
PC-3	24	0.046306	-0.29843	0.54343	0.78323
PC-4	5	0.70918	0.66537	0.22684	0.05419
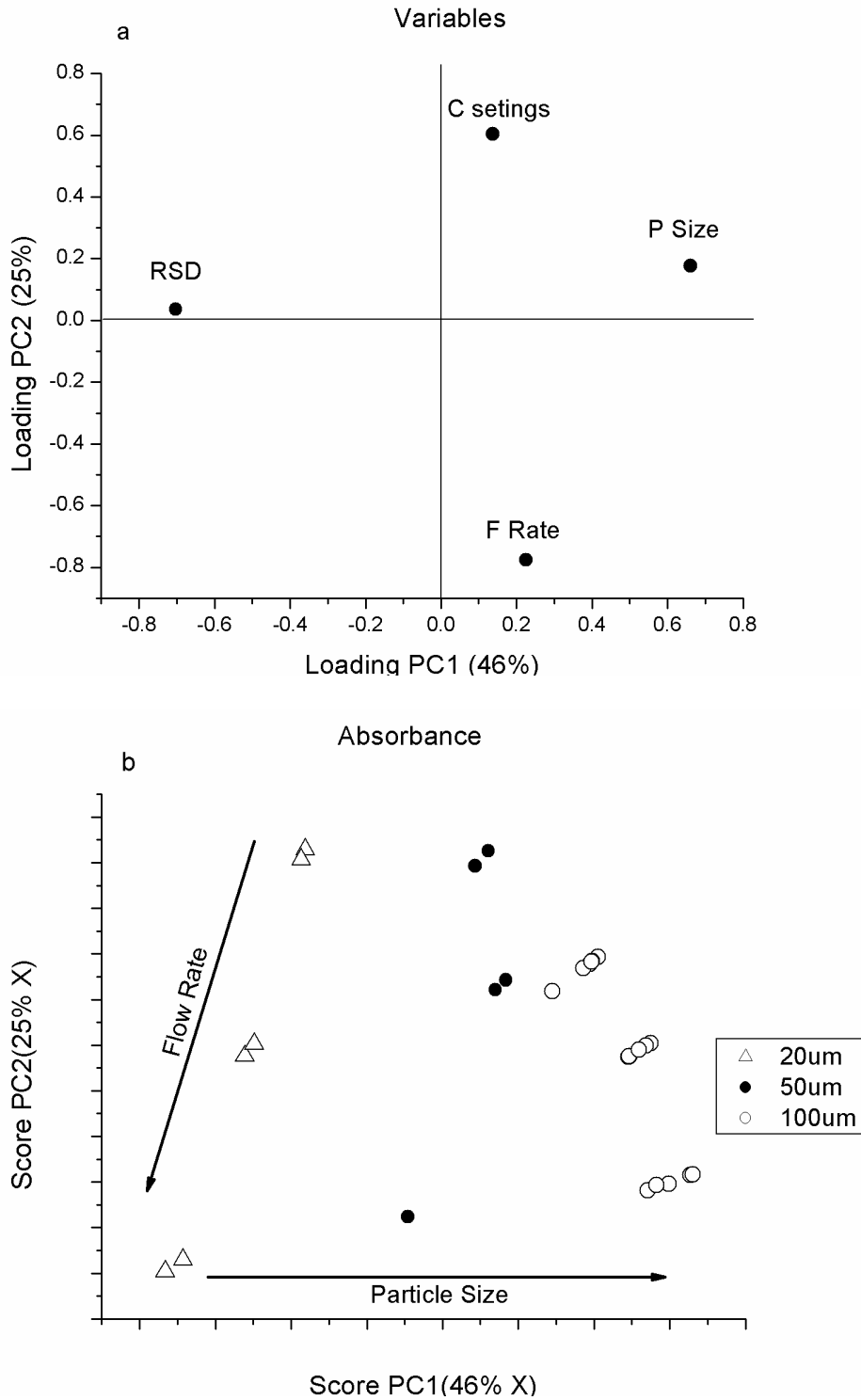
Figure 3.13 Loading and score plot of PCA of feeder process using MCC at three levels of particle size, three levels of flow rate and two different acceleration settings.

Table 3.7 PC Scores results of PCA analysis of gravimetric feeder process.

	PC-1	PC-2	PC-3	PC-4
PH101AN	-31.54866	-20.44174	-4.719769	-0.4778799
PH101BN	-17.29417	7.908206	-16.22662	-0.5741873
PH101BO	-16.03889	8.910956	-18.18654	0.4136749
PH101CN	-16.3109	25.6575	-7.051782	-0.5422241
PH101CO	-14.4395	27.15239	-9.971855	0.4396831
PH102AN	27.5105	-21.18886	-8.129098	-0.5505947
PH102AO	29.83938	-19.32855	-11.76211	0.4268907
PH102BN	28.31187	-3.584861	1.329211	-0.5168735
PH102BO	31.16959	-1.302133	-3.127922	0.4555007
PH102CN	27.99827	13.12853	12.52509	-0.4723756
PH102CO	29.36198	14.21789	10.3962	0.5144386
PH105AN	-74.62999	-26.10075	9.241016	-0.3603515
PH105AO	-82.51806	-32.40144	21.52998	0.7158841
PH105BN	-62.41907	0.6168647	0.9188193	-0.4369072
PH105BO	-60.4794	2.166287	-2.107648	0.5443401
PH105CN	-51.08283	26.63581	-6.040277	-0.5050088
PH105CO	-52.11794	25.80906	-4.430887	0.5049908
PH112AO	30.06245	-19.15037	-12.10974	0.4247347
PH112BN	28.41832	-3.499837	1.16333	-0.5179023
PH112BO	30.62136	-1.740043	-2.273569	0.4607995
PH112CN	21.87322	8.236016	22.07029	-0.4131751
PH112CO	28.47872	13.51237	11.77265	0.5229756
PH302A N	25.27999	-22.97053	-4.653093	-0.5290362
PH302A O	26.39745	-22.07787	-6.398236	0.4601582
PH302B N	28.36653	-3.541203	1.244036	-0.5174018
PH302B O	29.79766	-2.397991	-0.9899224	0.4687608
PH302C N	27.00922	12.33851	14.0664	-0.4628162
PH302C O	28.38288	13.43581	11.922	0.5239019

The PC scores 1 confirm the variation of samples in function of particle size; samples with

higher particle size (100 μm) were classified in the positive axis of PC1, particle size of 50 μm

has centered position in the PC 1, and samples with lower particle size (20 μm) appear at negative values of PC1.

The PC score 2 shows the variation of samples in function of flow rate and control setting, lower values of PC 2 were assigned to samples with flow rate of 10 g/min, the medium values of PC 2 correspond with a flow rate of 30 g/min, and higher values of PC 2 correspond to a flow rate of 30 g/min, and higher values of PC 2 correspond to a flow rate of 50 g/min (Figure 3.13 b).Figure 3.13 b also shows a direct relation of RSD values with optimal control settings. A thorough evaluation of Figure 3.14 and Table 3.5 could also lead to the observations using PCA will, but PCA provides a graphical and abbreviated way to describe the relation of variables and samples aggregation.

3.3.11 Feeding process of V-blended vs nano-coated materials

Using an identical setup for the Ktron feeder, nanocoated and V-blender material was compared to study powder continuity for three different mass flow rates and two levels of control settings. The measurements were performed using the NIR real time sensor of flow continuity. The results were summarized in Table 3.8. The interdependency of variables in the gravimetric feeder process required a method that allows visualize in a space of multiple dimensions, again PCA was the selected method to visualize the relation of variables.

PCA of gravimetric feeder results (Table 3.8) was performed to understand the relationship between coating level, flow rate, control settings and RSD. The first step in PCA was autoscaling of the data. The loading obtained on the PCA was summarized in Table 3.9 In the case of feeding pure ibuprofen usingthe K-Tron T20 gravimetric feeder, the principal source of variation was the control settings. PC loading 1 described 39% of the variation of the data, and revealed an inverse

relationship between the RSD and the control settings. The PC loading 1 shows a direct relation

between RSD and coated levels.

Table 3.8 RSD of ibuprofen feeding at different flow rate, control settings and coated method.

	RSD	COATED	F Rate (g/min)	C Settings
BBSDAN	23.603	0	10	0
BBSDAO	24.397	0	10	1
BBSDBN	19.627	0	30	0
BBSDBO	21.579	0	30	1
BBSDCN	38.826	0	50	0
BBSDCO	24.356	0	50	1
NCSDAN	36.247	1	10	0
NCSDAO	23.933	1	10	1
NCSDBN	28.301	1	30	0
NCSDCN	21.95	1	50	0
NCSDCO	21.95	1	50	1

Table 3.9 Loadings results of PCA analysis of gravimetric feeder process from V-blended vs Nano-coated ibuprofen.

	Variation (%)	RSD	COATED	F Rate (g/min)	C Settings
PC-1	39	0.599339	0.464794	0.107128	-0.64287
PC-2	28	0.078908	-0.52316	0.832179	-0.166
PC-3	18	0.652072	-0.61677	-0.4316	0.09007
PC-4	15	0.457568	0.360367	0.33124	0.742326

The second source of variation was split between flow rate and coated level; the PC loading

2 described 28% of the second variation, showed a direct relationship between the RSD and flow

rate; and described an inverse relation between coated level and RSD (Figure 3.14). The PC

loading 3 described the 19% of the variation of the data (not shown), and relate the inverse

variation coated level and RSD but show a dependence of flow rate again.
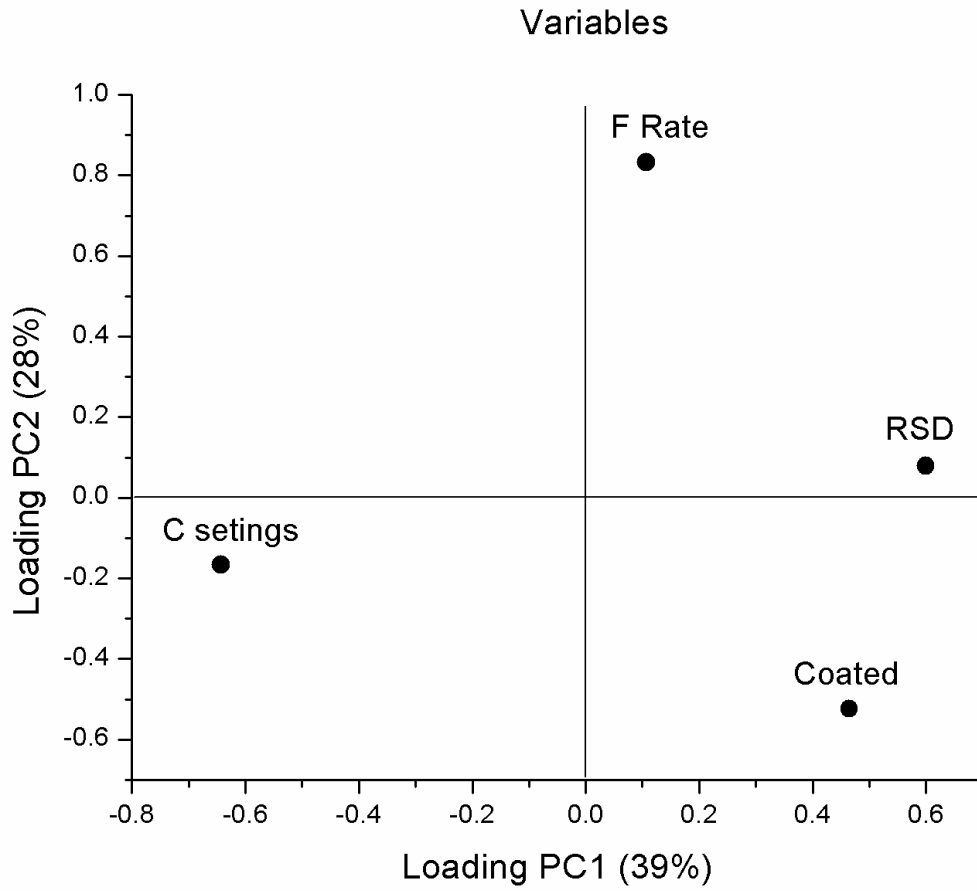
Figure 3.14 Score plot of PCA feeder process using nano-coated and V-blending ibuprofen at three levels of flow rate and two different acceleration settings.

3.4 Conclusion

Through characterization done via the novel application of in-line NIR spectroscopy, dry coating is shown to be very effective in powder flow enhancement and results in significantly improved flow uniformity during the voiding of blends of API powders. It is shown that the blends prepared from dry-coated APIs, ibuprofen and acetaminophen, had better flow intensity and uniformity as compared to the uncoated API blends. Angle of repose measurements corroborated the flowability results obtained from the real time NIR measurements.

The powder flow continuity depends of the combination of factors present in the flow process, this affirmation was valid for free fall powder process and feeding powder process. The range of study variables shows two principal sources of variation. In the free fall powder process, particle size was the principal source of variation. The second case when feeder controls the powder flow, control settings have the bigger source of variation.

The NIR method clearly shows that the surface modification of API powders via the dry coating method results in improved flow properties when compared with addition of flow aid done through industry standard methods. Dry-coated blends with higher API content showed much better flow properties as compared to the V-blender silica-added API blends. This is a significant result because most formulators need capability of handling higher API loadings for number of APIs having higher dosage requirement.

Chapter 4. Deconvolution of Chemical and Physical Information from Intact Tablets

Published in *Journal of Pharmaceutical Sciences*, 2009, *Volume 98, Numbers 8*, Pages 2747-2758. And *Applied Spectroscopy*, 2011, *Volume 65, Numbers 4*, Pages 459-465.

4.1 Summary

NIR spectra provide both physical and chemical information; however most research efforts have been directed to chemical applications where drug or moisture concentrations are determined. Research efforts directed to obtain physical information from NIR spectra have been very limited.[21, 28] The first section of this chapter describes the use of NIR spectroscopy for real-time determination of tablet compaction pressure in moving tablets. The compaction pressure was determined for lactose monohydrate tablets where the compaction pressures were varied from 117–700 MPa. This was a first step in efforts to develop methods for online measure of compaction pressure as input for real-time control and decision-making in tablet compression.

The second sections of this chapter used NIR spectroscopy to study pharmaceutical tablets with large variation in both chemical and physical variables; drug concentration (15–85% w/w) and compaction pressure (100–500 MPa). The traditional two-way calibration strategies, such as Partial Least Squares (PLS), do not allow the obtaining of multivariate model with good predictive ability (nin-linear predictions and prediction error over 8% w/w) with such significant variations in compaction pressure. The presented strategy uses Parallel Factor Analysis (PARAFAC) to deconvolute in-line NIR spectra in scores associated with drug concentration variation, and loadings related with wavelength range and compaction range. The PARAFAC deconvolution was followed by Multiple Linear Regression (MLR) to obtain the simple

calibration model with a better predictive ability on the whole compaction pressure range (prediction error less than 1.4% w/w).

The third section of this chapter describes the use of Near-infrared chemical imaging (NIR-CI) to study pharmaceutical tablets that undergo tablet relaxation. NIR-CI spectra of lactose monohydrate tablets were acquired and the spectral slope from each pixel in the data hypercube was used to assess tablet compaction and relaxation over the time. Tablets were prepared at compaction pressures of 100, 300 and 500 MPa using un-lubricated and magnesium stearate lubricated lactose monohydrate. Results show that NIR slope distribution is a function of applied compaction forces and magnesium stearate lubrication. The distribution of NIR slope values was studied using histograms and statistical parameters. The mean slope value yields a linear calibration curve that predicts tablet compaction pressure as a function of spectral slope. The NIR-CI slope measurements were also used to study tablet relaxation which occurs as tablets release some of the stored energy from compression. The NIR-CI slope method provides a qualitative description of the relaxation process and provides quantitative information describing relaxation through time.

4.2 Materials and Methods

4.2.1 Tablet Preparation

The materials chosen for this study were acetaminophen (micronized grade), supplied by Mallinckrodt, Inc., Hazelwood, MO. Commercial microcrystalline cellulose (MCC) 90 (JRS Pharma), lactose monohydrate, Flowlac 100 ® Ph. Eur/USP-NF/JP and magnesium stearate (MgSt) Kosher (Peter Greven Fett-Chemie GmbH & Co. Kg; Venlo, The Netherlands).

Seven mixtures of acetaminophen (APAP) and microcrystalline cellulose (MCC) were prepared covering a concentration range of 25–85% w/w of APAP every 10%. For this purpose, a total of 25 g of each mixture were prepared, weighing appropriate amounts of both pure ingredients, using an analytical balance with 0.00001 g of tolerance.

Aliquots of 350 mg were withdrawn from every mixture to obtain laboratory tablets with a diameter of 15mm, applying a compaction pressure of 100-500 MPa every 100 MPa (accuracy 29 MPa), using a manual single punch model 3912 Carver press. A total of 210 tablets were obtained (six replicates, seven APAP concentration levels and five compaction pressures).

Tablets with an average weight of 201±2 mg of pure-lactose or lubricated with 0.50% w/w MgSt were prepared for the relaxation study. The tablet height ranged from 2.50 – 2.95 mm and the diameter was 13.30 mm. Three groups of tablets were made with compaction pressures of 100, 300 and 500 MPa using a manual single punch model 3912 Carver press. The time spent at maximum compression was 20 seconds for each tablet. A total of 18 tablets were obtained (three individual preparations at every compaction pressure level). Each tablet subset was maintained in plastic sealed vials to avoid moisture absorption, and placed in closed desiccators after the initial measurement (marked as 0 hour). Two additional measurements were taken at 24 and 48 hour after the initial measurement. Two measurements were performed per tablet, top and bottom surface. 36 tablets of pure lactose at six levels of compaction pressure were prepared to real time determination of tablet compaction pressure in moving tablets.

The D_{90} and particle size distribution of raw material were determined from three replicates of the sample. Laser diffraction (Insitec T, Malvern Inc.) provided a volume mean diameter (VMD) of 187.33 µm, D_{90}= 168.15 µm, D_{50}= 73.62, and D_{10}= 23.01 µm. An acrylic 4-quart V-

blender was used to lubricate the lactose with MgSt. Lactose and MgSt were blended for 1 min and then placed into a closed desiccator to prevent moisture absorption.

In order to calculate the density, a sample of 3.3 g of monohydrate lactose was used to make flat tablets with a Carver punch of 28 mm of internal diameter. The compaction pressure was varied between 100 to 500 MPa, as stated above. Measurements of the dimensions (height and diameter) of the flat tablets were measured using a Dial Caliper Scienceware® 6411H45(shaped as a disk), and its weight are needed to calculate the density.

4.2.2 NIR Equipment and Spectral Acquisition

In-line acetaminophen tablet spectra were collected using a NIR spectrometer from CDI (Control Development Inc, South Bend, IN) equipped with a thermoelectrically cooled InGaAs diode array detector of 256 elements that provides a spectral range from 1097 to 2200nm. Diffuse reflectance spectra were obtained with a miniature probe consisting of a dual tungsten halogen light source, equipped with gold diffuse reflectors positioned at a 45 degree angle from the fiber optic probe and fixed at a distance of 11 mm over each tablet. The inner diameter of the fiber optic is 400 microns and its length is three meters. The spectra were obtained while the tablets were moving along a conveyor belt with a linear velocity of 60 tablets/min. The radiation of the two lamps from the NIR probe was focused on the center of the surface of each tablet. A total of six spectra were obtained per tablet (three spectra per each side rotating 120º after each one) while each tablet was moving under the lamps and the detector. The average spectrum of each tablet was used for the multivariate models. Before each spectral set was acquired, a reference spectrum was obtained using a CDH 50 Standard White disk (Albrillon), an organic microcrystalline fluorinated polymer that provides a constant reflectance level.

Spectra of acetaminophen tablets were collected with the Spec 32 (version *1.6.0.6*) software provided by Control Development (South Bend, IN), and MATLAB 7.1 (The Math-Works, Natick, MA) was used to evaluate and extract information from the spectra obtained.

The chemical imaging of lactose tablets used in the relaxation study were collected in diffuse reflectance mode using Malvern Instruments SyNIRgi Near Infrared Chemical Imaging system, equipped with a Stirling cooled InGaAs focal plane array detector consisting of 320 x 256 pixels for a total of 81,920 spectra per image cube recorded, a liquid crystal tunable filter (LCTF), microscope stage, and computer-controlled illumination. For these measurements, the data were collected using an objective that provides 38.9 micron per pixel magnification resulting in a sample area of 12.5 mm x10 mm. Samples were scanned over 1200 nm− 2450 nm spectral range with spectral point spacing of 10 nm and 8 coadded images per wavelength, each image plane or channel was scanned 4 times. Due to the difference in density distribution for the top and bottom of the tablet compact, all the NIR-CI presented was from the top side of the tablet. If any hot and cold pixel (bad pixels)[57] were detected, its value was replaced by the average value of surrounding pixel intensities. The spectral information was converted to absorbance. Spectra outside the sample surface were removed by masking. The mean of tablet NIR-CI slope was calculated using the average of all NIR-CI slopes (obtained from every pixel). The distribution of NIR-CI slope content in each pixel surface was studied and compared by using histograms that plot pixel number against slope NIR value. The mean, standard deviation, and skew and kurtosis were used to characterize distribution on the image histogram. The standard deviation describes the variation about the mean slope in the NIR-CI. Skew measures asymmetrical tailing, a positive skew indicating tailing towards higher values and a negative skew tailing toward lower values. Kurtosis gives information about the shape of the histogram

peak. As the kurtosis of a Gaussian distribution is 3, then kurtosis >3 indicates sharper peaks with a long tail whereas kurtosis <3 describes flatter peaks with a smaller tail.[58]

Pixis® CI software from Malvern was used for data acquisition, Isys® 5.0 software package version 1.0.4 for preprocessing and preliminary data investigation, MATLAB 7.1 (The Math-Works, Natick, MA) was used for data analysis.

4.2.3 Data Processing
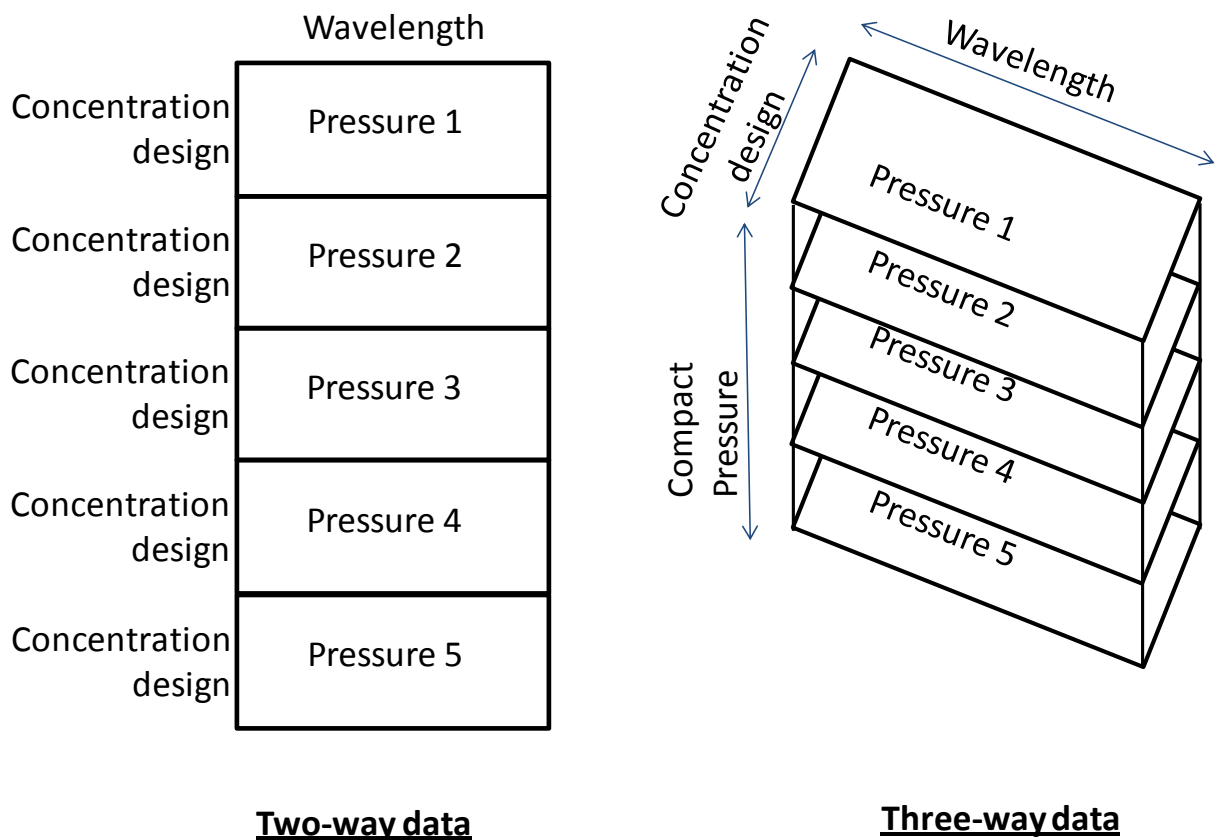
Figure 4.1 Two- and three-way data arrangement for the spectral sets.

Figure 4.1 shows the two- and three-way arrangement of spectral data sets, according to each source of variation. In the two-way data set, the first dimension (mode) corresponds to the

spectra and the second mode is related to the different concentrations and compaction pressure levels. The two-way calculations were performed using the chemometric software PLS Toolbox v4.2 (Eigenvector Research) under Matlab (v 7.0, The Mathworks). The three-way data set was arranged as follows: the first mode is related to the concentrations levels, the second mode is assigned to the spectra and the third mode related to the compaction pressure levels. The three way calculations were performed using also PLS Toolbox.

Two strategies were followed to develop calibration models for the APAP determination in intact tablets using two- or three-dimensional data sets. Figure 4.2 a) shows the use of Partial Least Squares to obtain the two-way calibration models. The spectral calibration set and the reference APAP concentrations were used to obtain the PLS model. Once the PLS regression vector is obtained, the APAP concentrations were calculated for the tablets in the prediction set. PARAFAC and MLR were selected as multivariate techniques to obtain the three-way calibration models, as described in Figure4.2 b) first, the calibration spectral set is decomposed by PARAFAC in scores (first mode, concentrations) and loadings (second and third mode, wavelengths and pressures, respectively). In the second step, the obtained calibration loadings are used to predict the scores from the prediction set. Finally, the calibration scores of the first mode and the APAP reference concentrations are used to calculate the MLR calibration model that allows the prediction of the APAP concentrations from the prediction set. The most common applications of MLR are based on specific wavelength selection, however in the present application the independent X-variables come from the PARAFAC decomposition using a whole wavelength range.
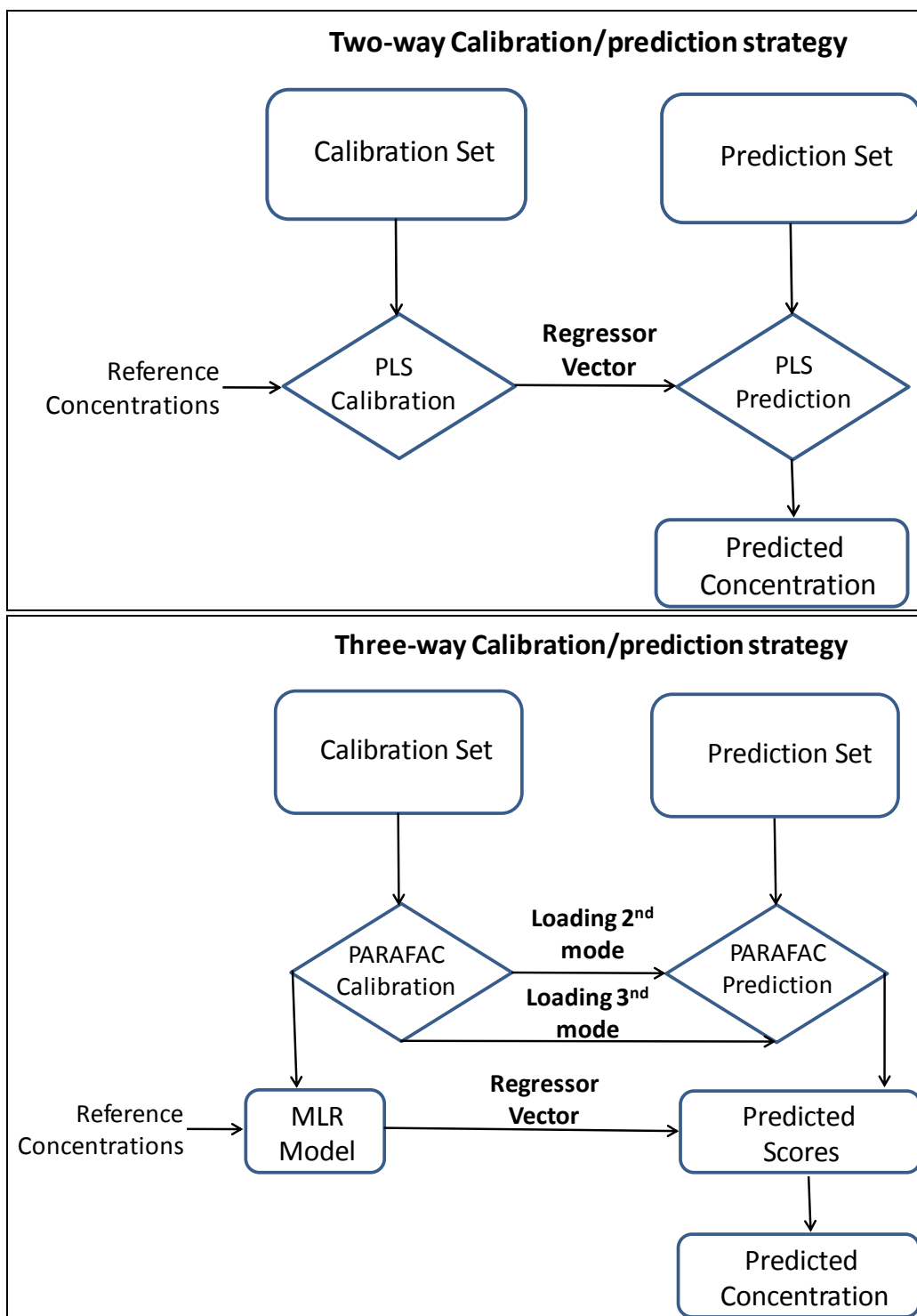
Figure 4.2 Schema of the two- and three-way calibration/prediction strategies (PLS and PARAFAC/MLR).

The entire wavelength range was used to model the data, in order to include as much spectral changes as possible due to chemical and physical changes. Before applying any kind of modeling, the data sets were centered across the concentration/compaction mode (2D data matrices) or across the concentration mode (3D data matrices). This pretreatment was applied to remove spectral differences due to uncontrolled sources of variation. Standard normal variate (SNV) and Savitzky-Golay derivatives (first and second order, second polynomial degree and fifteen points of moving window) were applied as spectral pretreatment along wavelengths mode. PLS Toolbox v4.2 (Eigenvector Research) under Matlab (v 7.0, The Mathworks) was used for the data pre-processing and modeling of the data. The quality of the calibration models was evaluated in terms of standard error of calibration (SEC), prediction (SEP), linearity, and correlation of the NIR versus reference results. The 95% confidence interval (two-tailed t-test, significance 95%, n-2 degrees of freedom) was calculated for the slope and intercept.

4.2.3.1 Slope algorithm and program

NIR chemical imaging of a sample consists in collecting a spectrum for each pixel in the focal plane array detector, about 81,920 spectra (320 x 256 pixels). The resulting spectra are stored in a three dimensional matrix or hypercube with X, and Y as spatial coordinates, and Z axis as diffuse reflectance scanned in a range of wavelengths. Two planes of information inside the NIR-CI hypercube were selected at wavelength λ_1 and λ_2 (Figure 4.3) to calculate the spectral slope of the p x q pixel inside the tablet imaging hypercube. Slope $M_{[p,q]}$ is a matrix of slope of the NIR spectra, where Z_1 and Z_2 represent the absorbance at the selected wavelengths $\lambda_1=1200$ nm and $\lambda_2=2240$ nm respectively.

$$\text{SlopeM}_{[p,q]} = \frac{Z_{1[p,q]} - Z_{2[p,q]}}{\lambda_1 - \lambda_2} \qquad (4.1)$$
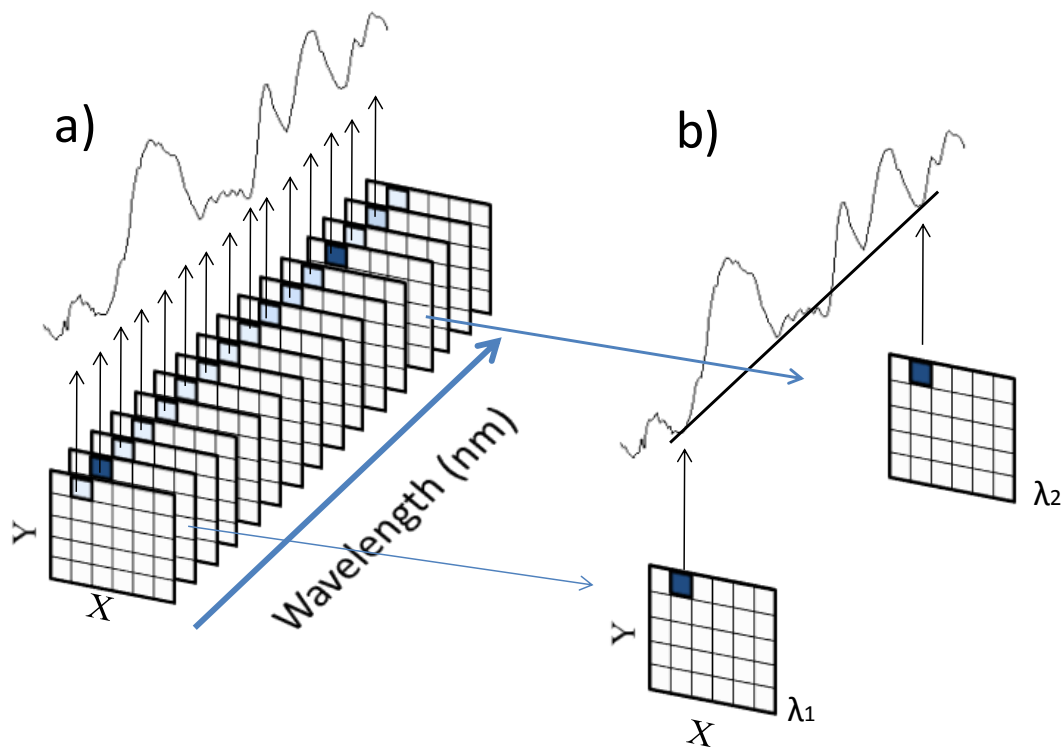
Figure 4.3 a) Schematic spectral hypercube. Each pixel is spatially located in the X-Y image plane. A representative NIR spectra associated with one pixel is shown in the third dimension. b) NIR spectral slope for one pixel inside the hypercube at two selected wavelength (λ_1 and λ_2).

The spectral hypercube is a matrix with dimensions <256x320x121>, 256 divisions in the X axes, 320 divisions in the Y axis and 121 divisions in wavelength range. The spectra have wavelengths between 1200-2450 (nm). A code was written in MATLAB to calculate the slope of the spectrum in every pixel.

The Matlab code written to calculate the slope matrix SlopeM$_{(PxQ),}$ is described as follows:

function slopeM = snirci(omega1, omega2,datafile);

S = load('datafile');

C = S.datafile(:,:,omega1);

D = S.datafile(:,:,omega2);

slopeM =(C-D)/(omega1- omega2);

imagesc (M);

figure(gcf);

4.3 Results and Discussion

4.3.1 Real time determination of tablet compaction pressure in moving tablets
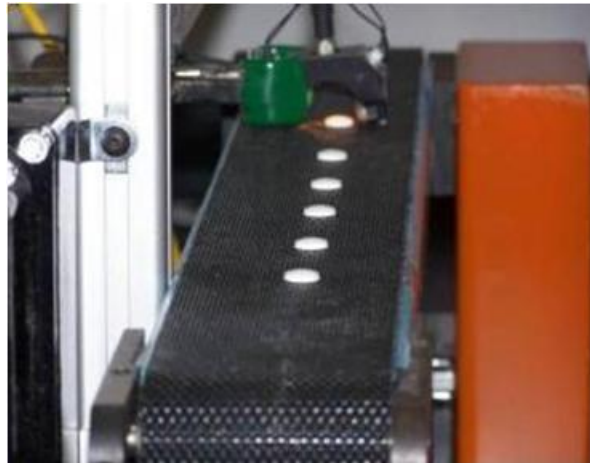
Figure 4.4 Set-up for NIR spectral acquisition of moving tablets.

On line NIR Spectra of 36 moving tablets at six different pressures were obtained to evaluate whether it was possible to measure the compaction pressure in moving tablets as shown in Figure 4.4. The spectra were obtained while the tablets were moving along a conveyor belt with a linear velocity of 60 tablets/min. The compaction pressure had a strong influence on the NIR spectra for the samples shown in Figure 4.5, the resulting spectra show an increase in the slope of the spectra obtained as a function of the applied pressure. The changes in the spectra were easily observed without spectral preprocessing or transformation.
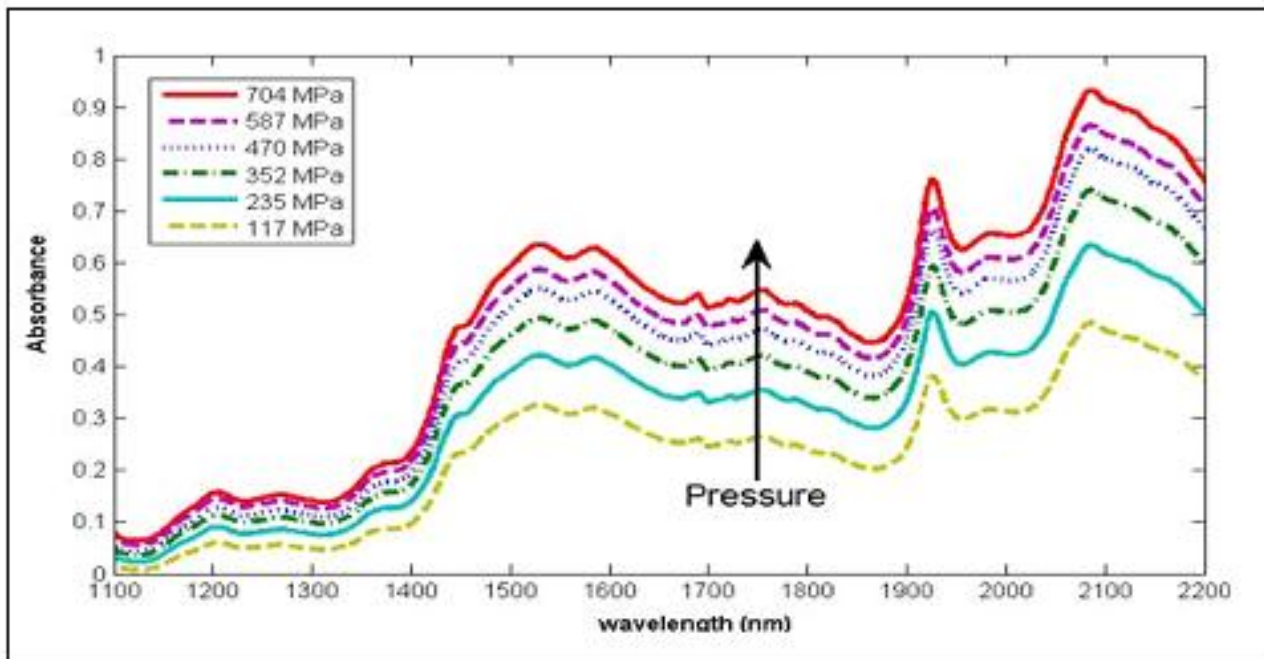
Figure 4.5 NIR raw spectra of moving lactose tablets at different compaction pressure.

A principal component analysis (PCA) was performed for 36 tablets of pure lactose, 6 tablets for each pressure, using the entire spectral range of 1107-2200 nm. The percent of total variation from the first factor was 99.92% and the cumulative variation with the second factor was 99.98%. The first principal component described the spectra as the applied pressure was increased, associated with a larger compaction pressure.

A partial least squares (PLS) calibration model was developed using first derivative spectra and 2 factors over the entire wavelength range. Regression analysis between cross validation results obtained with the model developed and reference pressure compaction applied, gave a coefficient of regression R^2=0.986, slope 0.99 ± 0.03 and intercept 5.73 ± 12.98, evidence of good agreement between the predicted and reference values.

The calibration model developed was also challenged through the prediction of an independent validation set, not used in developing the model. The results for the validation set are described below in Table 1, where the Standard Error of Prediction (SEP) for the compaction pressures was 22.5 MPa. The NIR spectra were obtained for tablets moving at about 60 tablets per minute.

Table 4.1 Determinations of compaction pressure for individual tablets.

Measured Pressure (MPa)	Predicted Pressure (MPa)
117	94.9
117	114
117	120
235	225
235	221
235	240
352	367
352	355
352	335
587	614
587	596
704	676
704	692
704	690

4.3.2 Deconvolution of Chemical and Physical Information

NIR infrared instruments may be considered cross-sensitive (capable of making two different measurements).[48] To evaluate the NIR cross-sensitive capacity, spectra of APAP moving tablets was acquired. Evaluation of the moving tablets spectra revealed that they include both chemical and physical information. The spectral response is very different depending on

which process variable (chemical or physical) was modified. Figure 4.6 a) shows the spectral

variation due to an increasing drug concentration.
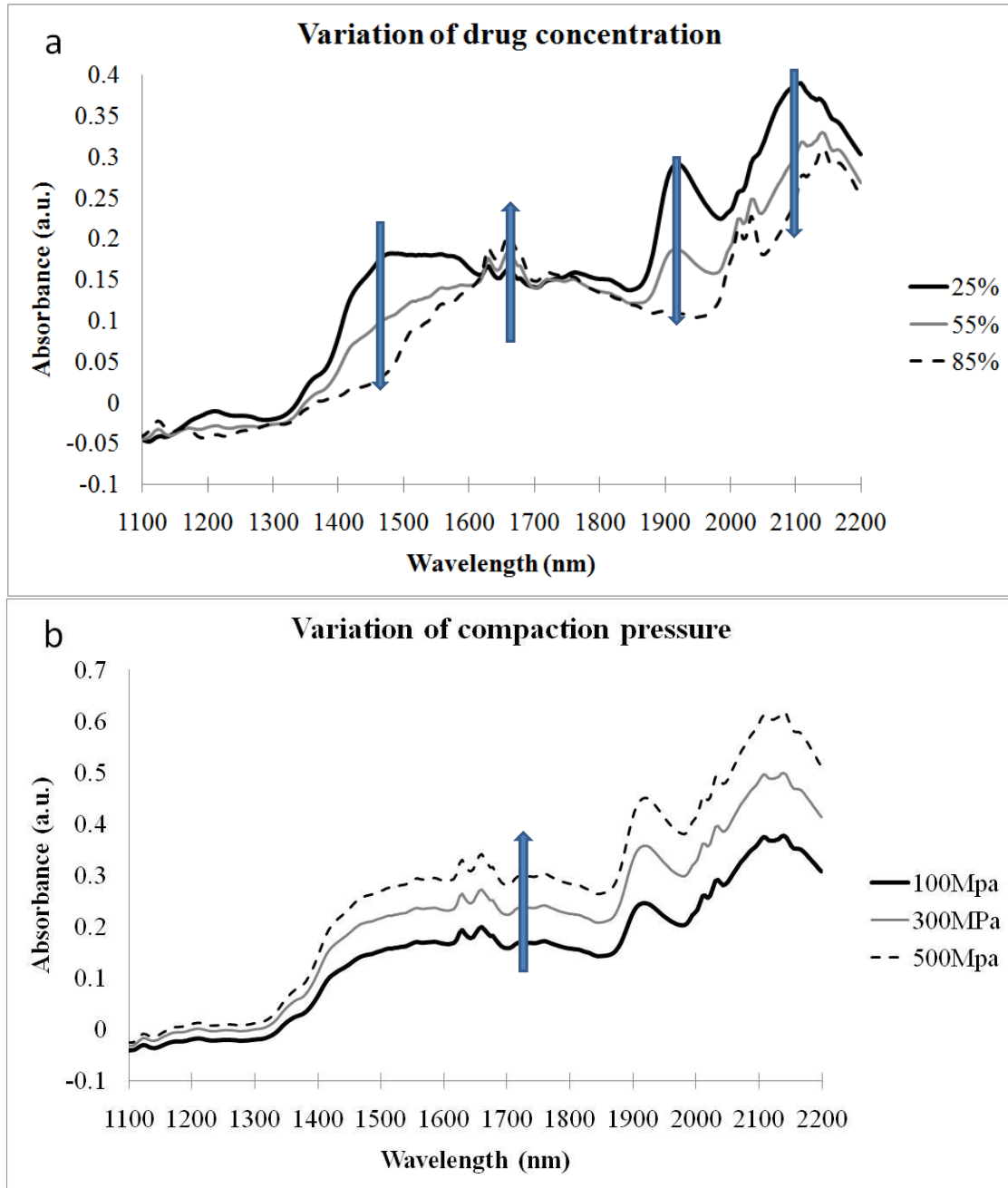
Figure 4.6 a) Spectral changes according to the variation of drug concentration at constant pressure. b) Spectral variation on compaction pressure at constant concentration.

The higher drug concentration results in a greater intensity of the bands related to the APAP and also results in a decrease of the intensity of bands associated with the excipients. Figure 4.6 b) shows that the increase in the compaction pressure is revealed as a higher slope in each spectrum.[59, 60]

The entire data set consisted of 210 spectra, obtained from the seven different concentrations and five levels of tablet compaction. The NIR spectral data set was analyzed by principal component analysis (PCA) in order to obtain relevant information about the influence of the chemical variation, and to visualize the spectral variability due to physical effects related to the changes in compaction pressure.

4.3.3 Principal component analysis of data set

Figure 4.7 shows the scores plot (PC1 vs. PC2) obtained from PCA of the spectra after applying different pretreatment (Absorbance, SNV, first, and second derivative).The SNV, extended multiplicative signal correction (EMSC) and derivative pretreatments have been used to reduce the multiplicative and additive effects that physical differences have on NIR spectra.[61, 62, 63, 64]
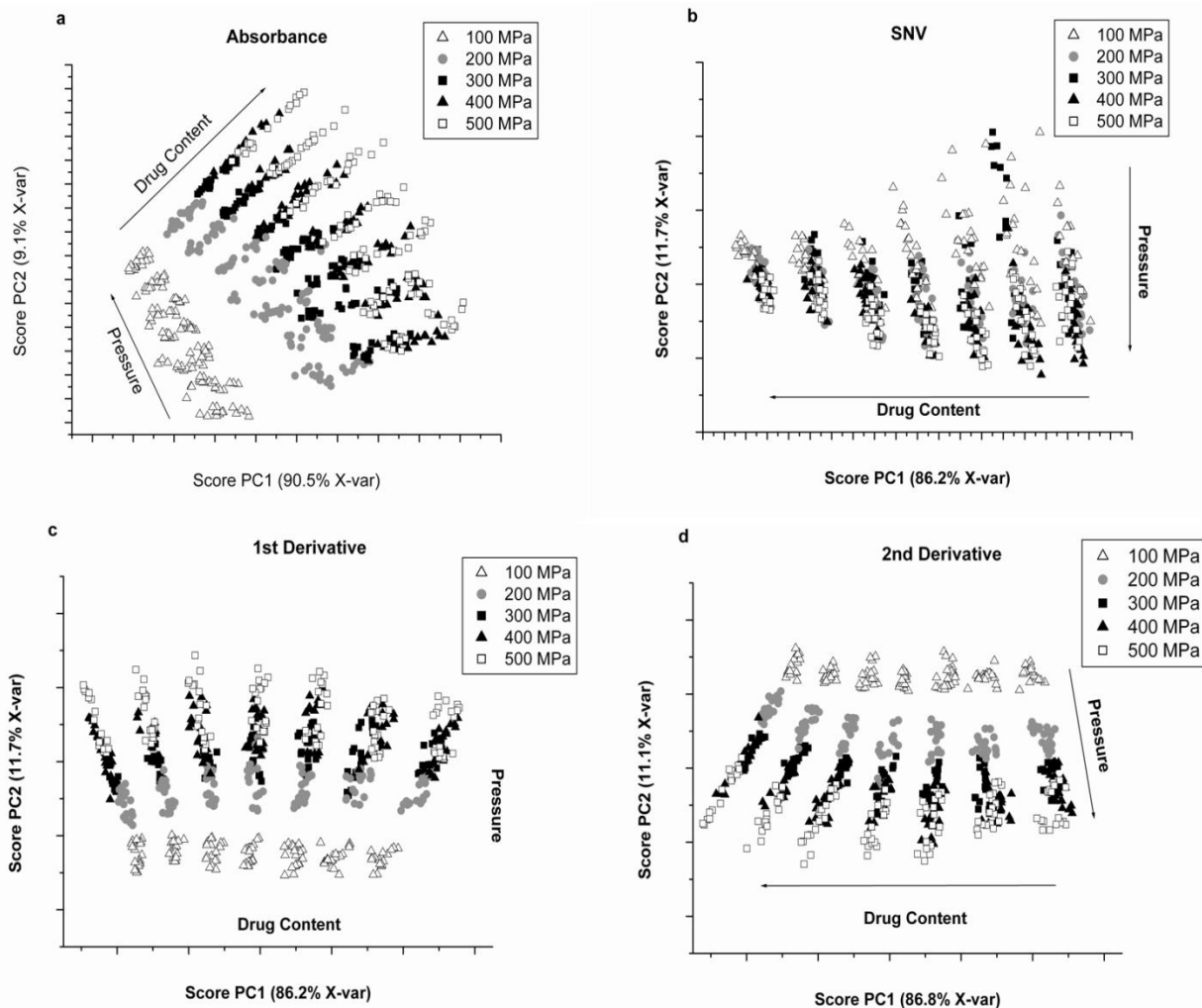
Figure 4.7 Scores plot (PC1 vs. PC2) obtained from PCA of the complete spectral data set after applying different spectral pretreatment (a) absorbance, (b) SNV, (c) first, and (d) second derivative. Arrows indicate the increasing amount of compaction pressure or drug concentration.

The explained variance for the first and second components is very similar in all cases, summarizing at least 98%, in all cases. The different plots show that the main source of variability of the spectra (chemical or physical), depends on the spectral pretreatment used to calculate the PCA. The scores plot of the absorbance spectra (Figure 4.7 a) shows that both first and second principal components explain information related with chemical and physical

variability clearly demonstrating that NIR spectroscopy provides both chemical and physical information. Both sources of variability have a great influence on the spectra, even after performing SNV, first or second derivatives to reduce the spectral changes due to the compaction pressure.

The compaction pressure effect has a great influence on the scattering of the reflected radiation. SNV and derivatives have been used to reduce the scattering effects on NIR spectra in many applications.[65] The application of these pretreatments to the data set was expected to reduce the spectral variation due to the compaction pressure, whereas the chemical related information would be highlighted. The scores plot of first derivative pretreatment (Figure 4.7 b) shows that the remaining spectral variation due to compaction pressure has been reduced (PC2 9% of X-variance), however, the scores clustering due to the tablet pressure is still remaining and clearly identifiable. The compaction pressure has a great influence on the slope of the NIR spectra of intact tablets, as the higher pressure resulted in a greater slope.

The second derivative pretreatment, which reduces the linear contributions along the wavelength range, should be the better option to reduce the physical influence on the spectra, because the larger compaction pressure the higher slope of the spectra (Figure 4.6 b). However, the scores plot of 2nd derivative pretreatment of Figure 4.7 c) reveals that the explained X-variance of PC2 is higher (11%), and far from reducing the segregation of the spectra due to compaction pressure, the distribution of the score according to the drug concentration has been distorted. The scores plot distribution after SNV pretreatment (Figure 4.7 b) shows that X-variance of PC2 is still high (12%), however the scores clustering has been highly reduced and

the main source of variability (PC1, 87%) is clearly related to the drug concentration of the tablets.

This general analysis of the PCA scores plot reveals the selection of the spectral pretreatment for the development of a calibration model for drug quantization in intact tablets is not trivial, because variation in the compaction pressure during tablet manufacturing cannot be completely removed and can cause a significant variation on the spectrum and possibly on the determination of drug content.

4.3.4 Two-Way Modeling (PLS)

The first approach to develop PLS calibration models for the determination of drug content in intact tablets entailed the selection of a calibration set. The first calibration set only included one compaction pressure level (200 MPa) and covered the whole drug concentration range (25–85% w/w). SNV and derivatives were tested as spectral pretreatments on the whole spectral range (1097–2200 nm). The set of tablets prepared at 200 MPa were split in 66/34% for the calibration model and external prediction set, respectively, in order to select the optimum number of PLS principal components reaching the minimum prediction error. Once the calibration model was established, it was used to predict the drug concentration for the rest of the tablets prepared at different compaction pressures (100, 300, 400, and 500 MPa).

Table 4.2 shows the figures of merit from the prediction using this initial PLS model calculated only with the 200 MPa compacted tablets. Independently of the spectral pretreatment used, the linearity for the prediction of the tablets compacted at 200 MPa is correct, being the slope and intercept not significantly different from one and zero, respectively. However, the predictions for the rest of compaction levels were not linear, being the slope lower than one

(~0.8) for the 100 MPa set and higher than one (~1.2) for the 500 MPa set. The model calculated in SNV is the only that presented a better predictive ability for the five compaction sets, but it is not appropriate to be used as a monitoring method for the drug content determination on the whole compaction range.

The PLS models described in Table 4.2 were obtained with the entire wavelength range. The selection of a better wavelength range, where the drug presents the most significant bands, should help to obtain simpler models with a better predictive ability. Different wavelength ranges were tested and the best predictive ability was reached using the 1500–1800 nm range. The number of principal components needed to define the model was two, one less than the previous approach using the whole wavelength range. However, no significant improvement on the predictive ability was obtained.

The figures of merit for the prediction of all the tablets sets are not shown because they are very similar to those presented in Table 4.2. In this initial approach, neither the spectral pretreatment nor the wavelength range selection allows to obtain PLS calibration models with a good predictive ability to quantify the drug content in intact tablets, compacted at a different pressure than those included in the calibration set. These experiments demonstrate that an NIR method for drug content established without taking into consideration variations in tablet compaction pressure, would not provide adequate results if the tablet compaction pressures changed after it is implemented.

The use of PLS models encompassing all the compaction pressure levels in the calibration set was also evaluated. The number of principal components needed to define these models was

greater (five principal components), because the calibration set includes more physical variability

(compaction pressure levels).

Table 4.2 Figures of Merit from the Predictions Using the PLS Model (1097–2200 nm, Calibration Set: 200 MPa)

Spectral Pretreatment	Compaction Pressure (MPa)	Slope	Intercept	Correlation	Standard Error of Prediction (SEP)
Absorbance (3 LV, SEC=6.01%)	100	0.781	14.9	0.995	10.45
	200	0.995[a]	-0.395[a]	0.995	6.2
	300	1.107	-5.94	0.996	9.54
	400	1.194	-11.5	0.995	9.98
	500	1.216	-14.1	0.995	10.23
SNV (3 LV, SEC=3.17%)	100	1.045	-1.7	0.996	7.87
	200	0.983[a]	0.883[a]	0.998	3.88
	300	0.966	2.39	0.998	6.71
	400	0.993[a]	0.769[a]	0.998	4.1
	500	0.97	1.774	0.998	6.54
First derivative (3 LV, SEC=3.67%)	100	0.82	13.4	0.995	9.9
	200	0.992[a]	0.029[a]	0.997	3.98
	300	1.085	-5.84	0.996	8.6
	400	1.162	-10.8	0.996	9.65
	500	1.184	-12.8	0.996	9.72
Second derivative (4 LV, SEC=3.89%)	100	0.816	-12.2	0.995	9.97
	200	0.994[a]	-0.088[a]	0.998	4.03
	300	1.069	-3.33	0.997	8.14
	400	1.172	-9.99	0.996	9.7
	500	1.21	-12.7	0.997	10.07

[a]Slope and intercept not significantly different of one and zero, respectively.

The SNV spectral pretreatment on the entire wavelength range provided the best predictive

ability. Table 4.3 shows the figures of merit for the predictions using the PLS model calculated

using samples of the whole pressure range, from 100 to 500 MPa. The predictive ability of this

model is slightly better than the calculated using only samples compacted at 200 MPa. The tablet

119

sets compacted at 100, 200, and 400 MPa are correctly predicted, being the slope and intercept not significantly different of one and zero, respectively. However, it is not still possible to predict correctly the drug content of the tablet compacted at 300 and 500 MPa, even though these compaction levels are included in the calibration set. This may be caused due to a nonlinearity due to the physical effects of compaction. Another approach was evaluated including only tablets compacted at 100 and 500 MPa in the calibration set. The obtained model was slightly simpler (four principal components), but the predictive ability for the whole compaction pressure tablets sets was not correct.

Table 4.3 Figures of Merit from the Predictions Using the PLS Model (SNV, All Wavelengths, Calibration Set: 100–500 MPa, 5 Principal components)

Compaction Pressure (MPa)	Slope	Intercept	Correlation	Standard Error of Prediction (SEP)
100	1.0024[a]	0.1446[a]	0.963	6.61
200	0.9955[a]	-0.0115[a]	0.997	1.82
300	0.9698	1.6348	0.997	2.12
400	0.9894[a]	0.7895[a]	0.997	1.67
500	0.9685	1.7986	0.998	1.82

[a]Slope and intercept not significantly different of one and zero, respectively.

The combination of a proper spectral pretreatment, the selection of a wavelength range and combination of tablets produced with different compaction pressures are not useful to model the chemical variability due to the drug content, when the physical variability is very large.[66] The calibration models are more complex (required more principal components) and presented a poor predictive ability. However, the predictions on drug content were acceptable when the variation in pressure is small. The two-way approaches to obtain PLS models for the drug quantization in intact tablets have in common that both chemical and physical variations are included in the second mode on the 2D data matrix, while the first mode is the wavelength range.

4.3.5 Three-Way Modeling

The three-way MLR–PARAFAC algorithm allows to deconvolute the spectral matrix and select the scores mainly related with the variation in drug concentration to calculate the calibration model.

The MLR calibration model only uses the chemical related scores, so the models are expected to provide a better predictive ability for the drug quantization in intact tablets, independently from the compaction pressure. The tablet set (210 spectra) was split in two subsets (calibration and prediction) by selecting one-by-one alternating samples. Each subset was arranged in a 3D matrix structure, obtaining two data sets of 105 samples each one (21 samples X 1104 wavelengths X 5 pressures). PARAFAC/MLR was used to calculate calibration models in absorbance, SNV, first, and second derivative spectral pretreatment. Each sample contained only two pure compounds (APAP and MCC). The number of PARAFAC components used in all the models was fixed to two, because explained variance and the core consistency obtained from the following tests were over 99% in all cases. The core consistency is a calculation similar to the explained variance of PCA but specific for three-way methods. Also, the use of three PARAFAC components was also tested, but no improvement on the obtained results was found. Figure 4.8 shows the scores and loadings obtained from the PARAFAC deconvolution. The scores plot of the first mode reveals a high linear correlation between the two variables (scores and concentration, r = 0.9984).
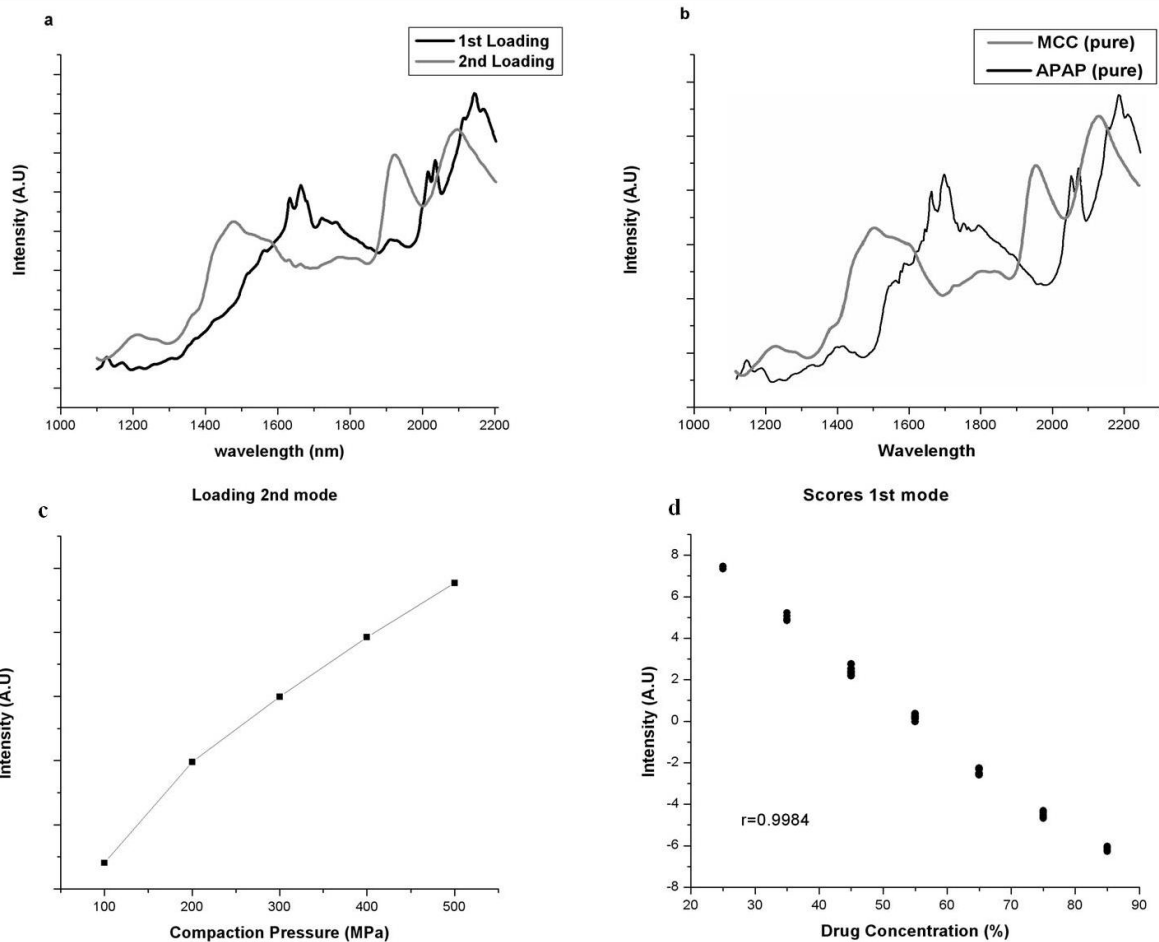
Figure 4.8 Scores and loadings obtained from the deconvolution using two PARAFAC components, no spectral pretreatment, and data centering on the second mode (drug concentrations).

The loadings obtained from the second mode show how the compaction pressure influences the average spectra. As the pressure increases, the absorbance also increases. The effect of the compaction on the spectra decreases at the higher pressures. This result is similar to the obtained with the visualization of the spectral changes (Figure 4.6) where the spectral slope increases as the compaction pressure does. This increase in the slope is weaker on the higher pressures. The last plot from Figure 4.8 shows the deconvolution of the third mode compared with the pure spectra of MCC and APAP. The two sets of spectra are virtually the same, with the exception of

the 1940 nm band, that is not present in the spectrum of the pure APAP, while the obtained loading presents one band. The deconvoluted physical information is obtained from the loading of the second mode that reveals the effect of the physical variation on the spectral changes. The deconvoluted chemical information is obtained from the scores of the first mode (highly correlated with the drug concentration) and from the loadings of the third mode (virtually identical than the pure spectra of MCC and APAP).

Table 4.4 Figures of Merit from the Optimization of Spectral Pretreatment Using the Strategy Calibration of PARAFAC–MLR

Spectral Pretreatment	Slope	Intercept	Correlation	Standard Error of Prediction (SEP)
CAL				
Absorbance	0.999[a]	0.069[a]	0.999	0.73
First derivative	0.999[a]	0.019[a]	0.999	0.38
Second derivative	0.987[a]	0.686[a]	0.994	2.29
SNV	0.999[a]	0.056[a]	0.999	0.65
PRED				
Absorbance	0.917	10.1	0.999	1.81
First derivative	0.918	6.4	0.999	1.91
Second derivative	0.907	0.394[a]	0.995	2.64
SNV	0.990[a]	1.12[a]	0.999	0.69

[a]Slope and intercept not significantly different of one and zero, respectively.

Table 4.4 shows the figures of merit obtained from the calibration models and the predictive ability for each spectral pretreatment. In this case, both calibration and prediction sets encompass the entire drug and compaction pressure ranges (25– 85% w/w and 100–500 MPa, respectively). The calibration statistics show that the linearity of the regression line between the model and the reference APAP concentration is correct, being the slope and intercept not significantly different to one and zero, respectively. All the spectral pretreatments used for the three-way calibration strategy allowed the correct modeling of the APAP concentration in intact tablets, independently

of the compaction pressure. However, only the SNV pretreatment allowed a good prediction (reduced prediction error, high correlation, and slope/intercept not different than one and zero). The rest of the models (absorbance and derivatives) presented nonlinear statistics from the prediction.

The three-way calibration/prediction approach requires that the dimensions of the wavelengths and compaction pressure modes (1104 and 5, respectively) should be the same in the prediction set and the calibration set. This requirement can be easily fulfilled during the development of the calibration model in the laboratory. However, during the routine use of the obtained method on a tableting machine, samples are obtained at a single compaction pressure and prediction sample sets cannot be set-up covering the 100–500 MPa range to fit the three-way method requirements. A strategy to design the prediction data set in such a way to adjust the requirements to the PARAFAC–MLR model was needed. The strategy developed consisted in using individual 3D matrices for each compaction level.

This is reached overlapping five times within the third mode (compaction) every single 2D data set of an individual compaction pressure, obtaining one 3D matrix for each compaction pressure (n spectra x 1104 wavelengths x 5). These 3D matrices fulfilled the dimension requirements of the PARAFAC–MLR model, allowing the prediction of the APAP concentration for each different compaction pressure. Following this strategy, the obtained model in SNV (Table 4.4) was used to quantify the drug content of the five individual 3D data sets (one for each compaction pressure).

Table 4.5 Figures of Merit from the Prediction of Separate Tablets Subsets According to Their Compaction Pressure, Using the SNV PARAFAC–MLR Model.

Compaction Pressure (MPa)	Slope	Intercept	Correlation	Standard Error of Prediction (SEP)
100	1.003[a]	0.325[a]	0.998	1.39
200	0.992[a]	1.62[a]	0.999	1.25
300	0.996[a]	2.50[a]	0.999	1.2
400	0.998[a]	0.029[a]	0.999	1.02
500	0.995[a]	0.956[a]	0.998	1.23

[a]Slope and intercept not significantly different of one and zero, respectively.

Table 4.5 shows the figures of merit obtained for these predictions. Every individual tablet set compacted at different pressures can be successfully predicted to quantify the drug concentration.

In all the cases, the prediction errors are low and the regression lines fulfill the linearity requirements, which conclude that this three-way strategy of calibration and prediction can be used for the monitoring of tablets in a pharmaceutical process, independently of the compaction pressure.

4.3.6 Density calculations using NIR spectra

The NIR is capable to monitoring changes on the surface of tablet. This changes can be related to the applied pressure and therefore with density. The tablet density, as many researchers stated, increase with applied pressure. As Figure 4.9 shows, the tendency of increasing density as the applied pressure increases; the relationship is not linear.
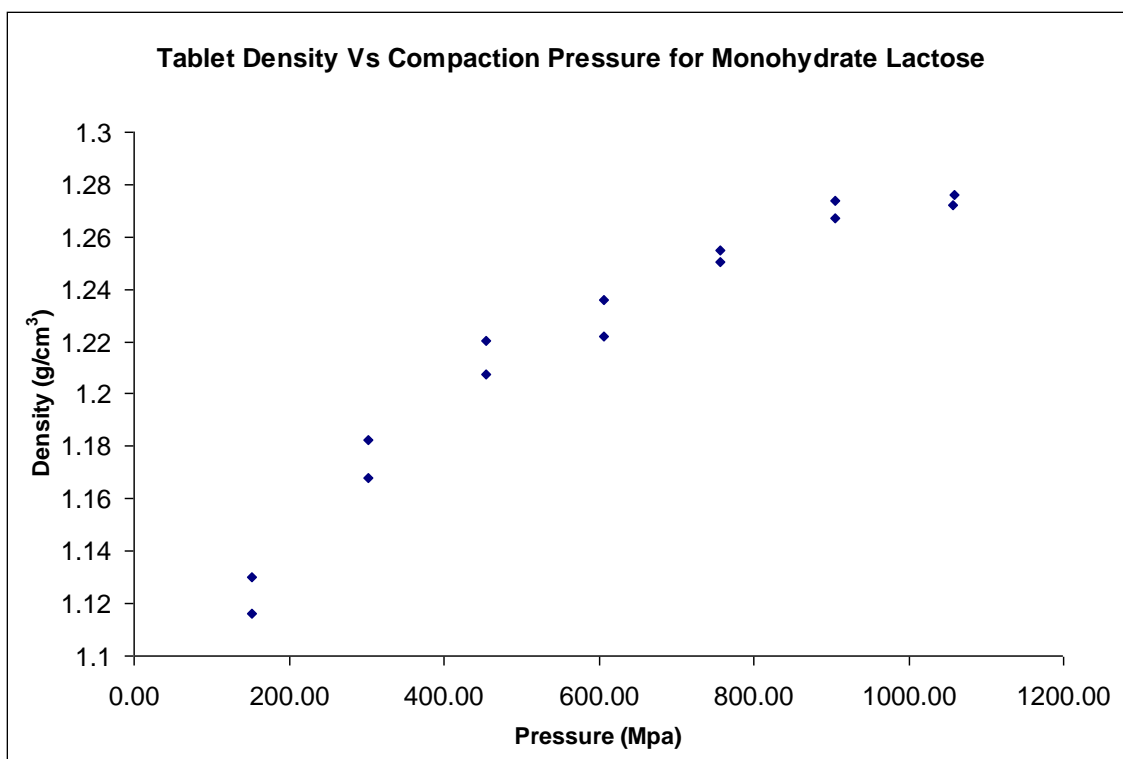
Figure 4.9 Tablet density vs Compaction Pressure

Previous studies had proved that the tablet density is not uniform across the tablet.[67, 68]There is a distribution that depends if the tablet is lubricated or nonlubricated.[68] The density profile shows that the density is lower in the center of the tablet; this is due to compaction pressure.[69] A possible explanation for this is that the density increases until the tablet compaction reaches a maximum, by this point (at higher pressure) the density will remain mostly constant. The density study was not continued in this study because geometry of commercial tablets not permit calculated the dimension using the caliper approximation.

4.3.7 Tablet compaction evaluated with NIR-CI slope
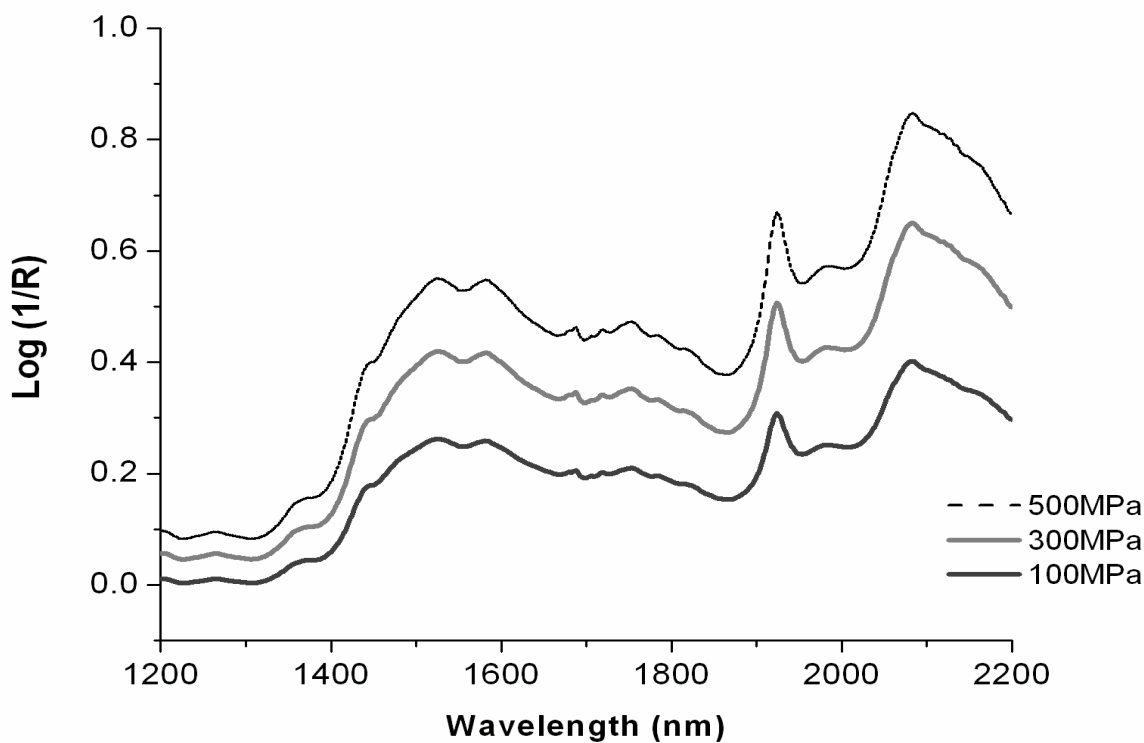
Figure 4.10 NIR-CI spectra of pure-lactose tablet at different compact pressure.

The compaction pressure applied to make the tablet has a strong influence on the NIR-CI spectra. NIR spectra with increasing slope values were obtained as a function of the applied tablet compaction pressure. The changes in the spectra can be observed even without any spectral preprocessing or transformation as shown in Figure 4.10. To further assess quantitatively the compaction at each tablet, a linear least squares regression was generated based on the measured applied compaction force of 6 lactose tablets and their average NIR-CI slope, determined as a mean value of all pixels on the top and bottom surfaces of those tablets. The data yields an equation for compaction (C). C =949.25*(NIR-CI slope) - 347.94, with R^2= 0.9987

127

and RMSEC=4.99 MPa. This equation further demonstrates the effect of tablet compaction pressure on the slope of the NIR spectra.

4.3.8 Spatial distribution of tablet compaction at different applied pressure
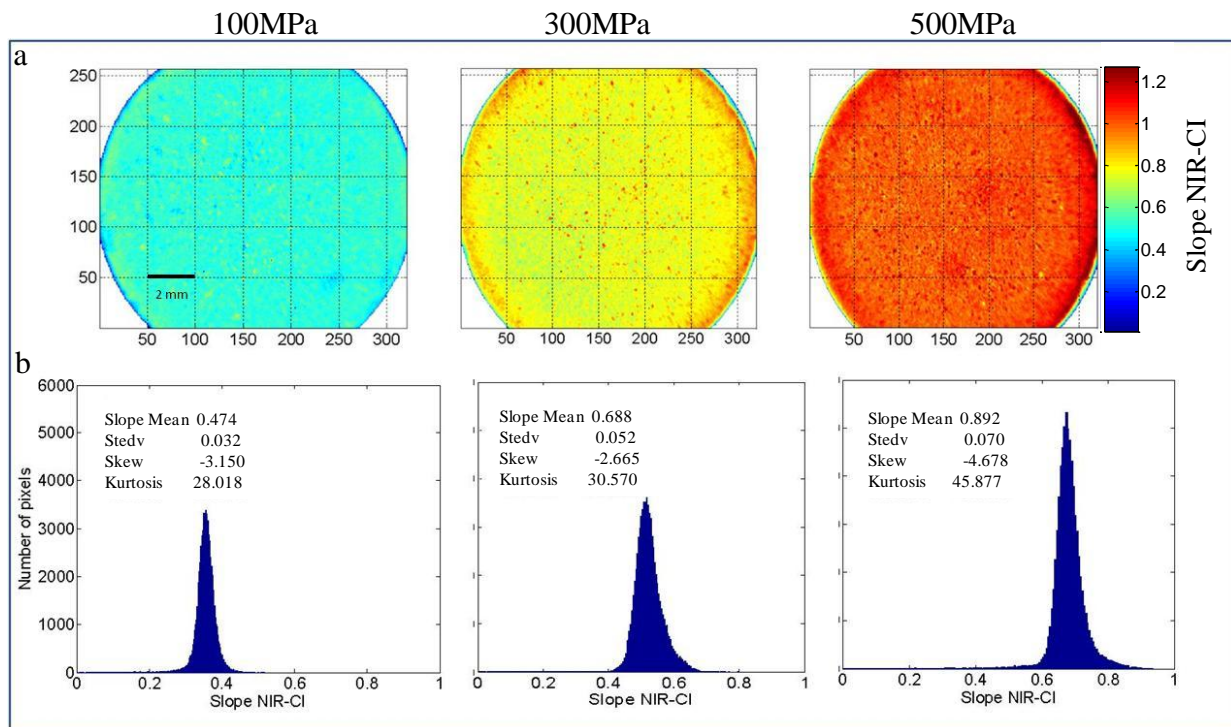
Figure 4.11 a) NIR-CI slope imaging of lactose-tablets, 0% w/w MgSt, at three levels of pressure (100, 300 and 500 MPa), the mapping was constructed with the slope NIR-CI of each pixel. b) Histogram of slope NIR-CI values at different compact pressure (100, 300 and 500 MPa).

Near-infrared data imaging of slope values is presented for three different pressures at 100, 300 and 500 MPa. Figure 4.11 shows the effect of pressure, with zones of high compaction evidenced in the image of the 500 MPa tablet, while the darker zones in the figure represent decreasing pressure in the tablet and low particle compaction, as observed in the 100 MPa image. The obtained results clearly show differences in the slope as a function of applied compaction forces.

Figure 4.11 a) was obtained using all the NIR-CI spectra collected with the focal plane array detector and the MATLAB program, where λ_1=1200 nm and λ_2=2240 nm. The two wavelengths selected are from the baseline of the spectra and were selected to minimize the effect of chemical differences such as moisture content. The objective is to obtain an image of the spectral slope based on physical, not chemical differences.

Table 4.6 Effect of current power on slope and absorbance values.

Current power (%)	Slope	Abs at 1220nm	Abs at 2240nm	Error relative to 88%		
				Slope	λ_1=**1220**	λ_2=**2240**
86	0.296	0.105	0.354	1.786	13.434	4.988
	0.297	0.104	0.354	1.924	12.893	4.958
87	0.296	0.097	0.346	1.752	5.092	2.672
	0.295	0.098	0.346	1.237	6.392	2.643
88	0.291	0.093	0.337	0.069	0.325	0.148
	0.291	0.092	0.336	-0.069	-0.325	-0.148
89	0.299	0.089	0.34	2.679	-4.117	0.831
	0.299	0.089	0.34	2.748	-4.117	0.861
90	0.296	0.064	0.312	1.649	-30.878	-7.274
	0.291	0.064	0.308	-0.137	-30.553	-8.462

Slope measurements were performed to develop a robust method for studying tablet relaxation. After obtaining a first set of spectra while studying the relaxation of a tablet, the optical configuration of the system could be changed to study another type of sample. Lamp adjustment may be required in order to continue with the tablet relaxation measurements. The NIR-CI operational manual provides guidance to avoid saturating the detector but fine adjustments are required to gain the highest throughput for the system and the current power could vary as shown in Table 4.6.

In this study the value of 88% of current power was taken as optimum but the values from 86 to 90% are also considered adequate. The slope measurements are more robust than absorbance measurements to variations in the throughput of the system, as observed in Table 4.6. The effect of vertical alignment of the sample stage positioning was also evaluated. The sample stage was moved 1 and 3 mm from the original position. In this situation the two methods showed similar robustness. Finally, the precision of absorbance and slope measurements was evaluated by collecting six spectra of a tablet.

The tablet was moved out of the stage and then inserted again before collecting each set of spectra. The standard deviation of spectral slope and spectral absorbance at 2240 nm was measured to evaluate the precision of the two measurements. The variations observed in the measurements were similar, with a standard deviation of 0.002 for absorbance and 0.003 for slope measurements. Thus, the optimization of instrument throughput in lamp adjustment has a greater effect on absorbance measurements than on slope measurements. The use of slope measurements does not require dedicating the NIR-CI instrument to the measurement of relaxation on a single tablet.

The longitudinal changes of axial tablet height were measured for lactose tablets at applied compression forces of 100, 300, and 500 MPa. The largest changes in tablet height are observed for the lactose tablets without MgSt compressed at 500 MPa as shown in Table 4.7. The lactose tablets with MgSt show a much lower expansion in tablet height.

Table 4.7 Tablet height measure at 0 hours and 48 hours.

	compaction pressures (MPa)	h_0 (mm)	h_1(mm)	ER%	
		T=0 h	T= 48 h		
Lactose 0% MgSt	100	2.9	2.95	1.75	1.77±0.02
	100	2.84	2.9	1.79	
	300	2.62	2.69	2.91	2.92±0.02
	300	2.59	2.67	2.94	
	500	2.64	2.78	5.31	4.80±0.71
	500	2.64	2.75	4.3	
Lactose 0.5 % MgSt	100	2.75	2.78	1.09	2.02±1.31
	100	2.59	2.67	2.94	
	300	2.58	2.62	1.4	1.19±0.28
	300	2.57	2.59	0.99	
	500	2.54	2.57	1.18	1.68±0.71
	500	2.56	2.62	2.2	

Tablet relaxation was confirmed by measuring the axial elastic recovery (ER) of the tablets after 48 hours of ejection from the die. The ER was calculated using equation 4.1, where h_0 is the minimum height of the tablet inside the die, and h_1 is the final height of the tablet 48 hours after ejection.

$$ER\% = \frac{h_1 - h_0}{h_0} x100 \qquad\qquad (4.1)$$

Table 4.7 shows the ER% for tablets prepared with fast flow lactose. The elastic recovery confirms tablet relaxation. The different compaction pressures result in significant differences in tablet porosity. The NIR slope is directly proportional to tablet particle compaction and tablet density, and the NIR slope is inversely proportional to porosity. These results constitute an opportunity to evaluate tablet relaxation using the slope NIR-CI method. Tablet relaxation is

depicted as porosity expansion through time.[29] Changes in porosity affect NIR spectra because as the porosity increases the air–particle boundary surface area increases and scattering thus increases.[70]

Calculation of the NIR slope variation has the advantage of not requiring pretreatment or transformation data for describing the tablet porosity or tablet compaction, and it is a simple measurement based on two wavelengths. NIR-CI could be used to follow the changes in tablet relaxation and evaluate the final physical properties of tablets.

4.3.9 Tablet Relaxation
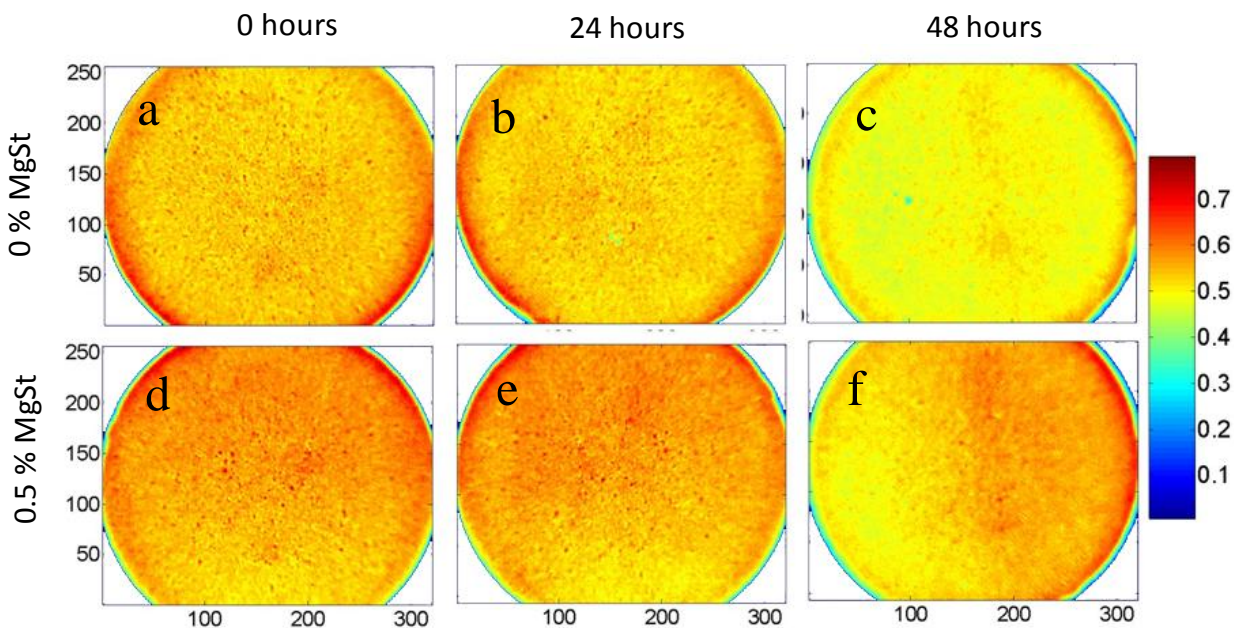
Figure 4.12 (a, b, c) Imaging of slope NIR-CI from lactose tablet compacted using 500 MPa without MgSt, at 0, 24 and 48 hours respectively. (d, e, f). Imaging of slope NIR-CI lactose tablet, compacted using 500 MPa with 0.5 % w/w of MgSt at 0, 24 and 48 hours.

Tablet relaxation of lactose tablets was evaluated using the NIR-CI slope method. The applied compaction pressure was 500 MPa in cylindrical tablets. Figure 4.12 presents the slope images of the tablets 60 seconds after ejection from the die and 24 and 48 hours after tablet ejection. Figure 4.12 a) shows the slope image for an un-lubricated lactose tablet only 60 seconds after ejection. The NIR-CI slope presents a nonuniform distribution, with lower slope values in the center of the tablet and higher slope values at the border because the friction from the unlubricated die wall resists powder motion and results in nonuniform distribution of the applied force.

The obtained results with slope NIR-CI were consistent with the study based on absorbance NIR chemical imaging performed by Ellison et al., who also observed a nonuniform force distribution.[71] The average value of the NIR-CI slope at 0 hours (Figure 4.12 a) was 0.544 (AU/nm). After 24 hours a decrease in the NIR spectral slope is observed as evidenced by the increasing yellow zones, indicating the occurrence of relaxation (Figure 4.12 b).

The calculated mean value of the NIR-CI slope was 0.534 (AU/nm); using the calibration curve developed, this NIR slope value corresponds to a compaction of pressure 477 MPa. The reductions in slope indicate increased porosity at 48 hours (Figure 4.12 c), showing expansion of yellow zones, with a mean NIR-CI slope of 0.488 (AU/nm) that corresponds to a compaction of 408 MPa. The decreasing values of slope from 0 to 48 hours were an indicative of tablet relaxation.

Figure 4.12 d) shows the slope image of a lubricated lactose tablet (0.5% MgSt) obtained 60 seconds after tablet ejection; the calculated mean slope was 0.562 (AU/nm) and predicted compaction value was 520 MPa. The slopes of this image do not appear to decrease significantly

after 24 hours as evidenced in Figure 4.12 e) the calculated value for the mean NIR-CI slope was

0.544 (AU/nm), corresponding to a compaction of 493 MPa. However, after 48 hours,

Figure4.12 f) shows a significant decrease of NIR spectral slope, with calculated mean NIR slope

of 0.534 (AU/nm), corresponding to a tablet compaction of 478 MPa. Figure 4.12 f) shows

significant differences in slope between the two halves of the tablet, showing the limitations of

the manual tablet press used.

Table 4.8 Results for tablet relaxation experiments for tablets compacted at 500 MPa. The tablet was compacted at 500 MPa and two levels of MgSt.

MgSt (%)	Time (h)	Mean Slope	Standard deviation	Coefficient of variation	skew	kurtosis
0	0	0.544	0.049	0.09	-3.986	45.119
0	24	0.534	0.047	0.088	-4.351	45.751
0	48	0.488	0.053	0.109	-5.745	53.099
0.5	0	0.562	0.057	0.101	-4.383	41.434
0.5	24	0.544	0.055	0.101	-4.24	37.968
0.5	48	0.534	0.067	0.125	-3.894	29.645

Table 4.8 shows results of the slope NIR-CI histogram analysis. The results show that

without MgSt the lactose tablets relaxed faster and in a greater proportion. Similar results were

obtained by Hwang, where for lactose fast flow tablets an inverse relationship between tablet

relaxation and MgSt level was reported.[72] Kurtosis values increase over time for lactose tablets

without MgSt, with a progressive diminution of slope values. The kurtosis values describe a

sharper peak on the histogram over time and a progressive concentration of values near the mean

NIR-CI slope value. For a lactose tablet with 0.5% MgSt the kurtosis decreased over time as

shown in Figure 4.13. This kurtosis indicated peak broadening and nonuniform tablet relaxation;

the histogram representation shows the bulk of pixels split in two subsets, a fraction that relaxed over time and a second set that remained at initial slope values.
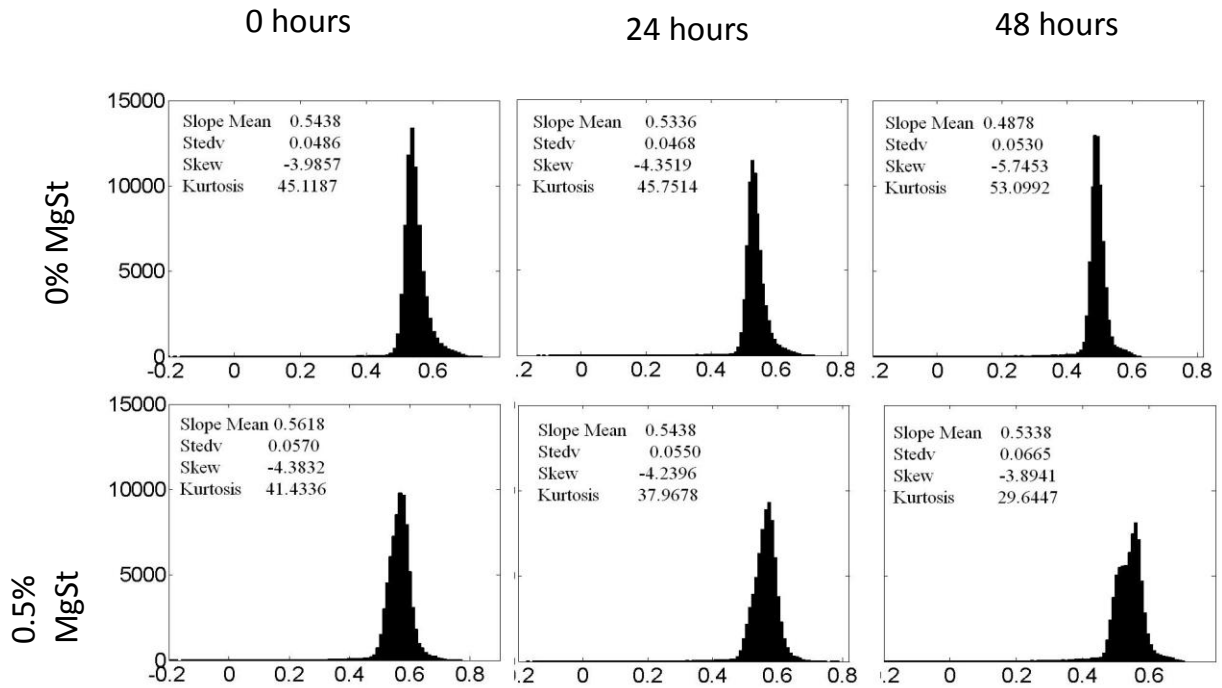
Figure 4.13 Histogram of slope NIR-CI values at different times, compact pressure 500 MPa and lactose tablets without lubricant and with 0.5% w/w of MgSt .

4.4 Conclusion

The PLS and PARAFAC/MLR approach was used to develop multivariate calibration models to predict chemical or physical parameters on many different kinds of samples, only acquiring the spectral response. The PLS calibration modelwas capable to predict chemical concentration handle compaction variation between 200-400 MPa. The PLS prediction model is not adequatewhen the range of physical variation is increased from 100-500 MPa. PARAFAC/MLR strategy was able to handle both sources of variation as separate modes, spread both chemical and physical information. The obtained PARAFAC/MLR models are less complex, because the number of components is lower and consequently the predictive ability is better. In the cases of tablet relaxation, Near-infrared chemical slope imaging is a simple and robust method that may be used to study tablet relaxation. The use of slope measurements does not require dedicating the NIR instrument to the measurement of relaxation on a single tablet. The relaxation process is affected by the use of magnesium stearate as a lubricant, and this effect is clearly observed in the images obtained. The resulting images could be used to compare different tablets from a manufacturing process.

5. Research Contributions

During formulation and pharmaceutical production, many of the critical variables are related to the physical properties of materials. Hardness, friability, solubility, homogeneity and fluidity of the particles are physical variables that define the design space where a pharmaceutical product meets quality requirements.

This research was a comprehensive effort to understand the physical information contained in NIR spectra obtained from pharmaceutical processes. NIR spectra obtained during powder flow, powder feeding, and tablets with significant differences in compaction pressure and tablet relaxation were study successfully using chemometric methods. The use of the physical information contained in NIR spectra also facilitates understanding the properties of pharmaceutical production processes.

The methodologies developed allow the use NIR spectroscopy as quality control system in real-time. In the specific case of powders flow, the in-line NIR spectroscopy is ready to evaluate the concentration and powder flow properties of a pharmaceutical formulation in the laboratory and the production plants. One important contribution of the study was following the mixing of powder particles during voiding, this result indicates the possibility of detecting segregation during the flow of particulate materials.

NIR spectroscopy showed that the powder flow continuity depends of the combination of factors present in the powder flow and feeding process. This affirmation was valid for free fall powder process and powder feeding processes. The range of variables studied shows two

principal sources of variation. In the free fall powder process, particle size was the principal source of variation. The case when feeder controls the powder flow, control settings show the largest source of variation. In both cases free fall and feeding process, NIR measurements in real-time can be converted into process control charts to achieve quality during production process.

In the cases of real-time NIR measurements of moving tablets, NIR spectra contain physical and chemical information. It was difficult to work with both a large variation in tablet compact pressure and API concentration. PARAFAC/MLR methods handle all variation in the physical and chemical ranges. This strategy is recommended in the development of pharmaceutical formulations or the development of pharmaceutical calibration models; however it could also be used for applications in other fields.

Near-infrared chemical slope imaging (NCSI) is a simple and robust method that may be used to study the distribution of hardness and tablet relaxation. The NCSI is also available to determine the impact of the geometry in the friability and relaxation of pharmaceutical tablets. The method developed could be used to compare different tablets from a manufacturing process.

5.1 Future Works

This research was focused in physical information contained in NIR spectra from separate unit operations. The next level of this research should be directed to consider all the units of a pharmaceutical process, using NIR and multi-block analysis. The implementation of NIR spectroscopy, multi-block PCA and multi-block PLS give the opportunity to understand the effect that process variable trajectories have in the final quality of pharmaceutical process.

6. References

1. Sarraguça, M. C. *et al.* Determination of flow properties of pharmaceutical powders by near infrared spectroscopy. *Journal of Pharmaceutical and Biomedical Analysis* **52**, 484–492 (2010).

2. Reich, G. Near-infrared spectroscopy and imaging: basic principles and pharmaceutical applications. *Advanced drug delivery reviews* **57**, 1109–43 (2005).

3. Jivraj, M., Martini, L. G. & Thomson, C. M. An overview of the different excipients useful for the direct compression of tablets. *Pharmaceutical Science & Technology Today* **3**, 58–63 (2000).

4. Swarbrick, B. Process analytical technology: A strategy for keeping manufacturing viable in Australia. *Vibrational Spectroscopy* **44**, 171–178 (2007).

5. Liltorp, K., Larsen, T. G., Willumsen, B. & Holm, R. Solid state compatibility studies with tablet excipients using non thermal methods. *Journal of pharmaceutical and biomedical analysis* **55**, 424–8 (2011).

6. FDA *Guidance for Industry Guidance for Industry PAT — A Framework for Innovative Pharmaceutical*. *Quality Assurance* (2004).

7. Gnoth, S., Jenzsch, M., Simutis, R. & Lübbert, a Process Analytical Technology (PAT): batch-to-batch reproducibility of fermentation processes by robust process operational design and control. *Journal of biotechnology* **132**, 180–6 (2007).

8. Sistare, F., St, L., Berry, P. & Mojica, C. A. Full Papers Process Analytical Technology : An Investment in Process Knowledge Abstract : *Organic Process Research & Development* **9**, (2005).

9. Jain, K. K. The role of nanobiotechnology in drug discovery. *Drug Discovery Today* **10**, 1435–1442 (2005).

10. Pasikatan, M., Steele, J., Spillman, C. & Haque, E. REVIEW: Near infrared reflectance spectroscopy for online particle size analysis of powders and ground materials. *Journal of Near Infrared Spectroscopy* **9**, 153 (2001).

11. Blanco, M. & Alcala, M. Content uniformity and tablet hardness testing of intact pharmaceutical tablets by near infrared spectroscopyA contribution to process analytical technologies. *Analytica Chimica Acta* **557**, 353–359 (2006).

12. Benedetti, C. *et al.* Cohesive, multicomponent, dense powder flow characterization by NIR. *International journal of pharmaceutics* **336**, 292–301 (2007).

13. Luypaert, J., Massart, D. L. & Vander Heyden, Y. Near-infrared spectroscopy applications in pharmaceutical analysis. *Talanta* **72**, 865–83 (2007).

14. Ramlakhan, M., Wu, C. Y., Watano, S., Dave, R. N. & Pfeffer, R. Dry particle coating using magnetically assisted impaction coating: modification of surface properties and optimization of system and operating parameters. *Powder Technology* **112**, 137–148 (2000).

15. Thalberg, K., Lindholm, D. & Axelsson, A. Comparison of different flowability tests for powders for inhalation. *Powder Technology* **146**, 206–213 (2004).

16. Freeman, R. Measuring the flow properties of consolidated, conditioned and aerated powders — A comparative study using a powder rheometer and a rotational shear cell. *Powder Technology* **174**, 25–33 (2007).

17. Mehrotra, A., Llusa, M., Faqih, A., Levin, M. & Muzzio, F. J. Influence of shear intensity and total shear on properties of blends and tablets of lactose and cellulose lubricated with magnesium stearate. *International Journal of Pharmaceutics* **336**, 284–291 (2007).

18. Castellanos, A., Valverde, J. & Quintanilla, M. The Sevilla powder tester: a tool for characterizing the physical properties of fine cohesive powders at very small consolidations. *Kona* **22**, 66–81 (2004).

19. Faqih, A. N., Alexander, A. W., Muzzio, F. J. & Tomassone, M. S. A method for predicting hopper flow characteristics of pharmaceutical powders. *Chemical Engineering Science* **62**, 1536–1542 (2007).

20. Schwedes, J. Review on testers for measuring flow properties of bulk solids. *Granular Matter* **5**, 1–43 (2003).

21. Barajas, M. J. *et al.* Near-infrared spectroscopic method for real-time monitoring of pharmaceutical powders during voiding. *Applied spectroscopy* **61**, 490–6 (2007).

22. Berntsson, O., Danielsson, L.-G., Lagerholm, B. & Folestad, S. Quantitative in-line monitoring of powder blending by near infrared reflection spectroscopy. *Powder Technology* **123**, 185–193 (2002).

23. Kitazawa, S., Johno, I., Ito, Y., Teramura, S. & Okado, J. Effects of hardness on the disintegration time and the dissolution rate of uncoated caffeine tablets. *The Journal of pharmacy and pharmacology* **27**, 765–770 (1975).

24. Siddiqui, A. & Nazzal, S. Measurement of surface color as an expedient QC method for the detection of deviations in tablet hardness. *International Journal of Pharmaceutics* **341**, 173–180 (2007).

25. Kirsch, J. D. & Drennen, J. K. Nondestructive tablet hardness testing by near-infrared spectroscopy: a new and robust spectral best-fit algorithm. *Journal of pharmaceutical and biomedical analysis* **19**, 351–62 (1999).

26.   Peinado, a, Vandenberg, F., Blanco, M. & Bro, R. Temperature-induced variation for NIR tensor-based calibration. *Chemometrics and Intelligent Laboratory Systems* **83**, 75–82 (2006).

27.   Skibsted, E. T. S., Westerhuis, J. A., Smilde, A. K. & Witte, D. T. Examples of NIR based real time release in tablet manufacturing. *Journal of Pharmaceutical and Biomedical Analysis* **43**, 1297–1305 (2007).

28.   Workman, J., Koch, M. & Veltkamp, D. Process analytical chemistry. *Analytical chemistry* **79**, 4345–63 (2007).

29.   Van Veen, B. *et al.* Pore formation in tablets compressed from binary mixtures as a result of deformation and relaxation of particles. *European journal of pharmaceutical sciences official journal of the European Federation for Pharmaceutical Sciences* **15**, 171–177 (2002).

30.   Zuurman, K., Van Der Voort Maarschalk, K. & Bolhuis, G. K. Effect of magnesium stearate on bonding and porosity expansion of tablets produced from materials with different consolidation properties. *International Journal of Pharmaceutics* **179**, 107–115 (1999).

31.   Van Veen, B., Bolhuis, G. K., Wu, Y. S., Zuurman, K. & Frijlink, H. W. Compaction mechanism and tablet strength of unlubricated and lubricated (silicified) microcrystalline cellulose. *European journal of pharmaceutics and biopharmaceutics : official journal of Arbeitsgemeinschaft für Pharmazeutische Verfahrenstechnik e.V* **59**, 133–8 (2005).

32.   Herschel, W. Experiments on the Refrangibility of the Invisible Rays of the Sun. By William Herschel, LL. D. F. R. S. *Philosophical Transactions of the Royal Society of London* **90**, 284–292 (1800).

33.   Chalmers John M. & Griffiths Peter R. *Handbook of vibrational spectroscopy*. 3862 (J. Wiley: 2002).

34.   Da-Wen Sun *Infrared Spectroscopy for Food Quality Analysis and Control*. 448 (2009).

35.   Williams, P. & Norris, K. *Near-Infrared Technology in the Agricultural and Food Industries*. (2001).

36.   Bakeev, K. A. *Process Analytical Technology: Spectroscopic Tools and Implementation Strategies for the Chemical and Pharmaceutical Industries*. 451 (Blackwell Publishing Ltd: Oxford, 2005).

37.   Atkins, P. & De Paula, J. *Atkins' Physical Chemistry*. *Chemistry* **116**, 1008 (Oxford University Press: 2006).

38.   Siesler, H. W. Introduction. *Near-Infrared Spectroscopy* (2007).doi:10.1002/9783527612666.ch01

39.   Wendlandt, W. W. & Hecht, H. G. *Reflectance spectroscopy*. (Interscience New York: 1966).

40.   Bohren, C. F. & Huffman, D. R. *Absorption and scattering of light by small particles*. (Wiley-Vch: 2008).

41.   Rantanen, J. *Near-infrared Reflectance Spectroscopy in the Measurement of Water as a Part of Multivariate Process Monitoring of Fluidised Bed Granulation Process*. (University of Helsinki: 2000).at <http://books.google.com.co/books?id=GDc2HQAACAAJ>

42.   Roggo, Y. *et al.* A review of near infrared spectroscopy and chemometrics in pharmaceutical technologies. *Journal of pharmaceutical and biomedical analysis* **44**, 683–700 (2007).

43.   Brereton, R. G. *Applied chemometrics for scientists*. *Applied Chemometrics for Scientists* **1**, 379 (John Wiley & Sons: 2007).

44.   Gaydou, V., Kister, J. & Dupuy, N. Evaluation of multiblock NIR/MIR {PLS} predictive models to detect adulteration of diesel/biodiesel blends by vegetal oil. *Chemometrics and Intelligent Laboratory Systems* **106**, 190–197 (2011).

45.   Brereton, R. G. Introduction to multivariate calibration in analytical chemistry. *The Analyst* **125**, 2125–2154 (2000).

46.   Bro, R. PARAFAC. Tutorial and applications. *Chemometrics and Intelligent Laboratory Systems* **38**, 149–171 (1997).

47.   Wold, S. PLS-regression: a basic tool of chemometrics. *Chemometrics and Intelligent Laboratory Systems* **58**, 109–130 (2001).

48.   Næs, T. *An User-friendly Guide to Multivariate Calibration and Classification*. (Nir Publications: 2002).at <http://books.google.com.co/books?id=UodrQgAACAAJ>

49.   Isaksson, T. & Griffiths, P. R. Optimal absorbance for transmission or reflection spectra measured under conditions of constant detector noice in the presence of stray radiation. *Applied Spectroscopy* **56**, 916–919 (2002).

50.   Vanarase, A. U., Alcalà, M., Jerez Rozo, J. I., Muzzio, F. J. & Romañach, R. J. Real-time monitoring of drug concentration in a continuous powder mixing process using NIR spectroscopy. *Chemical Engineering Science* **65**, 5728–5733 (2010).

51.   Pfeffer, R., Dave, R. N., Wei, D. & Ramlakhan, M. Synthesis of engineered particulates with tailored properties using dry particle coating. *Powder Technology* **117**, 40–67 (2001).

52.   Zhou, Q., Armstrong, B., Larson, I., Stewart, P. J. & Morton, D. A. V Improving powder flow properties of a cohesive lactose monohydrate powder by intensive mechanical dry coating. *Journal of pharmaceutical sciences* **99**, 969–981 (2010).

53.   Mujumdar, A., Wei, D., Dave, R. N., Pfeffer, R. & Wu, C.-Y. Improvement of humidity resistance of magnesium powder using dry particle coating. *Powder Technology* **140**, 86–97 (2004).

54.   Yang, J., Sliva, A., Banerjee, A., Dave, R. & Pfeffer, R. Dry particle coating for improving the flowability of cohesive powders. *Powder Technology* **158**, 21–33 (2005).

55.   Molerus, O. Theory of yield of cohesive powders. *Powder Technology* **12**, 259–275 (1975).

56.   Li, T., Donner, A. M. Y. D., Choi, C. Y., Frunzi, G. P. & Morris, K. R. A Statistical Support for Using Spectroscopic Methods to Validate the Content Uniformity of Solid Dosage Forms. *Journal of pharmaceutical sciences* **92**, 6–10 (2003).

57.   Hilden, L. R., Pommier, C. J., Badawy, S. I. F. & Friedman, E. M. NIR chemical imaging to guide/support BMS-561389 tablet formulation development. *International Journal of Pharmaceutics* **353**, 283–290 (2008).

58.   Gendrin, C., Roggo, Y. & Collet, C. Pharmaceutical applications of vibrational chemical imaging and chemometrics: a review. *Journal of Pharmaceutical and Biomedical Analysis* **48**, 533–553 (2008).

59.   Gupta, A., Peck, G. E., Miller, R. W. & Morris, K. R. Influence of ambient moisture on the compaction behavior of microcrystalline cellulose powder undergoing uni-axial compression and roller-compaction: a comparative study using near-infrared spectroscopy. *Journal of Pharmaceutical Sciences* **94**, 2314–2326 (2005).

60.   Gonza, J. M. A Process Analytical Technology Approach Based on Near Infrared Spectroscopy : Tablet Hardness , Content Uniformity , and Dissolution Test Measurements of Intact Tablets. **95**, 2137–2144 (2006).

61.   Barnes, R. J., Dhanoa, M. S. & Lister, S. J. Standard Normal Variate Transformation and De-trending of Near-Infrared Diffuse Reflectance Spectra. *Applied Spectroscopy* **43**, 772–777 (1989).

62.   Geladi, P., MacDougall, D. & Martens, H. Linearization and Scatter-Correction for Near-Infrared Reflectance Spectra of Meat. *Applied Spectroscopy* **39**, 491–500 (1985).

63.   Martens, H., Nielsen, J. P. & Engelsen, S. B. Light scattering and light absorbance separated by extended multiplicative signal correction. application to near-infrared transmission analysis of powder mixtures. *Analytical Chemistry* **75**, 394–404 (2003).

64.   Savitzky, A. & Golay, M. J. E. Smoothing and differentiation of data by simplified least squares procedures. *Analytical Chemistry* **36**, 1627–1639 (1964).

65.   Blanco, M., Bautista, M. & Alcalá, M. Preparing calibration sets for use in pharmaceutical analysis by NIR spectroscopy. *Journal of pharmaceutical sciences* **97**, 1236–1245 (2008).

66.   Blanco, M., Alcala, M., Gonzalez, J. & Torras, E. Near infrared spectroscopy in the study of polymorphic transformations. *Analytica Chimica Acta* **567**, 262–268 (2006).

67.   Eiliazadeh, B., Briscoe, B. J., Sheng, Y. & Pitt, K. Investigating density distributions for tablets of different geometry during the compaction of pharmaceuticals. *Particulate science and technology* **21**, 303–316 (2003).

68.   Djemai, A. & Sinka, I. C. NMR imaging of density distributions in tablets. *International journal of pharmaceutics* **319**, 55–62 (2006).

69. Busignies, V. *et al.* Quantitative measurements of localized density variations in cylindrical tablets using X-ray microtomography. *European journal of pharmaceutics and biopharmaceutics official journal of Arbeitsgemeinschaft fur Pharmazeutische Verfahrenstechnik eV* **64**, 38–50 (2006).

70. Short, S. M., Cogdill, R. P., Wildfong, P. L. D., Drennen, J. K. & Anderson, C. A. A near-infrared spectroscopic investigation of relative density and crushing strength in four-component compacts. *Journal of Pharmaceutical Sciences* **98**, 1095–1109 (2009).

71. Ellison, C. D., Ennis, B. J., Hamad, M. L. & Lyon, R. C. Measuring the distribution of density and tabletting force in pharmaceutical tablets by chemical imaging. *Journal of Pharmaceutical and Biomedical Analysis* **48**, 1–7 (2008).

72. Hwang, R. & Benannan, P. D. M. Lactose, Microcrystalline Cellulose, and Dibasic Calcium Phosphate. *Pharmaceutical technology* (2001).

Appendix A

M-file to read "spc" NIR spectra data. This M-file translates all NIR Spectra obtained in a batch process to a matrix in Matlab format. Additionally the algorithm gives the frequency and time of acquisition for every NIR spectra.

```
cd 'C:\MATLAB701\work\ Experiments\PH101BN'
MyFiles=dir('*.spc');
NIR=[];
TS=[];
for i=1:length(MyFiles)
   [data,xaxis,auditlog] = spcreadr(MyFiles(i).name);
timestamp=fieldnames(auditlog);
timestamp=timestamp{4}(end-7:end);
   TS=[TS;timestamp];
   NIR=[NIR;data];
end
[d,d,counts,TSunique]=grpstats(NIR,TS);
counts=counts(:,1)
TSunique=char(TSunique);
NumericTSUnique=[TSunique(:,[1 2]) TSunique(:,[4 5]) TSunique(:,[7 8])];
MyTime=[];
BaseTime=str2num(NumericTSUnique(1,[1 2]))*3600*100 + ...
str2num(NumericTSUnique(1,[3 4]))*60*100   + ...
str2num(NumericTSUnique(1,[5 6]))*100;

for i=1:length(NumericTSUnique)
DeltaMS=100/counts(i);
for j=1:counts(i)
MyTime(end+1)=str2num(NumericTSUnique(i,[1 2]))*3600*100 + ...
str2num(NumericTSUnique(i,[3 4]))*60*100   + ...
str2num(NumericTSUnique(i,[5 6]))*100      + ...
        DeltaMS*j;
end
end

% This script generates NIR WITH MATRIX SPECTRA, xaxis FREQUENTLY AND MyTime
% With delta time 1 / 100 second sample is the first time assume
% Zero.
```

Apendix B

M-file to calculate slope using NIR-CI data. This M-file Slope describes the grade of compaction along of a table surface.

```
%% REFERENCE: J. Ropero, Y. Colón, R.J. Romañach. Applied Spectroscopy, 2010
%%
%% INPUT:
%%  lambda1   imaging data matrix    (dataX x dataY)
%%  lambda2   imaging data matrix    (dataX x dataY)
%%
%%  datafile  threedimensional imaging data matrix x (dataX x dataY x lambda)
%%
%%
%% OUTPUT:
%%  slopeM     slope matrix of imaging data
%%
%% SUBROUTINES: center.m, invcente.m, plscvsim.m, plscvwim.m
%%
%% AUTHOR:  Jorge Ropero
%%          Copyright (c) 2010
%%          Analytical & Pharmaceutical Lab.
%%          University of Puerto Rico, Mayaguez Campus
%%
%% VERSION: 1.0 (27/05/2010)
%%
%%
clc
display('datafile')
lambda1
lambda2

%S = load('datafile');
%C = S.datafile(:,:,lamda1);
%D = S.datafile(:,:,lamda2);
%slopeM =(C-D)/(lamda1-lamda2);
%imagesc (M);
%figure(gcf);
%%
%%%%%%%%%%%%%%%%
%%  END
%%%%%%%%%%%%%%%%
```